UNIVERSITÀ DEGLI STUDI DI MILANO

Dipartimento di Fisica

Corso di Dottorato di Ricerca in Fisica, Astrofisica e Fisica Applicata
Ciclo XXXI

Theory of positronium interactions with porous materials

Settore Scientifico Disciplinare FIS/03

Supervisori: Professor Fabrizio CASTELLI

Professor Giovanni CONSOLATI

Tesi di Dottorato di:
Giacomo TANZI MARLOTTI

Anno Accademico 2018/19

Commission of the final examination:

External Member:
Prof. Roberto S. Brusa

External Member:
Prof. Grzegorz Karwasz

External Member:
Prof. Giovanni Consolati

Final examination:

Date 14/12/2018

Università degli Studi di Milano, Dipartimento di Fisica, Milano, Italy

Contents

Introduction

The purpose of this thesis work is a deep theoretical study of the physical characteristics and of the annihilation dynamics of a positronium atom (Ps) inside condensed matter, especially in porous and amorphous materials, to the aim of interpreting experimental observations. The need for improved theoretical models with respect to simple and well known examples found in past literature is justified by the lack of a simple explanation for the well known phenomenon of the lowering of the contact density, a quantum parameter describing the electron density at the positron position. Given that this parameter is experimentally accessible, connecting its value to specific properties would be extremely useful in the context of structural analysis of materials.

The thesis is organized as follows: in a first chapter we will review the physics of both Ps in vacuum and in matter. Special attention will be devoted to the introduction of the magnetic quenching effect and to the concepts of pickoff process and contact density, which are fundamental to understand the current research. In the second chapter we will describe the most famous models and theoretical techniques used in literature to describe Ps, particularly when a confinement effect in small cavities is present, together with their limitations and their failure in describing some experimental aspects.

In the third chapter we analyze a simple two-particle model we formulated to describe Ps confined in nanopores. This model is based on the observation that the confining potential acting on Ps is a net result of two independent and different contributions, acting on the electron and on the positron separately. In particular, a positive value for the positron work function, as derived by theoretical models and found, for example, in silica, suggests that the positron is attracted toward the medium and then is not confined *a priori*. The well known confining behavior of Ps is then related to the repulsive electron-electron interaction at short distances and to the strong Pauli exchange forces with bulk electrons. In this picture, it is the electron in *o*-Ps that prevents large overlap between Ps and electrons in matter.

By applying approximate semi-analytical techniques, a variational method approach, and finally a quantum montecarlo code, we were able to demonstrate that our model correctly describe the lowering of the contact density, obtaining also promising results in the comparison with experimental data. Despite that, this model was not fully satisfactory, because it is based on a macroscopic parameter, the positron work function, which is not clearly defined for all kind of materials, nor is it easy to obtain experimentally.

For this reason in the fourth chapter we reconsider the whole problem of Ps confinement in porous materials using a different approach, i.e. taking into full account exchange interactions with surrounding electrons. In particular, we will show how this problem can be treated by means of symmetry adapted perturbation theories (SAPT)

and local density approximation (LDA). Despite the difficulty of dealing with the full many-body wavefunction, we will show that, with a few reasonable approximations, it is possible to formulate a simplified model which accounts for the lowering of the contact density in a natural and simpler way. In turn, this will allow us to clarify some aspects of the pickoff process which still needed a theoretical description.

Part I
Theoretical background

CHAPTER 1

Positronium physics

In recent years the hydrogenlike bound state of an electron and a positron, namely the positronium atom (Ps), has been extensively studied in the context of structural analysis of materials. As a matter of fact, its characteristic behavior inside matter enables to extract useful information about the medium itself, effectively using Ps as a probe.

Experimentally, Ps is formed implanting positrons inside the material to be studied. While in metals positrons annihilate without forming a bound state, there is a vast class of materials where Ps formation mechanisms in bulk are accessible, as for example in zeolites[1], porous materials[2], amorphous and crystalline SiO2 [3], polymers[4] and many more. Ps formation is commonly related to many material-specific properties, like internal structure, electron density, positron work function and ionization energy. After a thermalization process in bulk[5] [6], the positron captures an electron from the host material and enters regions of low electron density(i.e. free spaces or pores) as a Ps atom[7], in particular in the long-living form of o-Ps (see later).

If pores are not interconnected, Ps will be confined inside these sites until its annihilation, a process which in turn is strongly related to the local properties of the material. This connection is usually provided by means of the pick-off annihilation process, in which the positron inside Ps annihilates with an external electron of the surrounding material. While in vacuum the annihilation rate depends on the electron density at the positron position (the contact density k [8]), in matter the pick-off process dominates as it strongly reduces the lifetime of the long-living component *o*-Ps from the vacuum value (142ns) to a few ns [9] .

Usually the pick-off signature of *o*-Ps obtained with PALS (Positron Annihilation Lifetime Spectroscopy) experimental techniques can be easily separated from faster annihilation processes related to other annihilation channels. Furthermore, the contact density can also be experimentally determined either by exploiting the magnetic quenching of Ps or by analyzing the $3\gamma/2\gamma$ generation ratio [10]. This enable to connect data with suitable models of the properties of Ps in small cavities and to obtain information on pore dimensions and other material characteristics.

In this chapter we give an overview of the Physics of Ps in vacuum and in matter, in order to introduce some concepts and properties that are necessary to understand the following work.

1.1 General properties of Ps in vacuum

1.1.1 Energy levels and annihilation rates

Positronium (Ps) is an atomic system consisting of an electron and its anti-particle, a positron, bound together via Coulomb force in a so–called exotic atom. Given that both

constituents are stable elementary particles without substructures, Ps is the simplest quantum electrodinamical bound system in nature, and the only relevant interaction is the electromagnetic one. Moreover it can be assumed that the two particles have the same mass m_e and opposite charge e.

Ps is hydrogen-like, but since the reduced mass is $\mu = m_e/2$, the bare values of the energy levels are reduced to half those found in the hydrogen atom, so that the binding energy of ground state positronium is approximately ≈ 6.8 eV in the non-relativistic approximation: [5]

$$\begin{aligned} E_{\text{not rel.}} &= -\frac{m_e e^4}{4n^2\hbar^2} \\ E^{\text{GS}}_{\text{not rel.}} &= -\frac{m_e e^4}{4\hbar^2} = -6.8 \text{ eV} \end{aligned} \tag{1.1}$$

The existence of this bound state was predicted by Mohorovicic [11] in 1934 and it was first detected from its annihilation properties γ–photons in 1951 by Deutsch at MIT [12].

Like for hydrogen, positronium ground state is almost degenerate with respect to its spin configuration. The singlet state ($S = 0, s_z = 0$) is called *para*-Positronium (*p*-Ps) and has an anti-symmetric spin configuration, while the triplet state ($S = 1, s_z = -1, 0, 1$) is called *ortho*-Positronium (*o*-Ps) and it has a symmetric spin configuration. In absence of an external magnetic field, the portion of Ps created in the two configurations is roughly $1 : 3$, being the *o*-Ps state triply degenerate. The small Hyperfine splitting Δ_{st} between the singlet and triplet spin configuration in the ground state $n = 1, l = 0$ Ps is given by[13, 14]:

$$\Delta_{\text{st}} = \frac{7}{6} E_{\text{RYD}} \alpha^2 \approx 8 \times 10^{-4} \text{eV} \tag{1.2}$$

where $4/6$ comes from the spin-spin interaction and $3/6$ from the one-photon virtual annihilation of *o*-Ps . The short-lived *p*-Ps lies lower in energy but since radiative transitions from triplet to singlet state are forbidden (under electric dipole approximation) *o*-Ps is stable in vacuum[15].

Unlike hydrogen there are some important differences between the two spin configurations due to their annihilation properties. Indeed, in order to conserve angular momentum and to impose CP invariance, Yang (1950) [16] and Wolfenstein and Ravenhall (1952) [17] concluded that positronium in a state with spin S and orbital angular momentum L can only annihilate into n_γ gamma–photons, where

$$(-1)^{n_\gamma} = (-1)^{L+S}. \tag{1.3}$$

Equation 1.3 predicts that annihilation of the *p*-Ps (1^1S_0) and *o*-Ps (1^3S_1) states can only proceed by the emission of even and odd numbers of photons respectively.

In both cases the lowest order processes dominate although observation of the five-photon decay of *o*-Ps has been reported [18]. The annihilation rate is directly connected with the number of photon created in each annihilation process by a factor of the order of the fine structure constant ($\alpha \simeq 1/137.036$)coming directly from the Feynman rules. This way *p*-Ps annihilation rate is about 10^3 times greater than that of the *o*-Ps . This means that the mean lifetimes of the two states are very different. The lowest order contrubutions to the annihilation rates for the $^1S_0$ and $^3S_1$ states of positronium with principal quantum number n were first calculated by Pirenne (1946) and Ore et al.(1949) [15, 19]

respectively, and are given by:

$$\lambda_{2\gamma}(n^1S_0) = \frac{mc^2\alpha^5}{2\hbar n^3} \tag{1.4}$$

and

$$\lambda_{3\gamma}(n^3S_1) = \frac{2}{9\pi}(\pi^2 - 9)\frac{mc^2\alpha^6}{\hbar n^3} \tag{1.5}$$

In the following, we will use $\lambda_{2\gamma}$ and $\lambda_{3\gamma}$ as a short notation for the ground state ($n = 1$) annihilation rates. It is found that $\lambda_{2\gamma} \simeq 8\,GHz$, whereas $\lambda_{3\gamma} \simeq 7\,MHz$.

The reciprocals of these annihilation rates are the lifetimes of the $^1S_0$ and $^3S_1$ states and they are around 124ps and 142ns respectively. Higher orders annihilation process are reduced approximately by a factor α for each additional photons and thus are commonly discarded. Given that *p*-Ps /*o*-Ps formation ratio in vacuum is $1/3$, we introduce here the spin-averaged annihilation rate

$$\bar{\lambda} = (\frac{1}{4}\lambda_{2\gamma} + \frac{3}{4}\lambda_{3\gamma}) = 2.01[\text{ns}]^{-1} \tag{1.6}$$

which will be extensively used throughout this work.

It is interesting to note that lifetimes of excited Ps states in vacuum, i.e. with $n > 1$, are much longer. Alekseev (1958)[20] calculated the lifetime against annihilation for Ps in the $2P$ states to be $> 10^{-4}$s , which is several orders of magnitude greater that the mean life for optical de-exitation. As an example, the $2P-1S$ transition has a characteristic lifetime of 3.2ns(in both spin configurations). The actual lifetime of an excited state may therefore be determined mainly by the lifetime of the atomic transition. Therefore, instead of the positronium annihilating directly in a $2P$ state, it is far more likely to make an optical transition to an $1S$ state, where annihilation than take place with standard rates $\lambda_{2\gamma}$ and $\lambda_{3\gamma}$.

1.1.2 The wavefunction of free Ps

As anticipated in the previous section, the non-relativistic description of Ps in vacuum can be done using the same two-body technique used for the hydrogen atom, the main difference being that, since positron's and electron's mass are equal, the center of mass will be in the middle between the two particles. The solution of the Schrödinger equation in free space is easily found by separating center of mass and relative position variables, $\boldsymbol{R}$ and $\boldsymbol{r}$ respectively:

$$\begin{aligned} \boldsymbol{r} &= \boldsymbol{r}_p - \boldsymbol{r}_e \qquad & \boldsymbol{R} &= \frac{\boldsymbol{r}_p + \boldsymbol{r}_e}{2} \\ \boldsymbol{p} &= \frac{\boldsymbol{p}_p - \boldsymbol{p}_e}{2} \qquad & \boldsymbol{P} &= \boldsymbol{p}_p + \boldsymbol{p}_e \end{aligned} \tag{1.7}$$

where $\boldsymbol{r}_p(\boldsymbol{r}_e)$ is the positron(electron) position. Since the hamiltonian is separable in these coordinates, its wavefunctions (solution of the eigenvalue problem) will factorize:

$$\Psi(\boldsymbol{R}, \boldsymbol{r}) = \Phi_k(\boldsymbol{R})\varphi_{nlm}(r, \theta, \phi) \tag{1.8}$$

The relative wavefunction φ depends on the well know quantum numbers (n, l, m)

$$\varphi_{nlm}(r, \theta, \phi) = R_{nl}(r)Y_{lm}(\theta, \phi) \tag{1.9}$$

where $R_{n,l}(r)$ is the radial part of the wavefunction, $Y_{l,m}(\theta, \phi)$ are the spherical harmonics functions. Φ_k describes the free motion of the center of mass, i.e. a plane wave parametrized by a wave vector $\boldsymbol{K}$. For the ground state, assuming for simplicity normalization of Φ_k on a large volume V, we explicitly have:

$$\begin{aligned} \Psi_{\text{GS}}(\boldsymbol{R}, \boldsymbol{r}) &= \frac{1}{\sqrt{V}} e^{i\boldsymbol{K}\cdot\boldsymbol{R}} R_{10}(r)Y_{00}(\theta, \phi) \\ &= \frac{1}{\sqrt{V}} e^{i\boldsymbol{K}\cdot\boldsymbol{R}} \frac{2}{\sqrt{4\pi}} (\frac{1}{2a_0})^{3/2} e^{-r/2a_0} \end{aligned} \tag{1.10}$$

where $a_0 = \frac{4\pi\epsilon_0\hbar^2}{m_e e^2} \approx 0.529\text{Å}$ is the Bohr radius.

The full ground state wavefunction will be just the product of the spatial and the spin component:

$$\Psi^{\text{Ps}}_{s,s_z}(p, e) = \Psi_{\text{GS}}(\boldsymbol{R}, \boldsymbol{r})\chi_{s,s_z}(\sigma_p, \sigma_e) \tag{1.11}$$

where we have introduced the spin-spatial coordinates $e = (\sigma_e, \boldsymbol{r}_e)$ and $p = (\sigma_p, \boldsymbol{r}_p)$, while χ_{s,s_z} are the well known eigenfunctions of S^2 and S_z:

$$\begin{aligned} \chi_{00}(\sigma_1, \sigma_2) &= \frac{s_\uparrow(\sigma_1)s_\downarrow(\sigma_2) - s_\downarrow(\sigma_1)s_\uparrow(\sigma_2)}{\sqrt{2}} \\ \chi_{10}(\sigma_1, \sigma_2) &= \frac{s_\uparrow(\sigma_1)s_\downarrow(\sigma_2) + s_\downarrow(\sigma_1)s_\uparrow(\sigma_2)}{\sqrt{2}} \\ \chi_{11}(\sigma_1, \sigma_2) &= s_\uparrow(\sigma_1)s_\uparrow(\sigma_2) \\ \chi_{1-1}(\sigma_1, \sigma_2) &= s_\downarrow(\sigma_1)s_\downarrow(\sigma_2) \end{aligned} \tag{1.12}$$

which describe the singlet *p*-Ps state and the 3 triplets *o*-Ps states respectively.

Beside the spin configuration, the most important parameter entering the description of Ps annihilation is the so-called contact density k_0. The contact density is defined as the probability of finding the electron at the positron position [8], and it's related to the spatial part of the wavefunction. The importance of this parameter is due to the fact

that the annihilation rates of both *p*-Ps and *o*-Ps in vacuum are proportional to k_0, so that Eq. 1.4 and Eq. 1.5 can be equivalently written as[14]:

$$\lambda_{2\gamma} = 4\pi r_0^2 c k_0 \tag{1.13}$$

for *p*-Ps and

$$\lambda_{3\gamma} = \frac{4}{9\pi}(\pi^2 - 9)\alpha\lambda_{2\gamma} \tag{1.14}$$

for *o*-Ps , where $r_0 = \alpha^2 a_0$ is the classical electron radius and c is the speed of light. In vacuum, the value in of the contact density k_0 can be easily derived with the help of a Dirac delta:

$$\begin{aligned} k_0 &= \int |\Psi_{\text{GS}}(R, \boldsymbol{r})|^2 \, \delta^3(\boldsymbol{r}_p - \boldsymbol{r}_e) \, d^3 r_+ \, d^3 r_- \\ &= \int |\Phi(R)|^2 \, |\varphi_{100}(r, \theta, \phi)|^2 \, \frac{\delta(r)}{4\pi r^2} r^2 \sin\theta \, dr \, d\theta \, d\phi \; d^3 R \\ &= \left| \frac{2}{\sqrt{4\pi}} (\frac{1}{2a_0})^{3/2} e^{-r/2a_0} \right|^2 \Bigg|_{r=0} \\ &= \frac{1}{8\pi a_0^3} \end{aligned} \tag{1.15}$$

where we have used the expression of the Dirac delta in spherical coordinates. The factor 8 in the denominator comes from the fact that the Ps Bohr radius is twice the hydrogen Bohr radius a_0.

1.2 The annihilation operator

As we've seen, positron annihilation rates with the bound electron of ground state Ps in vacuum are theoretically (and experimentally) well known and understood. This is not generally true in matter, where a fully quantum electrodynamical (QED) description of the electron-positron annihilation is not *de facto* possible.

As pointed out by many authors [21], this QED phenomenon can be described in a simpler way through the introduction of an effective absorption potential $-i\hbar\hat{\lambda}/2$ in the ordinary time-dependent Schrödinger equation of the quantum mechanical system under examination, where λ is a suitable loss rate operator. Being imaginary, this potential leads to an exponential decay of the positron (positronium) wavefunction, which accounts for particle loss and which rate can be determined via PALS experiment (see Sec. 1.6). The factor $1/2$ arises from the fact that the general definition is given in terms of the probability density:

$$\frac{d}{dt}|\psi|^2 = -\lambda|\psi|^2 \tag{1.16}$$

where as usual $\lambda = \tau^{-1}$ is the inverse of the lifetime.

However, this time-dependent approach is often pushed aside in favor of a time-independent one. In the standard theory of positron-atom scattering, for example, the system is usually described in terms of the Hamiltonian $\hat{H}_0$ including only the Coulomb potentials and not the absorption term. The wave function Ψ_0 thus obtained is then used to calculate the pair annihilation rate during the collision λ as expectation value of $\hat{\lambda}$:

$$\langle \Psi_0 | \, \hat{\lambda} \, | \Psi_0 \rangle = \lambda \tag{1.17}$$

In this context, this is justified by the fact that collision time is much shorter than Ps lifetime and the probability of pair annihilation during the collision is small[21, 22]. In general, it is assumed that the imaginary part of the energy is so small with respect to the real part that it can be treated as a perturbation of the time independent solution. As an example one may note that for *p*-Ps one has $\hbar\lambda_{2\gamma}/2 = 2.6\mu$eV, which is several order of magnitudes lower than the ground state excitation energy.

Historically, this approach was also widely used in the context of positron annihilation not only in metals, where a proper bound Ps state can not be formed, but also in liquids and condensed matter. In all cases, the form of $\hat{\lambda}$ is chosen in a way that its expectation value over the unperturbed positronium $1s$ wavefunction recovers known vacuum values.

The most common expression of the total annihilation operator for a positron surrounded by N electrons is the sum of N formally identical terms[1]

$$-i\frac{\hbar}{2}\hat{\lambda} = -i\frac{\hbar}{2}\sum_{i=1}^{N}\hat{\lambda}_i = N\hat{\lambda}_1 \tag{1.18}$$

each given by[9]:

$$\hat{\lambda}_i = 8\pi a_0^3 \delta^3(\boldsymbol{r}_p - \boldsymbol{r}_i)\left[\frac{1-\Sigma_{p,i}}{2}\lambda_{2\gamma} + \frac{1+\Sigma_{p,i}}{2}\lambda_{3\gamma}\right] \tag{1.19}$$

where $8\pi a_0^3$ is the inverse contact density of unperturbed positronium, r_p and r_i are positron and electrons coordinates, respectively, and $\Sigma_{p,i}$ is the spin exchange operator. In this approximation $\hat{\lambda}$ is basically a "contact operator" i.e., it is a linear combination of δ functions of the electron positron distance. The spin exchange operator Σ guarantees that the antisymmetric spin state (*p*-Ps) annihilate via 2γ emission while the symmetric spin state (*o*-Ps) via 3γ emission. It's easy to see that this form of $\hat{\lambda}_i$ is diagonal in the $n = 1$ subspace of unperturbed Ps and gives the correct annihilation value for *p*-Ps and *o*-Ps states in vacuum.

1.3 Positronium in matter

Positronium cannot be found in nature, but abundant emission of Ps in the vacuum has been observed by bombarding surfaces of different solid materials with a positron beam. However, positronium formation is just one possible outcome of the multiple annihilation channels of positron in matter. For this reason in the first part of this section we will review the main characteristics of positron annihilation in matter.

1.3.1 Positron annihilation in matter

Whenever a positron enters a medium or encounters an atom it will eventually annihilates with an electron at a rate which will depend on the local electron density[5]. In condensed matter for example, positron lifetimes in bulk are typically less than 500ps (if no Ps is formed), while in low density gases this can be order of magnitudes longer. Generally when a positron reaches the surface of a sample, it can either backscatter or enter into the material. The fraction of backscattered positrons will be strongly dependent on both

[1]The reader may note that for a system of more electrons, the expectation value must be calculated on a completely antysymmetric many body wavefunction.

the type of the material and implantation energy. On the contrary positrons entering a solid lose their energy very effectively through Coulomb scattering. This thermalization process is usually faster than the annihilation rate, so that the majority of positrons are thermalized before annihilation[23]. After this process the positron essentially remains in a free or delocalized state and it starts to diffuse around. In this phase it can either directly annihilate or be emitted back in the vacuum as slow e^+ or Ps.

In metals, positron behavior has been extensively studied by many authors. Given the possibility of describing bulk conduction electrons as an electron gas (HEG), metals provide indeed a natural framework to test *ab initio* perturbation theories of positron-electron interaction. Kahana [24] first showed that an accurate description of the total annihilation rate in many metals of any density can be obtained by iterating the screened electron-positron potential deduced in the high-density limit. In general, for a system of low energy electrons and positrons, the annihilation rate is directly proportional to the electronic density at the positron position. Given the Coulomb attraction, this quantity is strongly dependent on the short range correlations between the two annihilating particles. If one neglects positron-electron correlations, the resulting system of a positron interacting with an electron gas in a uniform background-charge (jellium) is recovered. This zero-order approximation is referred to as independent particle model (IPM). Improved calculations must include correlations. This is usually achieved through the introduction of an enhancement factor which describes the piling up of electrons around the positron (screening charge). We will review IPM and the enhancement factor in Section 2.3. We note here that at extreme low densities one would expect the positron to be correlated with just one electron in a quasipositronium atom. However, given the non-vanishing exchange interactions between electrons, there is complete mixing of triplet and singlet spin states, so that the state (and its annihilation rate) will be more similar to that of a positronium negative ion, as briefly discussed in subsection 1.5.

Experimentally it was discovered that real metals often exhibit a long-lived component in the annihilation spectra. It was soon realized that this can be easily explained by the formation of a spatially localized positron state. This in turn is linked to the presence of defects inside the metals, such as vacancies, voids, ionic centers and so on[25], characterized by a low electron density. In particular this is possible thanks to the high trapping probability of the positron, which makes experimental methods sensitive to defects already at low defect concentrations($\sim 10^{-6}$) [26]. First principle calculations for positron-annihilation in defected materials are usually performed in the framework of two-component density functional theory where the vacancy is approximated as a hole in the jellium background[27, 28]. These calculations assumed great importance especially in the study of voids in materials used in nuclear reactors technology, since they provide the only way to experimentally measure their size and distribution.

Electron-positron correlations play a major role also in the study of positron-atom interactions. Beside the enhancement of the electron-positron contact density, the main correlation effects in this case are the polarization of the atomic system by the positron and the virtual positronium formation[29]. As for metals, the first one is very important for calculating positron annihilation rate while the last two effects are crucial for an accurate description of positron-atom scattering.

While some quartz and ionic crystals exhibit only fast positron decay (for example in NaCl with a lifetime of $2.0\ 10^{-10}$s), other materials like common insulators and gas show widespread occurrence of an additional slow mode of decay. The situation is slightly different from what we saw before regarding defected metals because this time lifetimes are much longer. It is generally accepted that this is due to the formation of *o*-Ps [30]. Since, as opposite to metals, there are no free conduction electrons to interact with, Ps

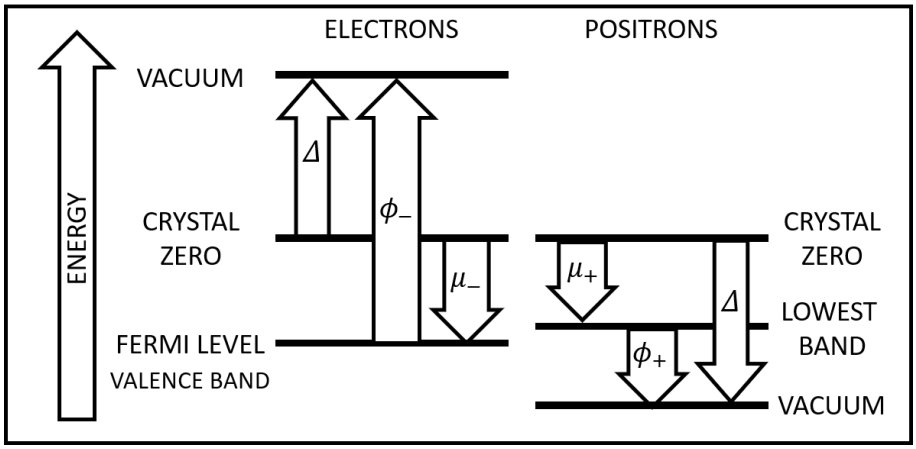

Figure 1.1: Schematic energy-level diagram for electron and positron in solids.

can be considered more or less isolated from the electronic charge of surrounding atoms. Before discussing the behavior of Ps, we will review the energetics of its formation in the next section.

1.3.2 Positron and electron energy levels in solids

In order to qualitatively understand positronium formation and trapping in solids, it is useful to introduce two standard measurable quantities: the positron work function and the positronium formation potential [31]. The work function is defined as the energy required to remove an electron or a positron from the material to a state at rest in the vacuum nearby the surface, and thus it strongly depends on the properties of the surface. In every standard band-structure calculation, both electron and positron energy levels are solved respect to a common reference level called *crystal zero*. However this level is defined for perfect infinite lattices without a surface and so it is a bulk property. For instance, the electron chemical potential μ_- is defined (see Fig. 1.1) as the distance of the Fermi level from the crystal zero. Similarly, the distance of the lowest positron energy level from the crystal zero is the positron chemical potential μ_+. The crystal zero is related to the Coulomb potential and it can be defined, for example, as the average electrostatic potential in the infinite lattice, or the average value of the electrostatic potential on the surface of the Wigner-Seitz cell. The surface effects are collected in a term called surface dipole Δ, that is just the energy distance between the electrostatic potential level, which a test charge feels in the vacuum, and the crystal zero. This quantity is the same for electron and positron but it has a different sign due to their opposite charge. The surface dipole depends on the electronic structure of the surface, especially on the spilling of the electron density into the vacuum. The electron work function ϕ_- is the distance between the absolute Fermi level and the vacuum level and thus is the sum of the electron chemical potential and of the surface dipole:

$$\phi_- = \Delta - \mu_- \tag{1.20}$$

In a similar way we can describe the positron work function:

$$\phi_+ = -\Delta - \mu_+ \tag{1.21}$$

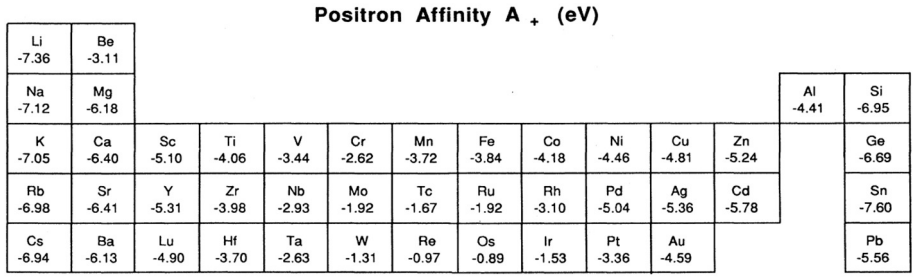

Figure 1.2: Calculated positron affinities A_+ (eV) for elemental metals and group-IV semiconductors (taken from "Theory of positrons in solids and on solid surfaces", Puska and Nieminen, [31])

As we have already seen, inside bulk metals or semiconductors, Ps can exists only as a quasi-particle (usually known as q-Ps) and is not stable. Near the surface, q-Ps can escape as free Ps into the vacuum, and the extraction of the thermalized positron and the Fermi-level electron costs the sum of the two work functions. When forming Ps outside the surface, the binding energy of $E_{\rm Ps} = -6.8eV$ is gained. The energy balance gives for the Ps formation potential $\epsilon_{\rm Ps}$:

$$\epsilon_{\rm Ps} = E_{\rm Ps} + \phi_+ + \phi_- \tag{1.22}$$

where ϕ_+ and ϕ_- are the positron and electron working function. The more negative $\epsilon_{\rm Ps}$ is, the more convenient is for the positron to form Ps. The negative of the sum of these two working functions is called positron affinity A_+. The sign convention is such that the more negative the positron affinity is, the deeper will be the positron energy level in the solid and the harder will be to extract it. We can rewrite Eq.1.22 as:

$$\epsilon_{\rm Ps} = E_{\rm Ps} - A_+ \tag{1.23}$$

Positron affinities and Ps formation potentials have been investigated and calculated by many authors [31, 29]. In Fig. 1.2 shows an example of calculated positron affinities for several elemental metals and semiconductors.

In metals, positron affinity is commonly a negative quantity. Its magnitude rises from the center of the transition-metal series towards left and right[31]. When the distances between the positive ions in the lattice are relatively large, the Coulomb repulsion felt by the positron will be small in the interstitial region. This is the qualitative explanation of the strong positron affinities found for example in alkali metals. However strong affinity values are found also in materials where bond distances are short (group-IV semiconductors like Si and Ge). This is due to the lattice having a structure (for example diamond structure) with large open interstitial regions where positrons can reside. In all these materials a free-positron or Ps-atom escape is therefore predicted to be not possible. On the other hand, there are materials where the magnitude of the positron affinity is small (transition-meta1 series). Usually these are used as efficient positron moderators since they have a large negative positron work function. Fig. 1.3 shows some positron bulk lifetimes τ calculated by Puska[31] for elemental metals and group-IV semiconductors. It is clear that where Ps formation is favorable, positron lifetimes are shorter due to the extremely short para-positronium lifetime component.

Positron Bulk Lifetime (ps)

Li 305	Be 137											Al 166	Si 221
Na 337	Mg 237												
K 387	Ca 297	Sc 199	Ti 146	V 116	Cr 101	Mn 103	Fe 101	Co 97	Ni 96	Cu 106	Zn 134		Ge 228
Rb 396	Sr 319	Y 219	Zr 159	Nb 122	Mo 111	Tc 95	Ru 90	Rh 93	Pd 103	Ag 120	Cd 153		Sn 275
Cs 407	Ba 315	Lu 199	Hf 149	Ta 117	W 100	Re 91	Os 86	Ir 87	Pt 94	Au 107			Pb 187

Figure 1.3: Calculated positron bulk lifetimes τ (ps) for elemental metals and group-IV semiconductors (taken from "Theory of positrons in solids and on solid surfaces", Puska and Nieminen, [31])

1.3.3 Ps formation

Positronium formation involves the capture by an incident positron of one electron of the surrounding, to form a bound state. The most simple framework where Ps formation is possible is that of positron-atom scattering, where the mechanism can be described by means of a rearrangement collision channel. In such a charge-transfer process, Ps may be formed in any excited state (with principal quantum number $n > 1$) provided that the kinetic energy of the incident positron, E , exceeds the difference between the ionization energy of the target,E_i , and the binding energy of the positronium in that state:

$$E \geq E_i - 6.8/n^2 \text{eV} \tag{1.24}$$

This inequality shows a threshold behavior. It is clear that positronium formation in the ground state is possible even at zero incident positron energy if the ionization energy of the target is less than 6.8eV (for example in alkali metal atoms). However in the most common situations, the threshold energy is a positive value (for example, it is at 6.8eV for atomic hydrogen and 17.8eV for helium)[5].

Positronium formation in solids strongly depends on material characteristic. As we saw, it is not possible in metals because of the large amount of free electrons interacting with the positron, which lead to a rapid annihilation. In insulators, Ps formation can be see as a two-step process where a Ps or a quasi-particle state is formed first in bulk and then it is emitted from the surface in vacuum as a Ps atom.

Historically, two main mechanism of Ps formation in bulk have been proposed: the *Ore model* and the *spur model*. Both can be energetically described by the positron work function ϕ_+ and the electron work function ϕ_- which have already been discussed in the previous section. We shall just recall here that, in metals, there is no band gap and energy states are filled up by electrons to the Fermi level so that it is straightforward to define the minimum energy required to extract them from the bulk. On the contrary in insulators the work function is associated with surface states (see the discussion in the previous section) which are usually higher in energy with respect to the valence states inside the bulk. Furthermore, the electron work function will be of the same order of magnitude of the band gap inside the material, usually well larger than 6.8eV so that Ps formation from a valence electron is an extremely hard process: the binding energy of Ps alone is not sufficient to compensate for the extraction of the positron and of the electron from the surface.

This difficulty is overcome by noting that the thermalization of positrons in an insulator is less efficient than in a metal.

The *Ore model* was first created to explain Ps formation mechanisms in gases. In this scenario, a Ps bound state is formed during the slowing down of a "hot" positron when its residual kinetic energy T_{e^+} is still high enough to pull out an electron from a molecule, leaving behind a positively charged radical. If I_G denotes the first ionization potential of a molecule, T_{e^+} must then be greater than $I_G - E_{\text{Ps}}$. At the same time an upper bound $T_{\text{Ore}}^{\text{Ps}} \leq I_G$ on the Ps kinetic energy must be present since otherwise electronic excitations and ionizations processes dominate and the species becomes unstable. These two thresholds define the so called "Ore gap". [32] In liquids and solids this model must be modified by taking into account the normally unknown affinities of the medium for electrons, positrons, and Ps atoms.[33] In a simplified picture, the Ore gap may be simply retrieved by substituting the binding energy of Ps in vacuum with that of a quasifree-Ps (qPs) in matter $E_{\text{qPs}} \leq 6.8\text{eV}$ and noting that the energy required to extract a valence electron is roughly equal to the band gap E_{gap}. The qPs atom in solid is a mobile system, as long as it is not trapped by a defect or self trapped in a phonon-cloud; it will eventually reach and escape from the surface with a residual kinetic energy of the order of few eV depending on the depth of formation and on the surface properties. We can write the maximum emission kinetic energy of qPs using the electron and positron work functions is given by:

$$T_{\text{Ore}}^{\text{qPs}} = -\phi_+ - \phi_- + T_{e^+} + E_{\text{qPs}} \tag{1.25}$$

Despite its general success, the Ore gap was shown to vanish for example in molecular liquids, which explains the inefficiency of the Ore mechanism there[6] and requires the introduction of other formation mechanisms.

On the other hand, if a positron fails to form Ps when still hot, it will find itself in a "spur", i.e in a group of reactive intermediates like free electrons, positive ions and various excited species and radicals created during its slowing down. In this case, if the average e^+-e^- distance in the spur is such that the Coulomb interaction energy is greater than the thermal one, a Ps atom can be generated[34]. This mechanism of Ps formation from thermal e^+ was proposed by Mogensen[33] and is called *spur model*. In the *spur model*, the energy needed to extract one excited electron to the vacuum level will be just $\phi_- - E_{\text{gap}}$ (which is usually just a few eV), and the maximum emission kinetic energy of Ps can be derived from Eq. 1.22:

$$T_{\text{spur}}^{\text{Ps}} = -\phi_+ - \phi_- + E_{\text{gap}} + 6.8\text{eV} \tag{1.26}$$

This process was studied for example in crystalline ice [35] and it was found to become more and more relevant at higher positron implantation energy T_{e^+}, where the Ps yield increases. The Ps yield probability can be expressed as: [36]

$$p(T_{e^+}) = p_{\text{max}} + (p_0 - p_{\text{max}}) e^{-\frac{1}{2}(\frac{T_{e^+}}{E_1})^\beta} \tag{1.27}$$

where p_0 , E_1 and β are suitable empirical parameters, while p_{max} is the maximum Ps yield in the bulk. After formation in bulk, Ps quickly thermalizes and diffuses inside the material until it eventually reaches the surface and if it finds favorable conditions it is emitted into vacuum.

Although the two models were long considered as alternatives, they should be viewed as complementary, and various experiments have detected a fraction of Ps formed by each process.

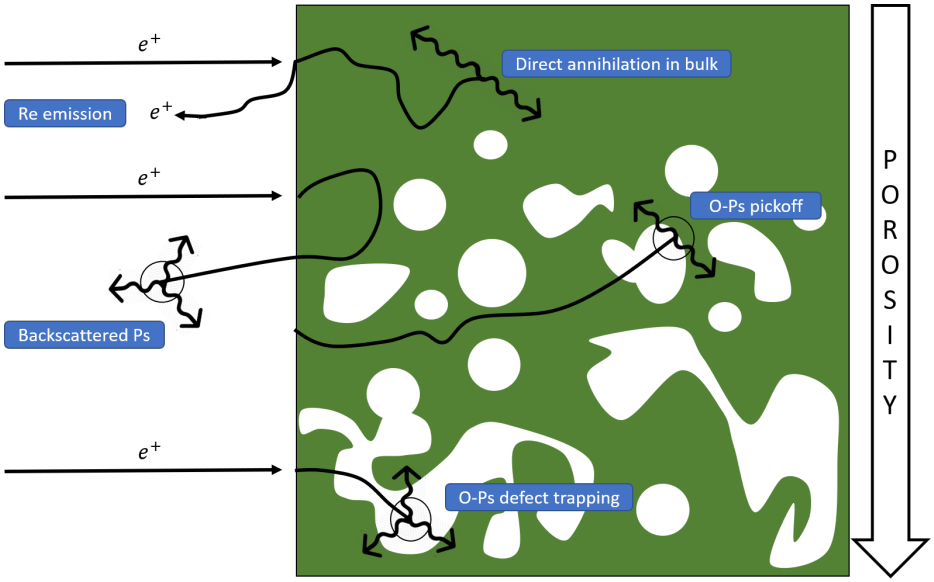

Figure 1.4: Schematic of the possible annihilation channels in porous materials.

Re-emission from the surface of a target under a positron beam is the most common mechanism of Ps production. However it exists also the possibility of Ps forming a trapped state inside the material itself. In liquids, for example, Ps is supposed to dig its own trap ("self-trapping"). In solids on the contrary, traps are geometrically defined by the rigid arrangement of atoms and molecules. In particular, Ps formation is well known in porous materials i.e. materials that present free spaces, dislocations or some sort of cavities in general. This particular situation is actually the object of the present work and we will discuss it in the next section.

1.3.4 Ps in porous materials

In insulating materials, Ps will preferentially locate in low-electron density regions, such as defects, pores, cracks, and voids in general. We saw that in metals it is the bare coulomb repulsion to force positrons into low-electron density vacancies. On the other hand in porous material, it's the reduced dielectric interaction present inside a void that energetically favors Ps trapping[37].

If a Ps or q-Ps is formed in the solid phase of a porous material, it will diffuse to the nearest pore's surface and it will eventually escape form bulk to enter inside of it, because in practice the pore works as a potential well for Ps. It will further localized there after loosing a small amount of energy by the numerous collisions with the pore wall. The confining behavior of Ps is commonly related to the Pauli exclusion principle which prevents Ps electron from entering an already occupied atomic orbital of the surrounding environment[38, 39, 40, 41]. This kind of Pauli repulsions become very strong at short distances so that the cavity becomes essentially a quantum well for the electron.

Ps spin state in the cavity region will be the projected onto the singlet or triplet configuration, leading to the usual *p*-Ps -*o*-Ps formation probability of $\frac{1}{4} - \frac{3}{4}$. This in turn leads to two distinct lifetime components in the annihilation spectra: a shorter one associated to *p*-Ps and a longer one associated to *o*-Ps . Those lifetimes are different from

their counterpart in vacuum, especially the triplet one. Indeed, the singlet interaction of Ps positron with surrounding molecular bound electrons of opposite spin shortens the lifetime of *o*-Ps by mixing in the fast 2γ decay mode during wall collisions.

The mechanism by which the Ps positron annihilates not with its bound electron but with a surrounding electron of opposite spin is called *pickoff* process. Pickoff is a fast 2γ annihilation channel which can shorten *o*-Ps lifetime from 142ns to as low as 1ns, and which reduces the $3\gamma/2\gamma$ branching ratio. Furthermore it is also the reason why *o*-Ps plays the key role in probing porous materials, as its description can be connected to the properties of the surrounding.

This can be easily seen in a classical picture where a single-particle Ps bounces around the cavity as a gas atom: the smaller the cavity, the higher the bouncing rate and the higher the pickoff annihilation, which can be seen as a surface effect.

The most general relations for Ps triplet/singlet annihilation rate in matter must then include the *pickoff* annihilation rate λ_{po} and they can be written as[9]:

$$\lambda_t = k_r \lambda_{3\gamma} + \lambda_{\mathrm{po}} \tag{1.28a}$$

$$\lambda_s = k_r \lambda_{2\gamma} + \lambda_{\mathrm{po}} \tag{1.28b}$$

where k_r represents the internal *relative* contact density, i.e. the ratio between the contact density in matter and in vacuum (Eq. 1.15), which is generally different from unity. Many different theoretical models connecting k_r and λ_{po} to material characteristics have been proposed and we will review the most important in the next chapter.

1.4 Ps in magnetic field

Besides pickoff process with external electrons, there is another factor which can deeply modify Ps annihilation properties even in vacuum: the presence of an external magnetic field. Given that it is experimentally simple to add such field to any Ps formation experiment, its effects are widely studied and many different treatments regarding Ps annihilation in the presence of magnetic fields are present in literature. Historically, the first one is due to Halpern[42] and it focused on studying the time variation of the probability amplitudes of the various states starting from the time dependent Schrödinger equation. On the other hand, a slightly different approach was used for example by Bisi[43, 44] and others. This time eigenstates are first calculated by standard perturbation theory in a time independent framework and annihilation is then taken into account as the expectation value over these eigenstates. In the following we'll give a complete review of the problem, underlying the differences. To keep a general notation we will call λ_s (λ_t) the annihilation rate of *p*-Ps (*o*-Ps) without magnetic field. In vacuum of course $\lambda_s = \lambda_{2\gamma}$ and $\lambda_t = \lambda_{3\gamma}$, while in matter their value may include pickoff annihilation as well.

The magnetic perturbation terms induced by a static magnetic field $\boldsymbol{B}$ in Ps hamiltonian reads[45]:

$$\hat{V}_B = +\mu_0 g_e \boldsymbol{s}_e \cdot \boldsymbol{B} - \mu_0 g_p \boldsymbol{s}_p \cdot \boldsymbol{B} \tag{1.29}$$

where g_e (g_p) and $\boldsymbol{s}_e$ ($\boldsymbol{s}_p$) are the electron(positron) gyromagnetic ratio and vector spin operator respectively. In practice, both the gyromagnetic ratios can be taken equal to the free electron gyromagnetic ratio $g = 2$ in common situations[2]. Taking the field direction

[2] Corrections with respect to this value are due to QED effects and the fact that Ps is a bound system and are usually so small they are neglected. For example, for a S-state, it has been calculated [46]:

$$g_e(n) = g(1 - \frac{5\alpha^2}{24n^2} - \frac{T}{2mc^2}) \tag{1.30}$$

along the z axis, $\hat{V}_B$ can be written using the Pauli matrices σ_z as:

$$\hat{V}_B = \frac{\mu_0 g B_z}{2}(\sigma_z^e - \sigma_z^p) \tag{1.31}$$

For this interaction, it turns out that the diagonal matrix elements over the spin basis states $|\Psi_{jm}\rangle$ (being j the eigenvalue of the total spin S^2 and m of the z component S_z) are zero, showing the well known fact that Ps has no linear Zeeman effect. The only non vanishing matrix elements are the off diagonals:

$$\begin{aligned} \langle\Psi_{00}|\,\hat{V}_B\,|\Psi_{10}\rangle &= \mu_0 g B_z \\ \langle\Psi_{10}|\,\hat{V}_B\,|\Psi_{00}\rangle &= \mu_0 g B_z \end{aligned} \tag{1.32}$$

Triplet states with $m = 1, -1$ are not affected by the field (their lifetime is left unchanged) while the $m = 0$ singlet and triplet states become mixed. Following Halpern, we'll start from the time dependent Schrödinger equation for these states:

$$i\hbar\frac{d}{dt}|\Psi_{10}(t)\rangle = \left[\hat{H}_0 - i\frac{\hbar}{2}\hat{\lambda}\right]|\Psi_{10}(t)\rangle + M_z\,|\Psi_{00}(t)\rangle \tag{1.33a}$$

$$i\hbar\frac{d}{dt}|\Psi_{00}(t)\rangle = \left[\hat{H}_0 - i\frac{\hbar}{2}\hat{\lambda}\right]|\Psi_{00}(t)\rangle + M_z\,|\Psi_{10}(t)\rangle \tag{1.33b}$$

where $\hat{H}_0$ is the unperturbed Ps hamiltonian,$M_z = \mu_0 g B_z$ and the imaginary potential term $-i\frac{\hbar}{2}\hat{\lambda}$, where $\hat{\lambda}$ is the annihilation operator (see 1.2), explicitly takes into account the particle loss due to annihilation. By definition $\hat{H}_0\,|\Psi_{jm}\rangle = E_{jm}\,|\Psi_{jm}\rangle$ and separating the time dependence of the amplitudes and phases of these states as:

$$\Psi_{10}(t) = A_{10}(t)\exp\left[-\left(i\frac{E_{10}}{\hbar} + \frac{1}{2}\lambda_t\right)t\right] \tag{1.34a}$$

$$\Psi_{00}(t) = A_{00}(t)\exp\left[-\left(i\frac{E_{00}}{\hbar} + \frac{1}{2}\lambda_s\right)t\right] \tag{1.34b}$$

we obtain:

$$i\hbar\frac{d}{dt}A_{10}(t) = M_z A_{00}(t)\exp\left[+\left(i\omega_0 - \frac{1}{2}\lambda'\right)t\right] \tag{1.35a}$$

$$i\hbar\frac{d}{dt}A_{00}(t) = M_z A_{10}(t)\exp\left[-\left(i\omega_0 - \frac{1}{2}\lambda'\right)t\right] \tag{1.35b}$$

where $\omega_0 = \Delta_{\text{st}}/\hbar$, $\Delta_{\text{st}} = E_{10} - E_{00} > 0$ is the hyperfine splitting (see 1.2) and $\lambda' = \lambda_s - \lambda_t$. This system of linear differential equations of first order can be solved differentiating for example 1.35a with respect to time and using the result in 1.35b to obtain:

$$\ddot{A}_{10}(t) - (i\omega_0 - \lambda'/2)\,\dot{A}_{10}(t) + \frac{M_z^2}{\hbar^2}A_{10}(t) = 0 \tag{1.36}$$

which solutions are of the form

$$\begin{aligned} A_{10}(t) &= C_1 e^{+\alpha_+ t} + C_2 e^{+\alpha_- t} \\ A_{00}(t) &= D_1 e^{-\alpha_- t} + D_2 e^{-\alpha_+ t} \end{aligned} \tag{1.37}$$

where T is the kinetic energy of the atom.

where D_1 and D_2 are related to C_1 and C_2 through Eq. 1.35a and with

$$\alpha_{\pm} = \frac{\left(i\omega_0 - \frac{1}{2}\lambda'\right)}{2}\left[1 \pm \sqrt{1 - \left(\frac{2M_z}{\hbar\left(i\omega_0 - \frac{1}{2}\lambda'\right)}\right)^2}\right] \tag{1.38}$$

Following [42] we assume $\lambda' \ll \omega_0$ and $M_z \ll \omega_0$ we take only the first order expansions:

$$\begin{aligned} \alpha_+ &= \left(i\omega_0 - \frac{1}{2}\lambda'\right) - \alpha_- \\ \alpha_- &= -i\frac{M_z^2}{\hbar^2\omega_0} - \frac{1}{2}\lambda'\frac{M_z^2}{\hbar^2\omega_0^2} \end{aligned} \tag{1.39}$$

so that finally we have:

$$\begin{aligned} \Psi_{10}(t) =& C_1 e^{-i(\frac{E_{00}}{\hbar} - \frac{x^2}{4}\omega_0)t} e^{-\frac{1}{2}(\lambda_s - \lambda'\frac{x^2}{4})t} \qquad (1.40a) \\ &+ C_2 e^{-i(\frac{E_{10}}{\hbar} + \frac{x^2}{4}\omega_0)t} e^{-\frac{1}{2}(\lambda_t + \lambda'\frac{x^2}{4})t} \\ \Psi_{00}(t) =& D_1 e^{-i(\frac{E_{00}}{\hbar} - \frac{x^2}{4}\omega_0)t} e^{-\frac{1}{2}(\lambda_s - \lambda'\frac{x^2}{4})t} \qquad (1.40b) \\ &+ D_2 e^{-i(\frac{E_{10}}{\hbar} + \frac{x^2}{4}\omega_0)t} e^{-\frac{1}{2}(\lambda_t + \lambda'\frac{x^2}{4})t} \end{aligned}$$

with $x = \frac{2Mz}{\hbar\omega_0}$. Eq.1.40 shows that it is possible to form linear combinations of $\Psi_{10}(t)$ and $\Psi_{00}(t)$ which decay with a simple exponential law. These states have then energies given by:

$$E_{00} - \frac{x^2}{4}\Delta_{st} \tag{1.41a}$$

$$E_{10} + \frac{x^2}{4}\Delta_{st} \tag{1.41b}$$

and decay rates

$$\lambda_s - \lambda'\frac{x^2}{4} \tag{1.42a}$$

$$\lambda_t + \lambda'\frac{x^2}{4} \tag{1.42b}$$

respectively. The same result could have been obtained with perturbation theory by a direct diagonalization of the $t = 0$ hamiltonian. The perturbed real eigenvalues for the energy in the $m = 0$ subspace are found to be[43]:

$$\tilde{E}_{10} = \frac{1}{2}\left[(E_{00} + E_{10}) + \Delta_{\text{st}}\sqrt{1 + x^2}\right] \tag{1.43a}$$

$$\tilde{E}_{00} = \frac{1}{2}\left[(E_{00} + E_{10}) - \Delta_{\text{st}}\sqrt{1 + x^2}\right] \tag{1.43b}$$

with eigenfunctions given by:

$$\tilde{\Psi}_{1,0} = \frac{\Psi_{1,0} - y\Psi_{0,0}}{\sqrt{(1 + y^2)}} \tag{1.44a}$$

$$\tilde{\Psi}_{0,0} = \frac{\Psi_{0,0} + y\Psi_{1,0}}{\sqrt{(1 + y^2)}} \tag{1.44b}$$

where $y = (\sqrt{1+x^2} - 1)/x$ satisfies $\lim_{B\to 0} y = 0$ and symbols in 1.44 are arbitrarily chosen in a way so that perturbed states and energies tend adiabatically to the respective unperturbed values at zero field:

$$\tilde{\Psi}_{j,0} \overset{B\to 0}{=} \Psi_{j,0} \tag{1.45}$$

The physical interpretation is that the perturbed *o*-Ps states contains an amount of *p*-Ps equal to $\frac{y^2}{1+y^2}$ and *vice versa*. As a result, annihilation rates for these states will modify accordingly (keeping in mind the orthogonality of the unperturbed states):

$$\tilde{\lambda}_t = \frac{y^2\lambda_s + \lambda_t}{1+y^2} \tag{1.46a}$$

$$\tilde{\lambda}_s = \frac{y^2\lambda_t + \lambda_s}{1+y^2} \tag{1.46b}$$

It's easy to note that Halpern results Eq. 1.41 and Eq. 1.42 are just the first order expansions in x of Eq. 1.43 and Eq. 1.46 respectively.[44]

To summarize, the quasi-degeneracy of Ps ground state in vacuum is broken when an external magnetic field is present. *o*-Ps and *p*-Ps become mixed and this opens the possibility for a 2γ decays also for the triplet state, which is the so called *magnetic quenching* effect.

1.4.1 The magnetic quenching parameter

Experimentally, it's useful to introduce the *quenching parameter* R which is defined as the ratio of the number of the annihilation events (count) in a given time interval $[t_1; t_2]$, with and without field.

The time interval is usually taken long enough to account for statistical weight. Since the magnetic quenching does not change much the annihilation rate of *p*-Ps , the instant t_1 is chosen in such a way to include the annihilation events from *o*-Ps as the main contribution, at the same time discarding background events such as the direct positron annihilation. In other words, this means that one neglects all the annihilation counts coming from the smaller lifetime components of a spectra $\lambda_i^{-1} \ll t_1$.

Assuming that the magnetic field does not change the ratio of Ps formed in *p*-Ps or *o*-Ps states($\frac{1}{4}$ and $\frac{3}{4}$ respectively), we call $n_1(n_3)$ the number of positronium atoms at time t in the singlet(triplet) state.

For the purpose of completeness we use here the explicit expressions for Ps annihilation rates in matter given in Eq.1.28, which were introduced in Section 1.3 and which will be extensively explained in subsequent chapters:

$$\lambda_t = k_r\lambda_{3\gamma} + \lambda_{\text{po}} \tag{1.47a}$$

$$\lambda_s = k_r\lambda_{2\gamma} + \lambda_{\text{po}} \tag{1.47b}$$

Following Bisi[43], the contribution to the two-quantum annihilation during the time dt given by *o*-Ps is found to be:

$$\frac{2}{3}\lambda_t e^{-\lambda_t t}\left(\frac{\lambda_{\text{po}}}{\lambda_t}\right) dt \tag{1.48}$$

for the two $m = \pm 1$ states and:

$$\frac{1}{3}\tilde{\lambda}_t e^{-\tilde{\lambda}_t t}\left(\frac{\tilde{\lambda}_{\text{po}}}{\tilde{\lambda}_t}\right) dt \tag{1.49}$$

for the $m = 0$ state, where in analogy with eq.1.46 we have defined

$$\tilde{\lambda}_{\text{po}} = \frac{y^2\lambda_s + \lambda_{\text{po}}}{1 + y^2} \tag{1.50}$$

At the same time the contribution to the three-quantum annihilation will be:

$$\frac{2}{3}\lambda_t e^{-\lambda_t t}(\frac{k_r\lambda_{3\gamma}}{\lambda_t})\, dt \tag{1.51}$$

and

$$\frac{1}{3}\tilde{\lambda}_t e^{-\tilde{\lambda}_t t}(\frac{k_r\lambda'_{3\gamma}}{\tilde{\lambda}_t})\, dt \tag{1.52}$$

respectively, with

$$\lambda'_{3\gamma} = \frac{\lambda_{3\gamma}}{1 + y^2} \tag{1.53}$$

If we admit the possibility of detecting only a fraction f of three-quantum decays, the total number of annihilation events will be proportional to:

$$\begin{aligned}
&\propto \int_{t_1}^{t_2} \left[\frac{2}{3}\lambda_t e^{-\lambda t}(\frac{fk_r\lambda_{3\gamma} + \lambda_{\text{po}}}{\lambda_t}) + \frac{1}{3}\tilde{\lambda}_t e^{-\tilde{\lambda}_t}(\frac{fk_r\lambda'_{3\gamma} + \lambda'_{\text{po}}}{\tilde{\lambda}_t})\right] dt \\
&= \frac{2}{3}(e^{-\lambda_t t_1} - e^{-\lambda_t t_2})(\frac{fk_r\lambda_{3\gamma} + \lambda_{\text{po}}}{k_r\lambda_{3\gamma} + \lambda_{\text{po}}}) + \\
&+ \frac{1}{3}(e^{-\tilde{\lambda}_t t_1} - e^{-\tilde{\lambda}_t t_2})(\frac{fk_r\lambda_{3\gamma} + y^2\lambda_s + \lambda_{\text{po}}}{k_r\lambda_{3\gamma} + y^2\lambda_s + \lambda_{\text{po}}})
\end{aligned} \tag{1.54}$$

It's easy now to evaluate the quenching R :

$$R = \frac{2}{3} + \frac{1}{3}\alpha\frac{e^{-\tilde{\lambda}_t t_1} - e^{-\tilde{\lambda}_t t_2}}{e^{-\lambda_t t_1} - e^{-\lambda_t t_2}} \tag{1.55}$$

with

$$\alpha = \frac{(fk_r\lambda_{3\gamma} + y^2\lambda_s + \lambda_{\text{po}})(k_r\lambda_{3\gamma} + \lambda_{\text{po}})}{(fk_r\lambda_{3\gamma} + \lambda_{\text{po}})(k_r\lambda_{3\gamma} + y^2\lambda_s + \lambda_{\text{po}})} \tag{1.56}$$

If all annihilation events in the time window are detected, then $f = 1$ and $\alpha = 1$. In practical situations the factor α differs from unity less than a few percent and it is little sensitive to the material[43]. Eq. 1.55 was extensively used to experimentally find the value of the relative contact density k_r. This is done by a least squared fitting procedure of the curve $R(B)$ to data obtained on samples with different applied magnetic field B[2, 47, 48, 49, 50, 51, 52].

1.5 The Ps negative ion

Here we briefly discuss the properties of the positronium negative ion Ps^-, because this element is often considered as a limiting case in many studies on Ps annihilation in materials. Ps^- is a well known three-body system[53, 54, 55, 56] which exists as a bound state only when the two electrons have opposite spin configuration. In this case, its ground state energy of $E \approx -7.13$eV is just slightly lower than that of the system of

Ps + free electron (~ -6.8eV). Its ground state wavefunction is usually separated in a spin and a spatial part by fixing an (arbitrary) positron spin direction:

$$\Psi_{\mathrm{Ps}^-}(p,1,2) = \phi_{\mathrm{Ps}^-}(\boldsymbol{r}_p;\boldsymbol{r}_1,\boldsymbol{r}_2)\chi_{00}(\sigma_1,\sigma_2)s_\uparrow(\sigma_p) \tag{1.57}$$

where χ_{00} is the electron-electron singlet spin distribution, $s_\uparrow$ represent the positron spin function and the spatial wavefunction ϕ_{Ps^-} satisfies the symmetric condition $\phi_{\mathrm{Ps}^-}(\boldsymbol{r}_p;\boldsymbol{r}_1,\boldsymbol{r}_2) = \phi_{\mathrm{Ps}^-}(\boldsymbol{r}_p;\boldsymbol{r}_2,\boldsymbol{r}_1)$.

Using the identity:

$$\chi_{00}(\sigma_1,\sigma_2)s_\uparrow(\sigma_p) = \frac{1}{\sqrt{2}}\chi_{11}(\sigma_p,\sigma_1)s_\downarrow(\sigma_2) - \frac{1}{2}(\chi_{00}(\sigma_p,\sigma_1) + \chi_{1,0}(\sigma_p,\sigma_1))s_\uparrow(\sigma_2) \tag{1.58}$$

and the analogue valid for $\chi_{00}(\sigma_1,\sigma_2)s_\downarrow(\sigma_p)$, the annihilation rate of Ps^- for a reference positron spin can be formally calculated as expectation value of the annihilation operator exposed in Eq. 1.18 and Eq. 1.19:

$$\lambda_{\mathrm{Ps}^-} = 2\bar{\lambda}8\pi a_0^3 \int |\phi_{\mathrm{Ps}^-}(\boldsymbol{r}_p;\boldsymbol{r}_p,\boldsymbol{r}_2)|^2\, d^3r_p\, d^3r_2 \tag{1.59}$$

and it was numerically found to be $\lambda_{\mathrm{Ps}^-} \approx 2.09[\mathrm{ns}]^{-1}$, a value very similar to the spin averaged annihilation rate of Ps in vacuum $\bar{\lambda} \approx 2.01[\mathrm{ns}]^{-1}$, which means that the total contact density is almost the same of the contact density of free Ps:

$$\begin{aligned}\int |\phi_{\mathrm{Ps}^-}(\boldsymbol{r}_p,\boldsymbol{r}_p,\boldsymbol{r}_2)|^2\, d^3r_p\, d^3r_2 + \int |\phi_{\mathrm{Ps}^-}(\boldsymbol{r}_p,\boldsymbol{r}_1,\boldsymbol{r}_p)|^2\, d^3r_p\, d^3r_1 \\ \approx \int |\Psi_{\mathrm{Ps}}(\boldsymbol{r}_p,\boldsymbol{r}_p)|^2\, d^3r_p \\ = k_0 = \frac{1}{8\pi a_0^3}\end{aligned} \tag{1.60}$$

Specifically, the numerical exact result is

$$\begin{aligned}\int |\phi_{\mathrm{Ps}^-}(\boldsymbol{r}_p,\boldsymbol{r}_p,\boldsymbol{r}_2)|^2\, d^3r_p\, d^3r_2 &= \int |\phi_{\mathrm{Ps}^-}(\boldsymbol{r}_p,\boldsymbol{r}_1,\boldsymbol{r}_p)|^2\, d^3r_p\, d^3r_1 \\ &= 0.02073 \text{ a.u.} \\ &\approx 0.52\ k_0\end{aligned} \tag{1.61}$$

This result is commonly explained as a classical picture of Ps^- where only one electron is closely bound to the positron while the other is loosely bound to the inner neutral Ps[57]. In this picture, the one half factor in the contact density comes from the normalization , i.e, from the symmetrization of the total wavefunction.

In other words, a bound Ps state in vacuum will repel electrons with the same spin and it will have only a small attraction to electrons of opposite spin, with an energy gain of $\Delta E \approx 0.3$eV.

1.6 Experimental techniques

One of the great virtues of using positrons and positronium as a probe is that they can penetrate deep into the inner of the sample. High energy positrons thermalize so fast

that one need only to consider low-energy nonrelativistic interactions with the surrounding matter [30]. As we saw, the annihilation rate and the momentum distribution of the emitted photons depend in many cases only on the product of the positron wave function times the wave function of the electron being annihilated. Thus it is clear that experimental measurements of the lifetime and momentum distribution give direct information about the interior of the sample.

A further advantage is that the information contained in the annihilation process is transported to the observer as high-energy gamma rays which escape without appreciable attenuation or scattering from reasonably small samples. This is in contrast with method where the surface properties of a solid under investigation may strongly influence the results as for example in x-ray emission.

Generally, positron annihilation techniques are mostly used to examine porosity. The two most driving industrial application are the the characterization of defect in nuclear reactor materials and of pores in dielectric materials, which are largely used in semiconductor industry[6].

Positron annihilation spectroscopy (PAS), sometimes specifically referred to as Positron annihilation lifetime spectroscopy (PALS), is a non–destructive spectroscopy technique to study voids and defects in solids. The technique operates on the principle that, when a positron or positronium annihilate through interaction with electrons of the material, they release gamma photons that can be detected.

Usually, positrons are produced from a radioactive source like the ^{22}Na isotope, with a process similar to β decay. The nuclear de–excitation also produces a gamma photon with energy 1.28MeV, which detection is used as a "starting signal" in most experiments (excluding trapping techniques). The time interval between the entering instant of the positron into the material, practically coincident to the starting signal, and the detection of gamma photons due to annihilation corresponds to the lifetime of a positron, or that of a positronium atom in the case of a formation of such a bound system.

When the positron enters the material uder examination, a great number of annihilation channels are possible, each with a characteristic lifetime $\tau_i = 1/\lambda_i$. The most important annihilation processes take place after an initial thermalization stage in which the positron loses its kinetic energy by scattering with electrons in the medium. After the thermalization process, the positron essentially remains in a free or delocalized state and starts to diffuse around. In this phase it can be emitted directly in vacuum (as e^+ or as Ps) or it can be trapped in a new surface state inside the material, from which it annihilates.

The total positron lifetime spectrum, *i.e.* the probability of an annihilation at time t, is the sum of these exponential decay components:

$$-\frac{dn(t)}{dt} = \sum_i I_i \lambda_i \exp^{-\lambda_i t} \tag{1.62}$$

with relative intensities I_i. Here $n(t)$ is the probability that a positron is still alive at time t after its emission. The lifetime spectrometer consists of a start and a stop detector, each of them made by coupling a fast scintillator to a photomultiplier. The timing pulses are obtained by differential constant–fraction discrimination. The time delays between the start and stop signals are converted into amplitude pulses the heights of which are stored into a multichannel analyser, so that the original lifetime components τ_i and their intensities I_i can be calculated.

In practice, the number of components used in the fitting analysis of a typical PALS spectrum is limited, given the difficulty in resolving components too close to each other.

In materials where Ps is formed (e.g. polymers, porous materials) this number is usually set to three: τ_1, τ_2 and τ_3. In the common interpretation, the shorter component $\tau_1 \sim 0.125$ns is associated to *p*-Ps annihilation, the intermediate lifetime $\tau_2 \sim 0.3 - 0.5$ns is due to direct positron annihilation while the longest $\tau_3 \sim 1 - 10$ns is associated to *o*-Ps annihilating via pickoff process. In some cases one may resolve up to three components associated to *o*-Ps , with a total of five lifetime values[58].

Despite the relationship between τ_1, τ_3 and Ps formation is widely accepted, its implications on the relative intensities I_1, I_3 of the two annihilation channels are rarely taken into account. Indeed, any model associating different annihilation rates to different Ps spin states, predicts by construction a $1/3$ probability ratio for *p*-Ps /*o*-Ps formation by an unpolarized positron. In turn, the ratio between the respective measured lifetime intensities must assume the same value, so that the condition

$$I_1 = \frac{1}{3} I_3 \tag{1.63}$$

must be imposed during the spectrum analysis. However, it is common practice to ignore condition 1.63 and let all the intensities vary during the fitting procedure. This way, given the greater number of free parameters, the fit convergence will improve. The reason for this choice may be a general lack of interest towards the shortest components of the spectrum, given that it is the longest one, τ_3, which is used to recover information on material properties. We want to stress that without condition 1.63 neither τ_1 nor τ_3 could in principle be associated to Ps states without introducing arbitrary assumptions on Ps formation mechanism.

Moreover, as we saw in section 1.4, useful information can be also found coupling PALS experiments with an external magnetic field.

This technique was often employed in the past to evaluate the contact density. However this is not the most practical method, and in fact it is possible to derive the contact density value, in the absence of magnetic field, from an accurate best-fitting analysis of lifetime spectrum experimental data if 1.63 is imposed. [2, 10] Using Eqs. 1.28, the contact density value can then be derived from[3]:

$$k_r = \frac{\lambda_1 - \lambda_3}{\lambda_{2\gamma} - \lambda_{3\gamma}} \tag{1.64}$$

Examples of contact densities calculated with this technique are given in Chapter 4 for a lot of different materials.

Finally, the less common technique of detection of the three quantum yield allows one to get an independent value of the relative contact density when the Ps features in the investigated medium are known.

[3]This method requires τ_1 to be measured with extreme accuracy, a drawback that can be overcome by modern experimental setup.

CHAPTER 2

Theoretical models

At present, the most used models describing Ps inside small cavities are based on the Tao-Eldrup (TE) approach [59, 60], which relates pick-off annihilation rates λ_{po} to pore sizes by considering Ps as a single quantum particle trapped inside an *infinite* potential well. At the state of the art, these models can describe various cavity geometry (e.g. the rectangular Tao-Eldrup model(RTE) [61]) and can easily include temperature as well as the effect of a *finite* potential well[62]. However, it has been pointed out that the single particle assumption, by definition, can give no information about the internal structure of the confined Ps, hence on the contact density parameter[38].

Fully *ab initio* treatments of a two-particle bound system inside a host material require huge computational efforts, mainly due to the fact that the adiabatic approximation, usually valid for heavy atom nuclei, cannot be applied to Ps. Recently, Zubiaga et al. [63] had derived a full-correlation positron potential for Ps interacting with a single He atom, which then they used to build a single particle Schrödinger equation for Ps inside a spherical pore structure in solid He. Although this approach is able to provide accurate distributions and pick-off annihilation rates for a small defect in a crystal structure, it requires extensive calculations for more complex systems.

Less expensive approaches still consider both Ps constituent particles as independent but use effective potentials to describe their interactions with the material. Depending on the chosen potential, these can range from simple models which can be solved analytically [64, 65], to ones that require numerical approaches like the variational method or Quantum Montecarlo (QMC) methods.

In this chapter we will review the main models starting from the one body models. We will dedicate a section to introduce QMC techiniques since a part of our work, which we will describe in the third chapter, involves their use.

2.1 One particle models

Historically, the first kind of models created to describe Ps behavior in porous materials are one-body models, in the sense that Ps is described as a single quantum particle. Interaction potentials between Ps atom and surrounding molecules are then commonly approximated by simple trapping quantum wells either *infinite* and *finite*.

Originally, Ps trapping concept was introduced by Ferrel to explain the unexpectedly long lifetime of the *o*-Ps atom found in liquid helium[30]. He suggested that due to the strong exchange repulsion between the *o*-Ps electron and electrons of the surrounding He atoms, Ps forms a nanobubble around itself. He also gave an estimate of the equilibrium radius R of the nanobubble by minimizing the sum of Ps energy in a spherically symmetric potential well ($E_{\mathrm{Ps}} = \pi^2\hbar^2/4mR^2$, where energy is measured in Rydberg) and

the surface energy $4\pi R^2\sigma$, where σ is the surface tension coefficient:

$$R = a_0 \left(\frac{\pi}{8\sigma a_0^2} \right)^{1/4} \tag{2.1}$$

To get an idea about the range of validity of this approximation, the Ps atom can be though of as a rigid sphere with a Bohr radius of $2a_0 \sim 0.1$nm, i.e. double the size of an Hydrogen atom. This is of the same order of usual molecular bonds, where the mean length is about $\delta = 0.15 - 0.2$nm. In mesoporous materials, cavities are in the range $2 - 50$nm and it is easy to see why a semi-classical single-particle picture of Ps in a quantum well is suited for the job. Surprisingly, this kind of approach works quite well also in nanoporous materials, where cavities are as small as a few tenth of nanometers. At this size, the internal structure of Ps begins to be relevant. Furthermore, the definition of a "cavity radius" is somehow tricky since the sharp potential barrier would have a gradient comparable in size to the pore dimension. The main goal of these early models was to explain the modification to Ps lifetime observed in PALS experiments. In particular the *pickoff* process where the positron in *o*-Ps annihilates with an electron of opposite spin from the surroundings.

2.1.1 The Tao-Eldrup model

The most popular model connecting the size of free spaces inside matter where *o*-Ps is located and its lifetime was proposed by Tao in 1972 [59] and later modified by Eldrup[60].

The localization of Ps, described as a single quantum particle, inside a spherical volume of size R_c was simplified by Tao into a strict confinement inside an infinite potential barrier of size $R_c + \Delta$, which basic idea is shown in Fig. 2.1 and explained below.

As a matter of fact, given the infinite strength of the confining potential, Ps wavefunction vanishes at a chosen boundary and outside. If this boundary coincide with the cavity, Ps has no overlap with surrounding electrons. This means in particular that pick-off annihilation could not take place. To take that into account, Tao assumed a boundary located at a shell of thickness Δ surrounding the cavity, and considered a constant pick-off rate, that is:

$$\lambda_{\text{po}} = P_{\text{out}} \lambda_{\text{bulk}} \tag{2.2}$$

where P_{out} is the probability of finding Ps in the region $[R_c; R_c + \Delta]$ and λ_{bulk} is the decay rate in bulk, which is assumed to be independent from the electron density of the material and equal to the average of the decay constant of *o*-Ps and *p*-Ps in vacuum (Eq 1.6) $\lambda_{\text{bulk}} \equiv \bar{\lambda} = 2.01[\text{ns}]^{-1}$.

The solution of such a model is a basic exercise of quantum mechanics, and the ground state Ps wavefunction results:

$$\Psi_{\text{TE}}(R) = \frac{1}{\sqrt{2\pi(R_c + \Delta)}} \frac{\sin\left(\pi R/(R_c + \Delta)\right)}{R} \tag{2.3}$$

so that finally

$$\begin{aligned} P_{\text{out}} &= 4\pi \int_{R_c}^{R_c+\Delta} |\Psi_{\text{TE}}(R)|^2 R^2 \, dR \\ \lambda_{\text{po}} &= \bar{\lambda} \left(1 - \frac{R_c}{R_c + \Delta} + \frac{1}{2\pi} \sin \frac{2\pi R_c}{R_c + \Delta} \right) \end{aligned} \tag{2.4}$$

This formula connects two generally unknown geometrical parameters, R_c and Δ, to the measurable annihilation rate. To be experimentally useful, it is assumed that Δ is an

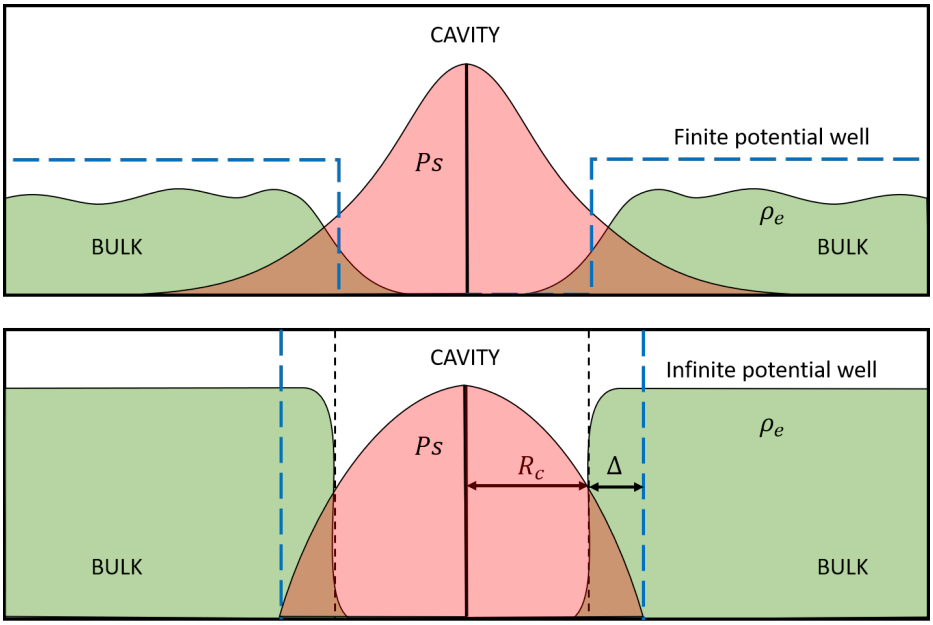

Figure 2.1: Schematic of the Tao Eldrup approximation. The description of a Ps atom in a finite potential well (top) is transformed into the simpler particle-in-a-box model (bottom). At the same time, the complex electron density profile is simplified into a step function, which vanishes in the inner part of the cavity and takes a constant value $\rho_e = k_0$ in a surface layer of thickness Δ. R_c is the cavity radius (free space region). The value of Δ is chosen in order to recover the correct pickoff annihilation rate.

universal constant which value is determined by fitting this model on materials where pore dimensions are known from different experiments.

The now commonly accepted value $\Delta = 0.166$nm was initially obtained from materials with void radii R_c in the range $R_c = 0.32 - 0.38$nm and with predicted lifetime between 2.45 and 3.2 ns. Generally, TE is considered valid only for nanometric sized cavities ($R_c < 2.5$nm)[66], where Ps excited states are not accessible by means of thermal energy.

As already said, equation 2.2 implicitly assumes no dependency of pickoff annihilation on the electron density of the material. One may naively assume that it can be derived from the more general expression (see Sec. 2.3),

$$\begin{aligned}\lambda_{\text{po}} &= \pi r_0^2 c\, 4\pi \int n_e(R)|\Psi_{\text{TE}}(R)|^2 R^2\, dR \\ &= \pi r_0^2 c \rho_e P_{\text{out}} \\ &\approx \bar{\lambda}\frac{\rho_e}{k_0} P_{\text{out}}\end{aligned} \tag{2.5}$$

by arbitrary fixing the electron density distribution of the material $n_e(R)$ to a constant value ρ_e corresponding to the contact density in vacuum k_0. This assumption has the advantage of reducing the number of parameters and furthermore it transfers all the complication in determining the value of Δ.

Such a constant electron density is in fact extremely high, being closer to values usually found in bulk rather than at the cavity surface. This is in contrast to the commonly accepted picture where the positron interacts only with a low-density surface layer of electrons belonging to outer atomic orbitals. However, the successful agreement between predicted radii and experimental data suggests that $\rho_e \sim k_0$ in fact in many materials. This is not surprising when one understands that the electron density $n_e(R)$ in Eq.2.5 is implicitly evaluated at the positron position $\boldsymbol{r}_p$. The condition $n_e(\boldsymbol{r}_p) \to k_0$ then resembles the low-density limit of Barbiellini enhancement factor used in many-body approaches, which we will discuss in Section 2.3.1 (Eq. 2.44).

TE completely removes the dependency on the material chemical properties from the annihilation rate, thus making this last one a matter of pure geometry. The interest of the chemist community together with the increase of experimental precision of PALS has recently raised the question of obtaining information not only on the geometry of the pores (R_c) but also on chemical properties of the surrounding medium. To this scope, many extension to TE have been proposed in the last decades. Some of them have the same number of free parameters as the TE, while others include additional parameter which have to be determined somehow.

2.1.2 Finite potential TE

Dutta et al.[62] considered the effect of a finite potential well, of height U_0 in the TE framework. This approach has several advantages. First, it removes the unphysical infinite potential barrier, which means in particular that a Ps bound state will disappear if cavity radius becomes too small. More importantly, it removes the need for a geometrical shell layer Δ, since this time Ps wavefunction can spread outside the cavity wall to the bulk where pickoff annihilation takes place. The general ground state solution of a

single particle in a spherical finite potential well is easily found to be:

$$\Psi_{\text{Dutta}} = \frac{1}{\sqrt{4\pi}}\sqrt{\frac{2\kappa_0}{1+R_c\kappa_0}}\begin{cases}\dfrac{\sin\eta_0 R}{R} & \text{if} R < R_c \\ \sin\eta_0 R_c \dfrac{e^{-\kappa_0(R-R_c)}}{R} & \text{if} R > R_c\end{cases} \tag{2.6}$$

where $\eta_0 = \sqrt{4mE_0/\hbar^2}$ and $\kappa_0 = \sqrt{4m(U_0 - E_0)/\hbar^2}$ and the energy E_0 is given by the eigenvalue condition $\eta_0 \cot(\eta_0 R_c) = -\kappa_0$. Pickoff annihilation will be proportional to the probability of finding the Ps in the surrounding matter, which now has the form

$$P_{\text{out}}^{\text{Dutta}} = 4\pi \int_{R_c}^{\infty} |\Psi_{\text{Dutta}}(R)|^2 R^2 \, dR \tag{2.7}$$

and following [62] it reads:

$$\lambda_{\text{po}} = \pi r_0^2 c \rho_e \frac{Z_{\text{eff}}}{Z} P_{\text{out}}^{\text{Dutta}} = \frac{1}{4}\lambda_{2\gamma}\frac{\rho_e}{k_0}\frac{Z_{\text{eff}}}{Z}P_{\text{out}}^{\text{Dutta}} \tag{2.8}$$

where $\frac{Z_{\text{eff}}}{Z}$ is the fraction of electrons effectively available per molecule for annihilation (usually only valence electrons since Ps does not penetrate in the core regions)[1]. In his work, Dutta considered also the possibility of replacing the sharp discontinuity introduced by the step potential with a smooth profile function for both the potential and the external electron density. Of course this requires the introduction of new parameters in the model. In the approximation that both functions vary with the same spatial profile, Dutta arbitrarily used:

$$\begin{aligned}\rho(R) &= \rho_0\left[1 - \frac{1+e^{-R_c/\Delta}}{1+e^{(R-R_c)/\Delta}}\right] \\ U(R) &= U_0\left[1 - \frac{1+e^{-R_c/\Delta}}{1+e^{(R-R_c)/\Delta}}\right]\end{aligned} \tag{2.9}$$

where Δ now represents the variation length. Since Δ/R_c is considered to be very small, it can be treated as a perturbation. This introduced an energy correction of $\delta E \sim E_0 \frac{2\pi^2\Delta^2\kappa_0^2}{3(1+\kappa_0 R_c)}$ and a new eigenvalue condition. The problem of finding the value of Δ was solved for liquids introducing an additional minimization condition for the energy, so that in this case the model has the same number of free parameters as the TE. In [62], via a fitting procedure over several experimental data with a lifetime in the range $3 - 10$ns, the authors found the empirical relationship between the pickoff lifetime and the potential height U_0 and the cavity radius:

$$\begin{aligned}\lambda_{\text{po}}^{-1}(R_c) &= 1.88 R_c[\text{ns}\mathring{A}^{-1}] - 5.07[\text{ns}] \\ U_0(R_c) &= A + B\exp[-(R_c - R_c')/D]\end{aligned} \tag{2.10}$$

with $A = 0.40$eV, $B = 1.25$eV,$R_c' = 3.44\mathring{A}$ and $D = 2.09\mathring{A}$. Even if this was found for liquids, the authors showed that the same relationship can extended without modification to molecular solids. We note that all predicted cavity sizes were lower than 1nm, making the model accurate for nanoporous material, exactly like the TE.

However many developments have been done to extend this model up to mesoporous materials ($R_c \approx 100$nm) by including both thermal excitation and different cavity geometry.

[1]Note that, given the implicit arbitrariness in the local electron density factor ρ_e, this expression is not in contrast with Eq. 2.5.

2.1.3 The rectangular Tao-Eldrup

Gidley et al showed how it is possible to extend TE maintaining physical simplicity and avoiding difficult calculations just by switching from spherical to rectangular pore geometry[61]. In the so called rectangular Tao Eldrup (RTE), Ps wavefunction has the product form:

$$\Psi_{ijk} = \psi_i(x)\psi_j(y)\psi_k(z) \tag{2.11}$$

where $x \in [0, a]$, $y \in [0, b]$, $z \in [0, c]$ and

$$\psi_i(x) = \sqrt{\frac{2}{a}} \sin\left(\frac{i\pi x}{a}\right) \tag{2.12}$$

are just the eigenfunction of the well known particle-in-a-box problem with energy eigenvalues

$$E_x = \frac{h^2}{16m}\frac{i^2}{a^2} \equiv E_0 \frac{i^2}{a^2} \tag{2.13}$$

with analogue results for y and z. The three free-parameters a, b, and c makes RTE easily adaptable to fit different expected geometries of the pores, from cubic to rectangular. Again, pickoff annihilation is taken into account introducing an outer shell of thickness Δ (identical for the three dimensions for simplicity) where Ps annihilates with $\bar{\lambda}$. If *o*-Ps is assumed to be in thermal equilibrium with the pore at temperature T, thermal average of the annihilation operator can be calculated as usual using the Boltzmann equation and density matrix $\lambda_{\text{RTE}} = \text{Tr}\{\rho\lambda\}$:

$$\lambda_{\text{po}} = P_{\text{out}}^{\text{RTE}}\bar{\lambda} + (1 - P_{\text{out}}^{\text{RTE}})\lambda_{3\gamma} \tag{2.14}$$

where $P_{\text{out}}^{\text{RTE}}$ given by:

$$P_{\text{out}}^{\text{RTE}} = 1 - F(a, \Delta, T)F(b, \Delta, T)F(c, \Delta, T) \tag{2.15}$$

with

$$F(x, \Delta, T) = 1 - \frac{2\Delta}{x} + \frac{\sum_{n=1}^{\infty} \frac{1}{n\pi} \sin\left(\frac{2\pi n\Delta}{x}\right) \exp\left(-E_0 n^2/x^2 kT\right)}{\sum_{n=1}^{\infty} \exp\left(-E_0 n^2/x^2 kT\right)} \tag{2.16}$$

being kT the thermal energy. The parameter Δ is usually chosen so that at $T = 0$ the RTE model (with a cubic configuration) agrees with the TE at small pore dimensions. However, once calibrated, RTE was showed to be successful in fitting PALS data from a wide range of pore dimensions, up to several micrometers. Also the temperature dependence of PALS experiment could be easily explained by RTE. It should be noted that in both these models, in principle one could arbitrarily fix the value of Δ (for example to the average bonding distance of surrounding molecules) and then use Eq.2.4 data to empirically find the annihilation rate in bulk λ_{bulk}.

Despite the success of the model, no theoretical efforts were made to prove its validity from fundamental principles.

2.1.4 Models based on classical mechanics

We mention here another simplified shape-free model for pore-size estimation which was recently proposed by Wada and Hyodo [67]. In their work the authors considered the classical picture of a finite-size Ps bouncing inside a cavity of generic geometry. This picture is valid when the Ps mean free path between collisions with the outer cavity

walls, $\bar{L}_{\text{Ps}}$, is much larger than the thermal Ps de Broglie wavelength $\lambda_{\text{Ps}} = h/\sqrt{4\pi mkT}$ (3.05nm at room temperature). For a finite-size Ps, $\bar{L}_{\text{Ps}}$ depends both on a parameter $\bar{\Delta}$ defining its effective mean size and on the mean free length of the pore $\bar{L} = 4V/A$ (in particular $\bar{L} = 4R_C/3$ for a spherical cavity):

$$\bar{L}_{\text{Ps}} = \bar{L} - 2\bar{\Delta} \tag{2.17}$$

The pick-off quenching rate of *o*-Ps is then simply given by the product of pick-off annihilation probability per collision with the cavity wall, P_A , and the collision frequency, $v_{\text{th}}/\bar{L}_{\text{Ps}}$, where v_{th} is the thermal velocity:

$$\lambda_{\text{po}} = P_A \frac{v_{\text{th}}}{\bar{L} - 2\bar{\Delta}} \tag{2.18}$$

The adjustable parameter $\bar{\Delta}$ may be chosen so that Eq.2.18 merges smoothly with the TE result for an arbitrary small value of cavity radius. This model proved to be in a good agreement with the RTE for cavity of size bigger than $\bar{L} > 1.28$nm, thus showing that the pickoff process is mainly related to the volume-to-surface ratio in mesoporous materials.

2.2 Two particle models

Given the increased success of PALS, the huge amount of available data required some new theoretical insight beyond the single particle approximation. The logical extension of TE-like models consists in taking separate degree of freedom for the positron and the electron forming Ps, so to have a two-particle wavefunction $\Psi(p, e)$, p and e being the spin-spatial coordinate of the positron and electron respectively. This way will be determined not only the center of mass wavefunction but also the internal structure of Ps. In particular this approach is the simplest one that is able to describe any variation of the contact density parameter k with respect to its vacuum value $k_0 = 1/8\pi a_0^3$. The interest of positronium community is usually limited to *o*-Ps , so that the spin part of the wavefunction is commonly neglected. The general expression for the contact density of a two particle wavefunction is

$$k = \int |\Psi(\boldsymbol{r}_p, \boldsymbol{r}_e)|^2 \delta(\boldsymbol{r}_p - \boldsymbol{r}_e)\, d^3 r_p\, d^3 r_e \tag{2.19}$$

where the integration is done over the entire configuration space. As usual in any two-particle system, Ps wavefunction is commonly written as a function of the relative and center of mass coordinate $\boldsymbol{r}$ and $\boldsymbol{R}$ (Eq. 1.7). If the problem is separable, the general form of the wavefunction will be

$$\Psi(\boldsymbol{R}, \boldsymbol{r}) = \Phi(\boldsymbol{R})\varphi(\boldsymbol{r}) \tag{2.20}$$

and the contact density can be written in the equivalent form:

$$k = \int |\Psi(\boldsymbol{R}, 0)|^2\, d^3 R \tag{2.21}$$

As for one body, two body models reduce the original multiparticle problem to a simpler one by using some effective potentials simulating the interaction with the medium. Usually these potentials are derived by means of macroscopic approaches, whose validity remains uncertain. Of course this come to a price since they naturally add more

and more free-parameters which have to be determined experimentally. Given the total hamiltonian H of the system, two main approaches can be used to numerically find the ground state, namely the variational method (VM) and the quantum monte carlo techniques(QMC). We will first review some simple two particle models which were solved by variational techniques.

2.2.1 The compressed Ps model

An approach somehow in between the one and two-particle models is due to Consolati, Quasso and Trezzi[10]. In their work "Swelling of Positronium Confined in a Small Cavity" the authors focused on the relative coordinate $\boldsymbol{r}$ instead of on the center of mass one. Whereas in TE like models the confinement acts only on the center of mass wavefunction, in this model the same vanish-at-boundary condition on $\varphi(\boldsymbol{r})$ is imposed. For simplicity they considered the center of mass stuck in the center of a spherical symmetric cavity, so that $\varphi(\boldsymbol{r}) = R_{nl}(r)Y_{lm}(\theta,\phi)$. Furthermore using $u(r) = rR(r)$ they solve the Hydrogen-like Schrödinger equation:

$$\frac{d^2u}{d\rho^2} + \left[\frac{1}{4} + \frac{n}{\rho} - \frac{l(l-1)}{\rho^2}\right] u = 0 \tag{2.22}$$

where n, l, m are the usual well known quantum numbers, $\rho = 2\kappa r$, $\kappa = \sqrt{m|E|}/\hbar$ and $n = 1/a_0\kappa$. The solution is then looked in the form $u(\rho) = \rho^{l+1}e^{-\rho/2}F(l,\rho)$ which may be familiar to the reader. The only difference with respect to the free-Ps case is that the series expansion for F must not vanish at infinity but at $r = 2R_c$ (if the center of mass is at the center of the cavity, the maximum radial distance r is related to the cavity diameter $2R_c$). This lead to a principal quantum number n which is no more integer but assumes real values, with a corresponding shift of the energy levels. F can be obtained numerically and the authors showed that a few dozens of terms are sufficient to discriminate among values of F lower than 10^{-6}.

The relative contact density is then given by

$$k_r = \frac{1}{n^2A^2} \tag{2.23}$$

where A is the normalization constant and both n and A depend on R_c. With this procedure, a numerical relationship between R_c and both n and k_r is obtained (with $l = 0$ for the ground state). It is found that n differs appreciably from unity only for $2R_c < 0.3$nm and the resulting relative contact density increases by decreasing the cavity radius. This simple model shows that the confinement alone inevitably leads to a compressed state, in contrast to the observed swollen Ps. Therefore, there must exist some other effect which may act on the contact density and which must be taken into account in more elaborate models.

2.2.2 The springs model

One of the few example of exactly solvable two particle model was due to McMullen and Stott in 1982[41]. In their work, the authors described all interactions acting on the electron-positron pair as harmonic potentials, different for each particle. These are in turn chosen to confine the Ps within a spherically symmetric cavity. The hamiltonian of this *Springs model* reads:

$$H = -\frac{\hbar^2\Delta_p}{2m} - \frac{\hbar^2\Delta_e}{2m} + \frac{1}{2}\kappa(\boldsymbol{r}_p - \boldsymbol{r}_e)^2 + \frac{1}{2}k_+r_p^2 + \frac{1}{2}k_-r_e^2 \tag{2.24}$$

where also the coulomb interaction between the electron and the positron is replaced by a harmonic attraction. The additional harmonic terms describe external fields acting on the two particles. These can be either attractive or repulsive. However a realistic choice of k_- would be positive, accounting for the Pauli exchange repulsion with the surrounding close-shell electrons, whereas a negative k_+ would describes the attraction of the positron to the surrounding ions. The solution of $H_0 = -\frac{\hbar^2\Delta_p}{2m} - \frac{\hbar^2\Delta_e}{2m} + \frac{1}{2}\kappa(\boldsymbol{r}_p - \boldsymbol{r}_e)^2$ is trivial in the center of mass frame:

$$\Psi_0(\boldsymbol{r}, \boldsymbol{R}) = \frac{1}{\sqrt{\Omega}} e^{i\boldsymbol{K}\cdot\boldsymbol{R}} \phi_n(\boldsymbol{r}) \tag{2.25}$$

where ϕ_n is an isotropic simple harmonic oscillator state with $n = (n_x, n_y, n_z)$. It is found that for the ground state the contact density reads

$$k = \left(\frac{m\omega_0}{2\pi\hbar}\right)^{3/2} \tag{2.26}$$

where $\omega_0 = \sqrt{2\kappa/m}$. To be consistent with the vacuum limit, the authors decided to set κ so that the free Ps dipole polarizability was recovered. This condition led to:

$$\kappa = \frac{e^2}{36a_0^3} \tag{2.27}$$

but of course other choices could have been done (for example one can choose κ so that the vacuum contact density is recovered $\kappa = \frac{\pi^{2/3}\hbar^4}{8ma_0^4}$). The general eigenstates of H were then found by a set of transformations and the final ground state reads:

$$\Psi_{\text{Harm}}(\boldsymbol{r}, \boldsymbol{R}) = \left(\frac{(k_u k_v)^{1/4}}{\pi}\right)^{3/2} e^{-(\sqrt{k_u}u^2 + \sqrt{k_v}v^2)/2} \tag{2.28}$$

where

$$\begin{aligned} \boldsymbol{u} &= \sqrt{2m}\boldsymbol{R}\sin\theta + \sqrt{\frac{m}{2}}\boldsymbol{r}\cos\theta \\ \boldsymbol{v} &= \sqrt{2m}\boldsymbol{R}\cos\theta - \sqrt{\frac{m}{2}}\boldsymbol{r}\sin\theta \end{aligned} \tag{2.29}$$

and k_v, k_u are given by:

$$k_{u/v} = 2\kappa + k_- + k_+ \pm \sqrt{4\kappa^2 + (k_+ - k_-)^2} \tag{2.30}$$

As expected, they found that the more k_- increase, the more the electron is confined, which leads to a compressed Ps with an higher contact density. On the other hand, the more negative k_+ the more the positron is polarized, which leads to a "swollen" Ps with a lower contact density. In between these two limits, there is a line in the space of parameters where with $k_r = 1$, e.e where the two effects precisely cancel. The authors suggested a simple picture to the physical origin of $k_\pm$ in which Ps is confined in a spherical cavity inside a dielectric: whereas the image forces, which attracts both the particles towards the walls, manage to pull the positron in the outer electronic shell, they can not overcome the strong repulsive exchange forces felt by the electron. This picture is somehow coherent with another famous model of confined Ps due to Stepanov.

2.2.3 The bubble model

One of the most successful attempt to go beyond TE for Ps annihilation in liquids is found in the work of Stepanov et al.[68]. Here Ps is pictured as confined inside a bubble which itself creates. In contrast to Ferrel, the authors point out that the formation of such a bubble can be related not only to exchange repulsion between electrons, but also to an enhancement of the Coulombic attraction of the positron-electron pair inside the cavity, where the dielectric screening is not present. In this *Bubble Model* the authors introduced in the hamiltonian two different potential terms for the positron and the electron in Ps together with a modified coulomb potential which takes into account the polarization of the medium:

$$H = -\frac{\hbar^2 \Delta_p}{2m} - \frac{\hbar^2 \Delta_e}{2m} + U_+(\boldsymbol{r}_p) + U_-(\boldsymbol{r}_e) - U_c(\boldsymbol{r}_p, \boldsymbol{r}_e, R_c, \epsilon) \tag{2.31}$$

where ϵ is the relative high frequency dielectric permittivity of the bulk. The main novelty of this simple model are the independent potentials U_+ and U_-, which are modeled using the positron and electron work functions ϕ_+ and ϕ_-[2]:

$$\begin{aligned} U_+(\boldsymbol{r}_p) &= \begin{cases} 0, & r_p < R_c \\ -\phi_+, & r_p > R_c \end{cases} \\ U_-(\boldsymbol{r}_e) &= \begin{cases} 0, & r_e < R_c \\ -\phi_-, & r_e > R_c \end{cases} \end{aligned} \tag{2.32}$$

The physical meaning of these form of potential is that if the work function is positive (i.e. it requires a positive work to be extracted from the bulk) the particle will be attracted to the bulk and vice versa. On the other hand U_c was calculated for every interparticle distance r solving the Poisson equation in the complex geometry of the uniform dielectric medium with a spherical hole, and turned out to be a complicated function of Legendre polynomials. The ground state solution was found by means of the variational method using the trial wavefunction:

$$\Psi_{\text{Step}}(\boldsymbol{r}, \boldsymbol{R}) = \frac{\exp(-r/2a - R/2b)}{8\pi\sqrt{a^3 b^3}} \tag{2.33}$$

where a and b are the variational parameter. After having found the best a, b, the contact density is evaluated using Eq. 2.19 while pickoff annihilation is accounted with the TE formalism 2.2 with $P_{\text{out}}^{\text{Bubble}}$ given by

$$P_{\text{out}}^{\text{Bubble}} = \int_{r_p > R_c} |\Psi(\boldsymbol{r}_p, \boldsymbol{r}_e)|^2 \, d^3 r_p \, d^3 r_e \tag{2.34}$$

which is just the probability of finding the positron outside the cavity wall. The Bubble model has a total of 4 parameters: R_c,ϕ_+,ϕ_- and ϵ which have to be determined with independent measurements. While ϵ and ϕ_- are easily accessible, this is not in general true for R_c and ϕ_+. As said in the previous section, in liquid there exist an extra equilibrium condition which can be used to relate R_c to the macroscopic surface tension σ.

It's straightforward to find that in the small radius limit $k_r = k/k_0 \to \frac{1}{\epsilon^3}$, which makes the Bubble model one of the few models capable of explaining the lowering of

[2]Note that in the original paper [68] the author used a different definition for the work functions, which leads to opposite signs. Here we stick with the common definition.

the contact density. On the opposite limit, the vacuum value is recovered for large cavities as expected. Regarding the pickoff-radius relationship, the predicted curves vary depending on the choice of $\phi_{\pm}$, and TE can be reproduced with the right choice of parameters.

One may argue that the variational wavefunction 2.33 is too simple to properly describe polarization effects due to surrounding medium. However the idea of introducing a dielectric medium in the description of confined Ps is not new and it was already studied with more powerful numerical methods for example by Bug et al. [69] in their QMC simulations (see Sec. 2.2.4). Surprisingly, differences of results are very little and are well compensated by the physical simplicity of the present description.

2.2.4 Quantum Montecarlo techniques

To solve the complex problems posed by these models, apart the variational method (used for example in the Bubble model), often Quantum Montecarlo (QMC) integration techniques are considered. The main goal of QMC is to calculate thermal-averages or ground-state expectation values of a many body system by representing the Schrödinger equation as a random walk in the multi-dimensional space.[70].

The most famous QMC method, the Path Integral Montecarlo (PIMC) is a powerful tool to numerically sample the canonical density matrix $\rho(\boldsymbol{R}, \boldsymbol{R}'; \beta) = \langle \boldsymbol{R}| \exp(-\beta \hat{H}) |\boldsymbol{R}'\rangle$ of a system in thermal equilibrium at an inverse temperature β, with a hamiltonian $\hat{H}$ [71]. The knowledge of the density matrix enables to find thermal averages of observables:

$$< \hat{A} >= \frac{\mathrm{Tr}\hat{\rho}\hat{A}}{\mathrm{Tr}\hat{\rho}} = \frac{1}{\mathrm{Tr}\hat{\rho}} \int A(\boldsymbol{R})\rho(\boldsymbol{R}, \boldsymbol{R}; \beta)\, d\boldsymbol{R} \tag{2.35}$$

where $\boldsymbol{R}$ represents the whole coordinates variables of the system (for a two-particle Ps system $\boldsymbol{R}$ is the six-dimensional position space of the two particles $(\boldsymbol{r}_p, \boldsymbol{r}_e)$) and the last equality holds only for operators which are diagonal in the coordinate representation.

In particular, for $\beta \to \infty (T \to 0)$ any system with discrete energy levels is dominated by its ground state Ψ_{gs}, so that $\rho(\boldsymbol{R}, \boldsymbol{R}; \beta) \sim e^{-\beta E_{\mathrm{gs}}} |\Psi_{\mathrm{gs}}(\boldsymbol{R})|^2$ and thermal averages become essentially expectation values over Ψ_{gs}. In this limit the sampling of the diagonal density matrix gives the ground state probability distribution of the system. Usually, such large value of β are not required if the corresponding energy remains smaller then the energy distance of the first excited state. This is just the situation which occurs when Ps is confined in a small pore, whereas for larger pores this approximation does not hold.

However, the density matrix of a quantum system is not generally known since its calculation requires the exact eigenstates of the Hamiltonian. The key aspect of any PIMC method is the possibility to use an exact Trotter decomposition to write the density operator at low temperature as a product of M high temperature ($\epsilon = \frac{\beta}{M}$) density operators:

$$\rho(\beta) = e^{-\beta \hat{H}} = \left[e^{-\frac{\beta}{M}\hat{H}}\right]^M = [\rho(\epsilon)]^M \tag{2.36}$$

With the help of this formula, the density matrix can be exactly decomposed as a multidimensional integral:

$$\begin{aligned} \rho(\boldsymbol{R}, \boldsymbol{R}; \beta) &= \langle \boldsymbol{R}| \rho(\beta) |\boldsymbol{R}\rangle \\ &= \int \langle \boldsymbol{R}| \rho(\epsilon) |\boldsymbol{R}_1\rangle \times \langle \boldsymbol{R}_1| \rho(\epsilon) |\boldsymbol{R}_2\rangle \\ &\cdots \times \langle \boldsymbol{R}_{M-1}| \rho(\epsilon) |\boldsymbol{R}\rangle \, d\boldsymbol{R}_1 \, d\boldsymbol{R}_2 \cdots d\boldsymbol{R}_{M-1} \end{aligned} \tag{2.37}$$

where M is a discretization variable.

The main advantage of this decomposition is that expressions for $\rho(\epsilon)$ in the high temperature limit are known and are introduced in a natural way using classical approximations. For example the primitive approximation [72] consist in neglecting commutation terms like $[T, V]$ in the hamiltonian (which are second order in ϵ) so that the density operator becomes:

$$e^{-\epsilon\hat{H}} \approx e^{-\epsilon\hat{T}} e^{-\epsilon\hat{V}} \tag{2.38}$$

Theoretically, convergence of the density matrix exists for the primitive approximation as $M \to \infty$. In the framework of a (two particle) confined Ps, the high temperature $\rho(\epsilon)$ can be written as a product of three parts:

$$\hat{\rho}(\epsilon) \approx \hat{\rho}_{\text{coul}}(\epsilon)\hat{\rho}_{\text{conf}}(\epsilon)\hat{\rho}_{\text{bulk}}(\epsilon) \tag{2.39}$$

In this expression, $\hat{\rho}_{\text{coul}} = \exp\left[-\epsilon(\hat{T}_+ + \hat{T}_- + \hat{V}_{\text{coul}})\right]$ is the density operator of a system of two particles interacting via an attractive Coulomb potential $\hat{V}_{\text{coul}} = -e^2/r$, i.e. the free Ps system. The strong singularity at the origin makes the coulomb potential unsuitable for a straightforward primitive approximation. For this reason many authors[73] use pseudo-potentials like the Yukawa potential:

$$\hat{V}_{\text{Yukawa}}(r; a) = -\frac{e^2}{r}(1 - e^{-r/a}) \tag{2.40}$$

which make the calculations fast and easy to set up at the cost of adding further arbitrary parameters on which the convergence must be tested.

However exact analytical expression for the propagator $\langle \boldsymbol{R}| \hat{\rho}_{\text{coul}}(\epsilon) |\boldsymbol{R}'\rangle$ exists and it can be expressed in a simple form using a special relation valid for the Coulomb potential[74, 75]:

$$\rho(\boldsymbol{r}, \boldsymbol{r}'; \beta) = \frac{1}{4\pi|\boldsymbol{r} - \boldsymbol{r}'|}\left(\frac{\partial}{\partial y} - \frac{\partial}{\partial x}\right)\rho_{l=0}(x, y; \beta) \tag{2.41}$$

With the help of this expression the full 3D density matrix can be obtain from the s-wave term alone. This form is particularly suitable for numerical calculation and $\hat{\rho}_{\text{coul}}$ was first tabulated by Pollock [76]. The advantage in using the exact propagator is that the resulting density matrix will be very accurate. Given the cost in computational time, the exact $\hat{\rho}_{\text{coul}}$ is commonly used only when the two particles are close to each other, i.e. their distance is less then a suitable cutoff radius R_{cutoff}, while the less expensive primitive approximation is used outside this region. The remaining terms in (2.39), $\hat{\rho}_{\text{conf}}$ and $\hat{\rho}_{\text{bulk}}$, are the approximations for the confining and bulk potential respectively.

PIMC methods have been used to study Ps trapped inside a cavity by many authors. In early works, the confining potentials were taken as infinite barrier for both the electron and the positron, an approximation leading to an increase of the relative contact density[73][77]. Furthermore no other potentials were considered so that the model was material-independent and essentially similar to a two-particle TE approach. In another series of works by Sterne and Bug [78][79], the authors described Ps-positron (electron) interaction with argon and silica sodalite replacing the infinite potential well with a more realistic Hartree potential built from the host electron density first obtained with density functional theory (DFT) calculations. This approach produced promising results but still requires material-specific calculations to determine the form of the potentials. Again, another type of QMC techniques, namely the Diffusion Montecarlo and the Variationl

Montecarlo, have been extensively used to study the ground and excited states of many Positronium-atom complexes[80, 81, 82], but these have never been applied to study Ps inside matter.

2.3 Many particle models

In order to further improve the description of Ps in matter, one has to include a certain number of external particles in the model. Whereas atomic nuclei play no direct role in the annihilation process, the presence of external electrons can introduce radical modifications. Given the indistinguishability with the Ps electron, this many-body problem has to be solved respecting Pauli exclusion principle and the total wavefunction Ψ must be completely antisymmetric:

$$\Psi(p;\cdots,i,\cdots,j,\cdots) = -\Psi(p;\cdots,j,\cdots,i,\cdots) \;\; \forall i,j \in [1;N] \tag{2.42}$$

where spin-spatial coordinates are implicit and p is reserved for the positron. In this kind of description, particle spin plays an active role on the annihilation and it should be treated with care. Finding the ground state of such a system is a cumbersome task which at the state of the art is faced by two-component density functional theory (DFT). This kind of approach is reserved to the study of positron annihilation in metals and crystal structures and it has never been used to study Ps. This is not a surprise since if all electrons are identical the concept of Ps, that is a positron bound to one specific electron, becomes blurry in condensed matter. However, other *ab initio* methods (e.g. configuration interaction (CI)) can be used to numerically solve systems where Ps interacts with a small number of electrons (e.g. Ps^-[55, 56], Ps-He [83] or a system of a positron and 4 electrons in a harmonic trap [63]). Furthermore, some formal theoretical analysis of Ps pickoff annihilation in the presence of external electrons have been done using full antisymmetrization of the wavefunction[84, 9]. In the following chapter we will review some of the first attempts to treat in a someway simple realization of a many-body formalism this problem. Here we only discuss an important and simple method for introducing positron-electron correlations.

2.3.1 The Independent Particles model and the enhancement factor

Positron annihilation in metals has been extensively studied by many authors[24]. In this context electrons are usually considered free, so that the problem reduces to the study of the annihilation rate of a positron in an uniform electron gas (Jellium) In earlier works the total wavefunction of the system Ψ was simplified into a product of a positron and an electron part. The so called "independent particle model" (IPM) (also known as "independent particle approximation" IPA) used uncorrelated one-body electron and positron densities $n_e(\boldsymbol{r})$ and $n_p(\boldsymbol{r})$ which were optimized by means of a DFT minimization. Electron and positron spins are commonly neglected in calculation in metals. An uniform spin distribution for electrons is assumed, so that for every positron spin direction the probability of forming a singlet-state is $\frac{1}{4}$ while a triplet state will occur with probability $\frac{3}{4}$. The spin part of the annihilation operator 1.19 is than taken equal to the spin averaged rate $\bar{\lambda}$ and $\hat{\lambda}$ becomes essentially a spatial delta function. This way all electrons are

treated equally and calculations are greatly simplified:

$$\begin{aligned}\lambda &= \pi r_0^2 c \int n_p(\boldsymbol{r}) n_e(\boldsymbol{r})\, d^3r \\ &= 8\pi a_0^3 \bar{\lambda} \int n_p(\boldsymbol{r}) n_e(\boldsymbol{r})\, d^3r\end{aligned} \tag{2.43}$$

where the prefactor is due to the Sommerfeld result for the positron annihilation in a homogeneous electron gas (see Eq. 1.13 for comparison)[24, 85].

It was soon realized that electron-positron correlation effects describing the screening charge of the electrons around the positron play a major role in the annihilation process. This fact is specially relevant at low density, where a Ps like bound state will be formed, thus enhancing the electron density at the positron position. Since the screening length is usually short, this effect can be described in a local density approximation (LDA) and the common approach due to Barbiellini is to introduce in 2.43 an enhancement factor $\gamma(\boldsymbol{r})$ given by the amplitude of the electron density on the positron site. [86][87]:

$$\lambda = 8\pi a_0^3 \bar{\lambda} \int \gamma(\boldsymbol{r}) n_p(\boldsymbol{r}) n_e(\boldsymbol{r})\, d^3r \tag{2.44}$$

Apart from this short-range enhancement, the mean electron density and states remain unperturbed. This is confirmed by the fact that 2γ angular distribution, hence the momentum density, shows relatively weak changes with respect to IPM[88].

In this context, the formal expression of the enhancement factor requires the knowledge of the true wavefunction of the system, and for a positron interacting with N electrons is given by:

$$\begin{aligned}\gamma(\boldsymbol{r}_p) &= \sum_{i=1}^{N} \int \frac{|\Psi(\boldsymbol{r}_p; \boldsymbol{r}_1, \cdots, \boldsymbol{r}_N)|^2}{n_p(\boldsymbol{r}_p) n_e(\boldsymbol{r}_p)} \delta^3(\boldsymbol{r}_p - \boldsymbol{r}_i)\, d^3r_1 \cdots d^3r_N \\ &= N \int \frac{|\Psi(\boldsymbol{r}_p; \boldsymbol{r}_p, \boldsymbol{r}_2 \cdots, \boldsymbol{r}_N)|^2}{n_p(\boldsymbol{r}_p) n_e(\boldsymbol{r}_p)}\, d^3r_2 \cdots d^3r_N\end{aligned} \tag{2.45}$$

The form of $\gamma(\boldsymbol{r}_p)$ is typically approximated within the local density approximation (LDA) as function of the electron density only. In literature, many different parametrizations of the enhancement factor exist, which are derived from calculations done on a system of a single positron immersed in an electron gas of mean density ρ[88, 89, 90]. As an example, we report the fitting result obtained by Mitroy and Barbiellini [89]:

$$\gamma(\rho) = 1 + 1.23 r_s + 0.8295 r_s^{3/2} - 1.26 r_s^2 + 0.328 r_s^{5/2} + \frac{1}{6} r_s^3 \tag{2.46}$$

where r_s is the electron gas parameter (in atomic units)

$$r_s = \left(\frac{3}{4\pi\rho}\right)^{1/3} \tag{2.47}$$

It is a known fact that the first two terms in Eq. 2.46 are fixed to reproduce the high-density random phase approximation limit (RPA), while the last term reproduce the low-density limit of Ps atom:

$$\lim_{\rho \to 0} \rho\gamma(\rho) = k_0 \tag{2.48}$$

Approximations based on Eq. 2.44 have proven to be powerful when combined with a two-component DFT calculation in various systems ranging from metals to liquids.

Part II
Modeling Ps in porous materials

CHAPTER 3

A two-particle model for Ps confinement in nanoporous materials

From an experimental point of view, existing models describing Ps in porous materials, which we described in the previous chapter, are not fully satisfactory. This is due to the fact that they either fail to predict the lowering of the contact density or they lack in simplicity since they rely on extensive material-specific calculations.

Recently we have introduced a two-particle model to describe Ps confined in nanopores by combining the generality of TE approach with specific chemical properties of the surrounding material[38, 39]. Our model is based on the observation that the confining potential acting on Ps is a net result of two independent and different contributions, acting on the electron and on the positron separately. In particular, a positive value for the positron work function, as derived by theoretical models[31] and found, for example, in silica[91], suggests that the positron is attracted toward the medium and then is not confined *a priori*. The well known confining behavior of Ps is then related to the repulsive electron-electron interaction at short distances and to the strong Pauli exchange forces[38, 40] with bulk electrons. In this picture, it is the electron in Ps that prevents large overlap between Ps itself and electrons in matter. This fact is confirmed by scattering experiments of Ps off noble gas atoms and molecules. Indeed, despite the mass and charge difference, the total cross section of Ps is found to be identical to that of a bare electron, hence showing that exchange effects dominates the short-range interaction[92].

By applying approximate semi-analytical techniques, the variational method and, more recently, QMC calculations, we were able to demonstrate that our model correctly describe the lowering of the contact density, obtaining also promising results in the comparison with experimental data on this quantity and on the pick-off annihilation rate, connected with the pore radius and the positron work function. This chapter is mainly an extended review of the work already published by us in [38, 39].

3.1 Theory

Starting from the previous observations and assuming for definiteness a spherical cavity of radius R_c centered on the axes origin, we write the Hamiltonian operator for a system of 2 particles with same mass m and opposite charges $\pm e$ subjected to different potentials:

$$H = \frac{p_1^2}{2m} + \frac{p_2^2}{2m} - \frac{e^2}{|q_1 - q_2|} + V_{\text{conf}}(q_1) + V_{\text{bulk}}(q_2) \tag{3.1}$$

where $\boldsymbol{q}_1(\boldsymbol{q}_2)$ is the position of the confined electron (positron). V_{conf} and V_{bulk} describe the particles specific interaction with the surrounding medium. The key concept behind our model of Ps trapped inside a pore is that the strong confining potential V_{conf} is mainly

due to the Pauli exclusion principle. As such it is felt only by the electron and can rapidly grow to large values near the surface of the cavity. Although its modelization as a finite well may sounds more physically plausible, the mathematical complications introduced by this assumption would not light up the important aspects of the problem. Besides its maximum value, one can argue that also the shape of this potential, which should strongly depend on the specific type of system in exam (atomic species, geometry of surrounding lattice, temperature, etc), may have some effects on the overall problem. To avoid such complications, we will assume a spherical quantum well with infinite depth:

$$V_{conf}(q_1) = \begin{cases} 0 & \text{if} \quad |\boldsymbol{q}_1| < R_c \\ \infty & \text{if} \quad |\boldsymbol{q}_1| > R_c \end{cases} \tag{3.2}$$

where R_c defines the radius of the cavity, eventually in a conventional way.

On the other side, the complex interactions between the positron and both bulk electrons and nuclei can be collected into a bulk potential V_{bulk}. This potential acts only on the positron and in first approximation can be taken as equal to the opposite of the positron work function ϕ_+ deep inside the bulk, and zero in the electron-confining cavity. This way we assume that with a positive value of the positron work function ϕ_+, the positron is attracted to the bulk and perceives a free volume cavity as a potential barrier. As for V_{conf}, the shape of V_{bulk} between the two limiting values depends on the system under examination. In particular, using a spherical symmetric step potential approximation, the transition may not exactly lay at the cavity wall R_c as it does for V_{conf}.

For this reason, in our first approach to this matter we considered the presence of a transition surface layer of thickness Δs, representing the offset between the outermost position accessible to the electron and the region where positron bulk properties become predominant. Such an offset, which can be either negative and positive *a priori*, was fixed by us at $\Delta s = +0.17$nm. This choice was done having in mind an analogy with the famous Δ layer already introduced in the TE model (Sec. 2.1.1). As a matter of fact, we found out that different reasonable choices of Δs around the TE suggested value of Δ had negligible effects on our results, as shown in [38]. In that paper, as detailed later, we used approximate semi-analytical techniques to derive the contact density from the TE inspired decomposition of the electron-positron interaction with the medium. The lowering of the contact density, which is the primary goal of our model, was demonstrated and a promising correspondence with experimental Ps lifetime data was found, under simplified assumptions on the electron density in the medium.

This preliminary success pushed us to find more accurate solutions using numerical methods, which we are going to discuss in the following. For the sake of minimizing unknown quantities in the model, we first noted that the introduction of the Δs parameter, which in fact is not experimentally known, can be avoided by a proper rescaling of the positron work function. This can be easily explained by this heuristic reasoning. Given that the bigger the offset, the bigger the distance between the confined positron and the bulk, the overall "pulling strength" of V_{bulk} must be proportional in first approximation to the ratio $\phi_+/(R_c + \Delta)$. This way, a vanishing offset would qualitatively yield the same results if a "scaled" work function $\tilde{\phi}_+ = \phi_+(R_c + \Delta)/R_c$ is used. However since $R_c \gg \Delta$ is expected in all practical situations, the difference between these two quantities is surely lower than the experimental accuracy of available data. For this reason Δs can be neglected here. Then, at variance with [38], we write the bulk potential simply as:

$$V_{bulk}(q_2) = \begin{cases} 0 & \text{if} \quad |\boldsymbol{q}_2| < R_c \\ -\phi_+ & \text{if} \quad |\boldsymbol{q}_2| > R_c \end{cases} \tag{3.3}$$

The time independent Schrödinger equation of our model reads:

$$\left[\frac{p_1^2}{2m}+\frac{p_2^2}{2m}-\frac{e^2}{|q_1-q_2|}+V_{\text{conf}}(q_1)+V_{\text{bulk}}(q_2)\right]\Psi(q_1,q_2)=E\Psi(q_1,q_2) \tag{3.4}$$

A first attempt of solution of 3.4 was given by us in [38] by means of the usual center of mass $\boldsymbol{R}$ and relative coordinate $\boldsymbol{r}$. Noting that the center of mass is not strictly confined inside the cavity (as long as the electron is), we separated the total wavefunction as a product of a plane-wave like factor times a relative motion part $\tilde{\varphi}_R(\boldsymbol{r})$:

$$\Psi(\boldsymbol{r},\boldsymbol{R})\simeq\frac{1}{\sqrt{\tilde{V}}}e^{i\boldsymbol{K}\cdot\boldsymbol{R}}\,\tilde{\varphi}_R(\boldsymbol{r})\quad(|\boldsymbol{R}+\boldsymbol{r}/2|<R_c)\ , \tag{3.5}$$

Here $\tilde{\varphi}_R(\boldsymbol{r})$ is a semi-analytical function which depends parametrically on $\boldsymbol{R}$ and takes into account the confinement effects. Given that an expression for $\tilde{\varphi}$ can be easily calculated in some limiting situations (i.e. in the center of the cavity and deep inside bulk), we constructed it as a piecewise continuous function on different R intervals. Although rudimentary, this form of $\Psi(\boldsymbol{r},\boldsymbol{R})$ was already capable of showing some interesting features like the lowering of the contact density.

To calculate a more accurate solution of Eq. 3.4, we introduce now a non–standard change of coordinates that is more suitable for the present situation where the system is dominated by the confining and the coulombic potentials. This new coordinates are given by

$$\begin{cases}\boldsymbol{r}=\boldsymbol{q}_2-\boldsymbol{q}_1\\ \boldsymbol{p}=\boldsymbol{p}_2\end{cases}\quad\begin{cases}\boldsymbol{r_e}=\boldsymbol{q}_1\\ \boldsymbol{P}=\boldsymbol{p}_1+\boldsymbol{p}_2\end{cases} \tag{3.6}$$

and they satisfy the usual commutation relations:

$$\begin{aligned}\left[\hat{r_e}_i,\hat{P}_j\right]&=[\hat{r}_i,\hat{p}_j]=i\hbar\delta_{ij}\\ [\hat{r_e}_i,\hat{r}_j]&=\left[\hat{r}_i,\hat{P}_j\right]=[\hat{r_e}_i,\hat{p}_j]=\left[\hat{P}_i,\hat{p}_j\right]=0\end{aligned} \tag{3.7}$$

Here $\boldsymbol{r_e}$ is again the confined electron position, while $\boldsymbol{r}$ represents the relative distance with the positron. With this variables the Hamiltonian operator in Schrödinger representation becomes (in atomic units):

$$\begin{aligned}H&=-\frac{1}{2}\nabla_{r_e}^2-\nabla_r^2+\boldsymbol{\nabla}_{r_e}\cdot\boldsymbol{\nabla}_r-\frac{1}{r}+V_{\text{conf}}(r_e)+V_{\text{bulk}}(\boldsymbol{r_e},\boldsymbol{r})\\ &=H_0+V_{\text{mix}}\end{aligned} \tag{3.8}$$

where we have separated the mixing Potential

$$V_{\text{mix}}=\boldsymbol{\nabla}_{r_e}\cdot\boldsymbol{\nabla}_r+V_{\text{bulk}}(\boldsymbol{r_e},\boldsymbol{r}) \tag{3.9}$$

from an "unperturbed" hamiltonian

$$H_0=-\frac{1}{2}\nabla_{r_e}^2-\nabla_r^2-\frac{1}{r}+V_{\text{conf}}(r_e) \tag{3.10}$$

It can be easily shown that the Hamiltonian H_0, which contains both the V_{conf} and the coulombic potential, is separable and has exact solutions. For completeness we will

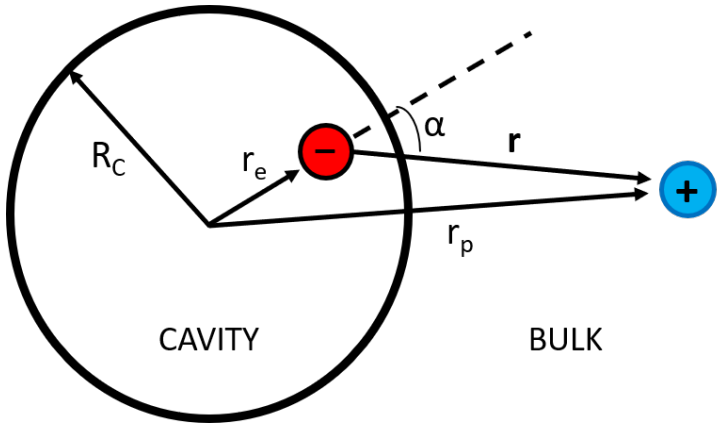

Figure 3.1: Coordinates used in Eq. 3.15.

derive its eigenfunctions in Appendix A. For the ground state energy and wavefunction, one has

$$E_0 = \frac{\pi^2}{2R_c^2} - \frac{1}{4} \tag{3.11}$$

and:

$$\Psi_0(\boldsymbol{r}_e, \boldsymbol{r}) = \frac{1}{N} \frac{\sin(\pi r_e / R_c)}{r_e} \exp[-\frac{r}{2}] \tag{3.12}$$

respectively.

We note that the separation in Eq. 3.8 can wrongly suggests to consider $\hat{H}_{\text{mix}}$ as a "small" perturbation and to study the problem in the perturbation theory framework. However we found out that while V_{bulk} is indeed small, the term $\boldsymbol{\nabla}_{r_e} \cdot \boldsymbol{\nabla}_r$ is not, so that any perturbative approach fails in practice.

Given the spherical symmetry, the problem is symmetric both with respect to axial rotation around the direction of $\boldsymbol{r_e}$, and with respect to a rigid rotation of both particles around the center of the cavity. In particular it is invariant under the inversion operator $I : (\boldsymbol{r}, \boldsymbol{r_e}) \to (-\boldsymbol{r}, -\boldsymbol{r_e})$ which preserves the angle α between the two vectors $\boldsymbol{r_e}$ and $\boldsymbol{r}$. From these considerations, it seems natural to search for a ground state wavefunction which depends only on the absolute values $r \in [0; \infty]$, $r_e \in [0; R_c]$ and on the angle $\alpha(\boldsymbol{r}, \boldsymbol{r_e}) \in [0; \pi]$ between them, which satisfies:

$$\cos\alpha = \sin\theta \sin\theta_e \cos(\phi - \phi_e) + \cos\theta \cos\theta_e \tag{3.13}$$

where (r, θ, ϕ) and (r_e, θ_e, ϕ_e) are the spherical coordinates for $\boldsymbol{r}$ and $\boldsymbol{r}_e$ respectively. The volume element in these new coordinates is $d\Omega = r_e^2 r^2 \sin\alpha \, dr_e \, dr \, d\alpha$, as expected. Furthermore, for any function $f(r_e, r, \alpha)$ having the same symmetries of the system one has:

$$\begin{aligned} \int\int f(r_e, r, \alpha) \, d^3\boldsymbol{r}_e \, d^3\boldsymbol{r} = \\ = 8\pi^2 \int_0^{R_c} \int_0^{\infty} \int_0^{\pi} f(r_e, r, \alpha) r_e^2 r^2 \sin\alpha \, dr_e \, dr \, d\alpha \end{aligned} \tag{3.14}$$

where the factor $8\pi^2$ comes from integration over the "mute" angular coordinates. By using these variables, the new Hamiltonian of the system assumes the form:

$$\begin{aligned}\tilde{H} =& -\frac{1}{2}\left[\nabla^2_{r_e} + 2\nabla^2_r + \frac{2{r_e}^2 + r^2 + 2rr_e\cos\alpha}{r^2{r_e}^2}\nabla^2_\alpha\right.\\ &- 2\cos\alpha\nabla^2_{r_e,r} + 2\frac{\sin\alpha}{r}\nabla^2_{r_e,\alpha} + 2\frac{\sin\alpha}{r_e}\nabla^2_{r,\alpha}\\ &\left.+\ \frac{2}{r_e}\nabla_{r_e} + \frac{4}{r}\nabla_r + \frac{2{r_e}^2\cos\alpha + r^2\cos\alpha + 2rr_e}{r^2{r_e}^2\sin\alpha}\nabla_\alpha\right]\\ &- \frac{1}{r} + V_{\text{conf}}(r_e) + V_{\text{bulk}}(r, r_e, \alpha)\\ =& H_{\text{conf}} + V_{\text{bulk}}\end{aligned} \tag{3.15}$$

where H_{conf} collects H_0 and the kinetic part of V_{mix}.

Calculation of the relative contact density requires the knowledge of the two–particle ground state wavefunction $\Psi_{GS}(r_e, r, \alpha)$ in $\vec{r} = 0$, integrated over the electron position in the cavity[38]. The general definition was given in Eq. 2.19- 2.21 and with current notation reads

$$k_r = 8\pi \int |\Psi_{GS}(\boldsymbol{r}_e, \boldsymbol{r}_p)|^2\, \delta(\boldsymbol{r}_e - \boldsymbol{r}_p)\, d\boldsymbol{r}_e\, d\boldsymbol{r}_p \tag{3.16}$$

where 8π is the inverse of the contact density of Ps in vacuum in atomic units. The expression of the delta function in spherical coordinates with azimuthal symmetry is:

$$\delta(\boldsymbol{r}) = \frac{1}{2\pi}\frac{\delta(r)}{r^2}\frac{\delta(\alpha)}{\sin\alpha} \tag{3.17}$$

Combining Eq. 3.17 and Eq. 3.14 with Eq. 3.16, the final expression for the relative contact density reads:

$$k_r = 4\int_0^{R_c} |\Psi_{GS}(r_e, 0, 0)|^2 r_e^2\, dr_e \tag{3.18}$$

For the pickoff annihilation rate, we use here the approximation given in Eq. 2.5:

$$\lambda_{\text{po}} = \bar{\lambda}\frac{\rho_e}{k_0}P^+_{\text{out}} \tag{3.19}$$

which is proportional to the probability of finding the positron in the electron cloud outside the cavity:

$$P^+_{\text{out}} = \int_{|\boldsymbol{r}_e + \boldsymbol{r}| > R_c} |\Psi_{GS}(r_e, r, \alpha)|^2 r_e^2 r^2 \sin\alpha\, dr_e\, dr\, d\alpha \tag{3.20}$$

The factor ρ_e represents the (constant) *effective* electron density at the positron position. As a matter of fact, this quantity is extremely hard to estimate both because it has a very specific dependence on the physical properties of the material surrounding the cavity, and because it depends on electron-positron correlations effects.

Here we follow a simplified analysis carried out by Ferrel [30] and successfully used in molecular substances by Dutta [62] (as seen in Eq. 2.8), where it is assumed that the positron "samples" only the fraction Z_{eff} of electrons laying in outer molecular shells and does not penetrate in core regions. These electrons in turn can be roughly thought as uniformly spread out over the molecular volume. A suitable approximate expression

Table 3.1: Experimental data on relative contact density κ_r and pick–off lifetime τ_{po} for some selected molecular solids. The column τ' reports the lifetime normalized with respect to the effective electron density ρ_-, calculated using the atomic Van der Waals radii (see text), taken from Ref. [93]: $H = 0.11$, $C = 0.17$, $N = 0.155$, $O = 0.152$, $Si = 0.21$ nm.

Name	formula	κ_r	τ_{po} [ns]	ρ_- [nm^{-3}]	τ' [ns]	marker
Octadecane (liquid)	$C_{18}H_{38}$	0.69 ± 0.07	2.92 ± 0.03	189.5	2.05	■
Octadecane (solid)	$C_{18}H_{38}$	0.85 ± 0.05	1.5 ± 0.01	198	1.1	■
Butyl–PBD	$C_{24}H_{22}N_2O$	0.88 ± 0.11	1.41 ± 0.07	241.3	1.26	◇
Benzene	C_6H_6	0.71 ± 0.06	3.26 ± 0.03	102.7	2.4	▲
Polyethylene	$(C_2H_4)_n$	0.6 ± 0.06	2.6 ± 0.05	170.3	1.6	•
2,5–diphenyl–1,3,4–oxadiazole (PPD)	$C_{14}H_{10}N_2O$	1.05 ± 0.11	1.22 ± 0.01	252.3	1.14	▼
Bhyphenil	$C_{12}H_{10}$	0.82 ± 0.06	1.14 ± 0.01	307.8	1.0	△
Polyethylene terephthalate (Mylar)	$(C_10H_8O_4)_n$	0.78	1.82	274.8	1.85	⋆
Amorphous silica	a–SiO_2	0.95 ± 0.03	1.59 ± 0.02	433	2.55	□
Guaiazulene	$C_{15}H_{18}$	0.64	1.84 ± 0.01	279	1.79	◯
Polymethylmethacrylate(PMMA)	$C_5H_8O_2$	0.65 ± 0.03	2.23 ± 0.04	255.5	2.11	•
p–terphenyl (doped with anthracene)	$C_{18}H_{14}$	0.8 ± 0.02	1.43 ± 0.01	277.5	1.47	♦
p–terphenyl (doped with chrysene)	$C_{18}H_{14}$	0.83 ± 0.02	1.16 ± 0.01	274.6	1.18	▽

for molecular volumes can be obtained by considering each constituent atom as a sphere defined by the *Van der Waals radius*.

As already pointed out in our previous work[38], the best way to compare experimental data on *o*-Ps pick–off lifetimes $\tau_{po} = 1/\lambda_{\mathrm{po}}$ from different materials, with the corresponding quantity calculated with our model, is to normalize this lifetimes with respect to the electron density (evaluated with the procedure explained below) by defining the quantity $\tau' = \tau_{po}\,\rho_e/\kappa_0$, as suggested directly by the general expression 2.5 for λ_{po}. Then this quantity retains the relevant information on the system. In Tab. 3.1 we report data on Van der Waals radii for relevant atomic elements, together with chemical formulae and calculated electron densities for some molecular solids of interest. In order to estimate the electron density of a specific material, we used the simple relation:

$$\rho_e = \frac{Z_{\mathrm{eff}}}{V} \tag{3.21}$$

where $V = \frac{4\pi}{3} R^3_{\mathrm{vdw}}$ is the volume relative to the *Van der Waals radius* of an atom.

3.2 Variational method

To numerically solve the full Schrödinger equation of the system we used the Ritz variational method to find an approximated ground state wavefunction. The method consists of choosing a basis set of parameter-dependent trial wavefunctions $\Psi_n[\epsilon]$, and finding the linear combination $\tilde{\Psi} = \sum_n C_n \Psi_n[\epsilon]$ for which the expectation value of the energy $\left\langle \tilde{\Psi} \middle| \tilde{H} \middle| \tilde{\Psi} \right\rangle$ is the lowest possible. As it is well known, the variational method deeply relies on the choice of the basis set, which must be done wisely. These wavefunctions can be quite general and parameter dependent but they must satisfy the correct boundary conditions of the problem.

Following Fülöp et al.[40] and inspired by the form of the wavefunctions of H_0 (see eq. (3.12)) we introduce the following ansatz for the basis set:

$$\Psi_{ijk}[\epsilon](r_e, r, \alpha) = \psi^{(1)}_i(r_e) \cdot \psi^{(2)}_j(r) \cdot \psi^{(3)}_k(\alpha) \tag{3.22}$$

The three components are given by

$$\begin{aligned} \psi_i^{(1)}(r_e) &= (R_c^2 - r_e^2)^i \quad i = (1, \cdots, N_1) \\ \psi_j^{(2)}(r) &= r^{j-1} e^{-r/\epsilon} \quad j = (1, \cdots, N_2) \\ \psi_k^{(3)}(\alpha) &= \cos^{k-1}\alpha \quad k(1, \cdots, j) \end{aligned} \tag{3.23}$$

where N_1 and N_2 determine the size of the basis expansion while the condition $k \leq j$ must be present in order to make the wavefunction single-valued everywhere. The polynomial expression of $\psi^{(1)}$ makes numerical calculation faster and is suggested by the Taylor expansion of the particle-in-a-box ground state $\sin(\pi r_e/R_c)/r_e$ (see Appendix A). Also note that the correct boundary conditions for the electron wavefunctions are satisfied: $\psi_i^{(1)}(R_c) = 0$ and $\frac{d\psi^{(1)}}{dr_e}(0) = 0$. On the other hand, the form of $\psi^{(2)}$ resembles the radial part of the well known hydrogenic wavefunctions. Here ϵ is an additional adjustable parameter, representing the possibility of a homogeneous swelling of the Bohr Ps radius (for free Ps, $\epsilon = 2a_B$), and with respect to which the energy is also minimized. Finally, $\psi^{(3)}$ accounts in a simple way for possible polarization effects. These functions are neither normalized nor orthogonal. However, the variational method with minor theoretical modifications can be applied also with a non orthogonal basis set.

Our total trial wavefunction can be expanded on this basis set:

$$\tilde{\Psi} = \sum_i^{N_1} \sum_j^{N_2} \sum_{k \leq j} C_{ijk} \Psi_{ijk}[\epsilon] \tag{3.24}$$

The energy minimization requires the calculation of the hamiltonian matrix

$$H^{\epsilon}_{nn'} = \langle \Psi_{ijk} | \, \tilde{H} \, | \Psi_{i'j'k'} \rangle \tag{3.25}$$

as well as the overlap matrix

$$S^{\epsilon}_{nn'} = \langle \Psi_{ijk} | \Psi_{i'j'k'} \rangle \tag{3.26}$$

for every value of the parameter ϵ. Due to the simple form of the basis functions, $(H_{\text{conf}})^{\epsilon}_{nn'}$ matrix elements can be calculated analytically, however $(V_{\text{bulk}})_{nm}$ must be calculated numerically.

We performed the analytical calculation with Mathematica 10 and we subsequently evaluated the numerical solution of the eigenproblem with a C++ code. For every set of (R_c, ϕ_+), the lowest eigenvalue was minimized as a function of ϵ to obtain the ground-state energy E_{GS}, and the eigenvector $\tilde{\Psi}$ corresponding to this eigenvalue was determined to be the approximate ground-state wavefunction. Finally, the relative contact density and the pickoff lifetime was calculated from $\tilde{\Psi}$.

3.3 Numerical results

Here we discuss the obtained results with reference to selected suitable values for the work function and cavity radius. Generally speaking, for the calculation of the energy, a base functions set of $N_1 = 3, N_2 = 3$ was sufficient, while the contact density and the pickoff annihilation rate calculations required more care. For relatively low values of ϕ_+ (below 5.9eV) a base functions set of $N_1 = 5, N_2 = 5$ already gives good results, in the

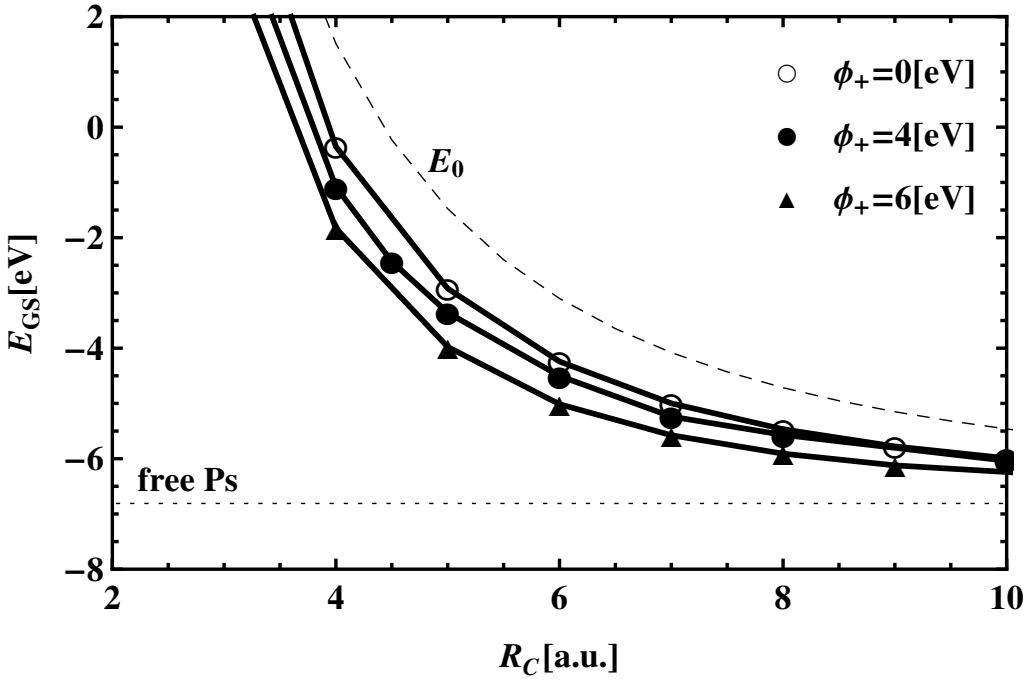

Figure 3.2: Ground state energy as a function of the cavity radius R_c (in atomic units), for different values of the positron work function ϕ_+. The straight dotted line represents the energy of free Ps in vacuum (-6.8eV) while the dashed line marked E_0 represents the exact ground state energy of H_0. In the limit $R_c \to \infty$ the energy of free Ps is recovered. Picture taken from [39].

sense that any further increase of this number has a negligible influence on the calculated values of $E_{\rm GS}, k_r, \lambda_{\rm po}$. It turns out that in order to fit almost all available experimental data, this range of values for the positron work function is sufficient. On the other side, for greater values of ϕ_+ the behavior of the wavefunction started to change drastically and the number of basis set needed to reach the same accuracy increase exponentially, making it manifest the need of a modified basis set. Anyway, during our calculations we decide to use a basis set with $N_1 = 6, N_2 = 6$. The resulting ground state energy energy is plotted in Fig 3.2 as a function of the confining radius R_c in atomic units ($R_c = 1$ corresponds to the value of the Hydrogen Bohr radius). For large radii, free Ps energy of -6.8eV is recovered. The confinement tends to increase the energy with respect to free Ps, while the bulk potential has a lesser effect.

The mixing term $V_{\rm mix}$ in (3.9) leads to a distortion of the relative wavefunction of the positron around the electron position. As plotted in Fig 3.3, the positron is strongly polarized toward the inner of the cavity via $\boldsymbol{\nabla}_{r_e} \cdot \boldsymbol{\nabla}_r$, while its attraction toward the outer bulk is mainly due to $V_{\rm bulk}$.

In fig. 3.4 we plot a section of the electron radial probability $P(r_e)$ defined as :

$$P(r_e) = \int |\Psi(r_e, r, \alpha)|^2 r^2 \sin\alpha \, dr \, d\alpha \tag{3.27}$$

It can be seen that an increase in the strength of $V_{\rm bulk}$ results in the electron being attracted to the cavity walls.

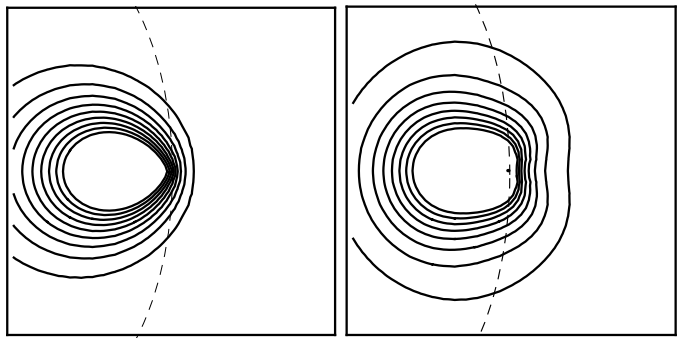

(a) $\phi_+ = 0$eV **(b)** $\phi_+ = 6$eV

Figure 3.3: Polarization of the relative wavefunction of the positron around the electron, for a cavity $R_c = 5$ a.u.. The electron position is fixed at the wall of the cavity, which is located on the left side of both figures.

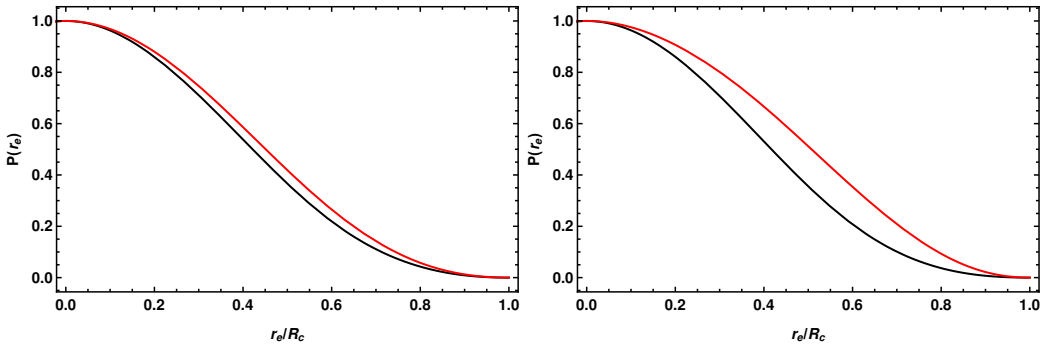

(a) $R_c = 5(a.u.)$ **(b)** $R_c = 10(a.u.)$

Figure 3.4: Electron radial probability $P(r_e)$ for a cavity with $R_c = 5$ a.u.(left) and $R_c = 10$ a.u.(right) as a function of the electron radial position r_e/R_c. To provide a better comparison, functions are arbitrarily renormalized to have $P(0) = 1$. The dark lines correspond to $\phi_+ = 0$ eV while the red ones correspond to $\phi_+ = 6$ eV. The effect of the bulk potential is to increase the probability of finding the electron near the walls.

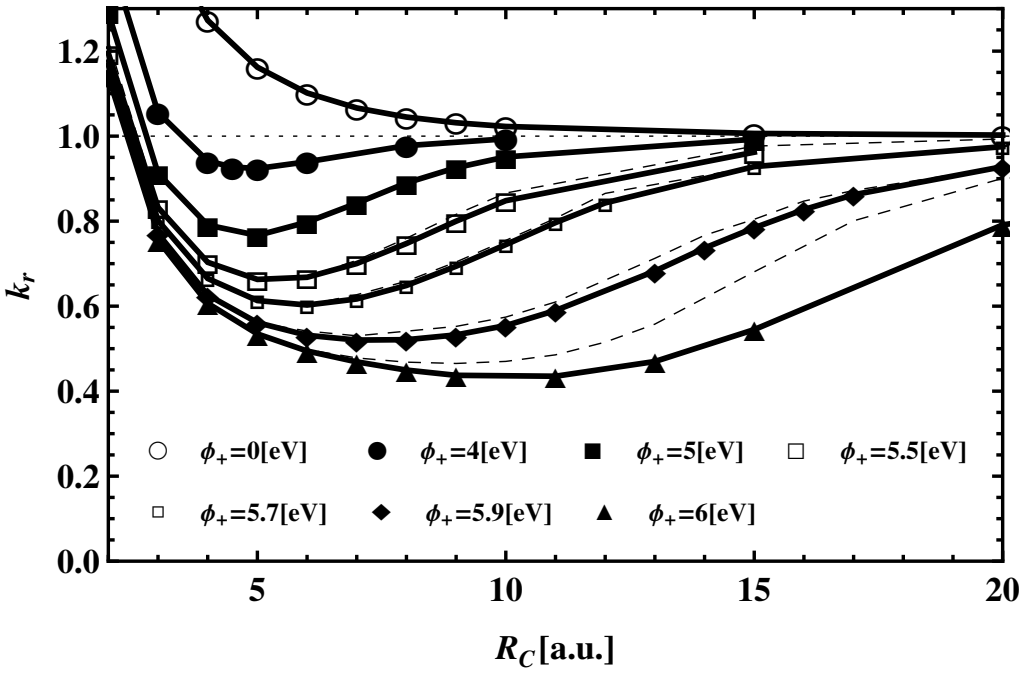

Figure 3.5: Relative contact density k_r as a function of the confining radius R_c, for some values of the positron work function ϕ_+. Full lines are calculated with the basis set $N_1 = 6, N_2 = 6$, while the dashed lines are calculated with the basis $N_1 = 5, N_2 = 5$. The distance between those lines can be considered as a raw error estimation. Picture taken from [39].

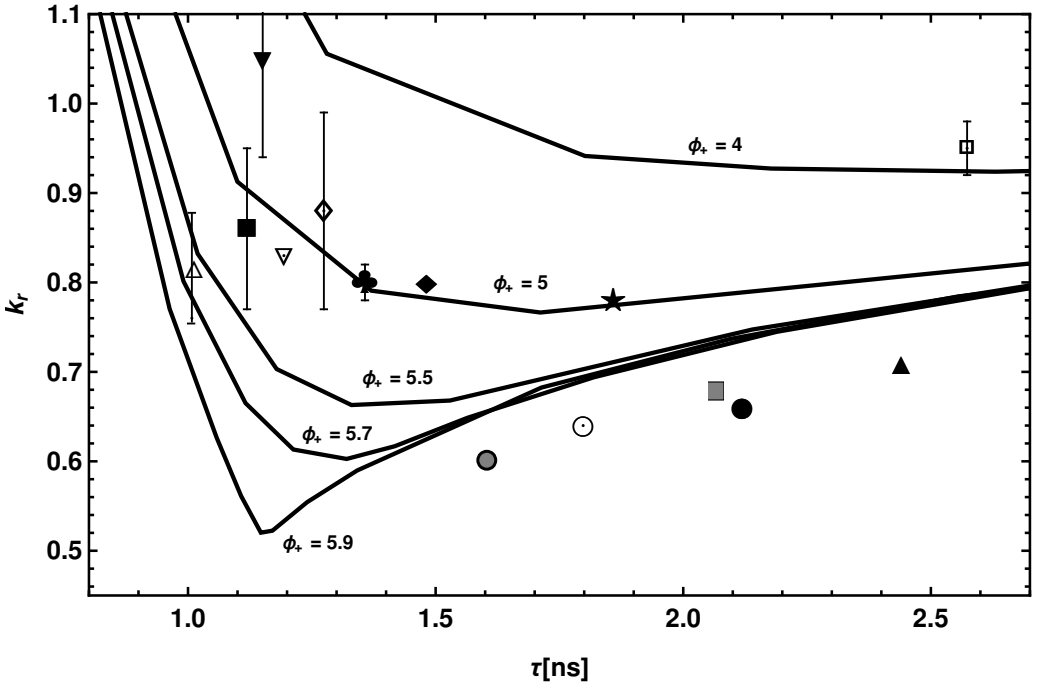

Figure 3.6: Relative contact density k_r of Ps as a function of its lifetime τ, for different values of the positron work function ϕ_+(in eV). Selected lines are calculated with the basis set $N_1 = 6, N_2 = 6$.

The resulting relative contact density k_r is plotted in Fig. 3.5 as a function of the confining radius R_c and for some values of the positron work function ϕ_+. The effect of lowering of the contact density, with respect to its vacuum value, shows up when $\phi_+ > 3$eV. This value is slightly larger than the results found in our previous work [38], but the qualitative trend is recovered. In the point cavity limit $R_c \to 0$ the electron is stuck at the origin and the Schrödinger equation of the hydrogen atom is recovered, where $k_r \to 8$. On the other hand when $R_c \to \infty$ free Ps solution is recovered, with $k_r \to 1$.

Experimental data for Ps in small cavities usually directly concern the *o*-Ps lifetime $\tau = \frac{1}{\lambda_{\text{po}}}$. In Fig. 3.6 we plot some curves joining points corresponding to calculated values of k_r and τ for a fixed ϕ_+ and different R_c.

Known experimental data for some materials are normalized as we discussed before Eq. 3.21, and are indicated by markers in Fig. 3.6. It must be noted that this kind of representation is the better choice to compare theoretical and experimental data, because it is very difficult to gain independent information on the positron work function and on the pore sizes for most materials. The general trend shows a lowering of the contact density and of the o-Ps lifetime for smaller cavities, as expected. There is a good agreement between our theory and experimental data for a large group of hydrocarbon molecular solids. On the other hand, some compounds stand below the line $\phi_+ \sim 6$eV, probably because their effective electron density is lower than our estimation, so that their position in the picture should be shifted to the left.

3.4 QMC calculation

To confirm numerical results obtained with the variational method, we performed PIMC calculation as discussed in Sec. 2.2.4.

We followed the same approach recently used by L.Larrimore et all [73] in a study of Ps confined within a spherical cavity, the only difference from this being the fact that in our model the infinite step potential is felt by the electron only, then the expression of matrix elements of the density operator reads:

$$\begin{aligned}&\langle \boldsymbol{r}_+\boldsymbol{r}_-|\,\hat{\rho}_{\text{conf}}(\epsilon)\,|\boldsymbol{r}'_+\boldsymbol{r}'_-\rangle = \\ &= \begin{cases} 1-\exp(-\dfrac{(r_c^2-r_-^2)(r_c^2-r_-^{'2})}{2\epsilon r_c^2}) & \text{if } r_- \le r_c \\ 0 \qquad \text{otherwise} \end{cases}\end{aligned} \tag{3.28}$$

For the bulk potential part of the density operator we used the symmetrical primitive approximation:

$$\langle \boldsymbol{r}_+\boldsymbol{r}_-|\,\hat{\rho}_{\text{bulk}}(\epsilon)\,|\boldsymbol{r}'_+\boldsymbol{r}'_-\rangle = \exp(-\epsilon\frac{V_{\text{bulk}}(\boldsymbol{r}_+)+V_{\text{bulk}}(\boldsymbol{r}'_+)}{2}) \tag{3.29}$$

To avoid possible problems due to ionization and to speed up the convergence of the calculation we also introduced a fictitious confinement potential of the form (3.28) to keep the positron inside a sphere of radius $Rc_{\text{max}} >> Rc$.

The set of moves used in our Metropolis code comprehend the exact sampling of the kinetic energy through the Levy construction and a rigid translation which improve the sampling of the potentials.

Our calculations used a chain of $M = 1000$ beads with $\beta = 100$a.u.. Such large M is required in order to keep discretization parameter $\epsilon = \frac{\beta}{M}$ reasonably small for values of β^{-1} much less than $3/16$, the Ps ground to-first-excited state energy gap. Several million steps were simulated to accumulate statistics in order to obtain accurate values (within 1%)of the probability distributions of $\boldsymbol{r}_e, \boldsymbol{r}_p$ and r.

The contact density k_r was found by a fitting procedure of the relative probability distribution while the probability of finding the positron outside the cavity could be easily obtained by the tail of the radial probability distribution.

To better understand the effects of the confining and bulk potentials, in Fig. 3.7 we plotted the probability distribution of the relative distance r between the electron and the positron, for two values of cavity radius and two different positron work functions. In the top panel we chose a very small cavity radius $R_c = 3$a.u. to make the confining effect evident, while we used a bigger $R_c = 7$a.u. in the bottom one. In both pictures, the black dashed lines represent the free-Ps 1S relative distribution, as given in Eq. 1.10. It is clear that the confining potential tend to squeeze the radial distribution, hence enhancing its contact density value with respect to the free case. This effect becomes relevant only in very small cavities, and it almost disappears for $R_c > 7$a.u.. The effect due to the bulk potential is exactly the opposite: a higher value of the positron work function (red lines) leads to a stronger potential, which in turn tends to swell the wavefunction reducing the contact density.

Some insight on pickoff annihilation rates comes from viewing the distribution functions of the radial distances r_p and r_e of the two particles from the center of the cavity as plotted in Fig. 3.8. Again, two values of cavity radius are used (top,bottom) together with two different positron work functions (blue,red). Whereas electronic density is close to

the distribution of a single particle in a hard cavity (black dashed line), this is not true for the positron, which can be easily found in bulk, i.e. in the region where pickoff process naturally occurs. This loosely confinement of the positron is only due to its coulomb attraction to the inner electron and it is opposed by the bulk potential, which pulls the positron outside the cavity wall. To provide a further comparison, we plotted the radial distribution as given by the TE model, where Ps center of mass is confined in a cavity of radius $R_c + \Delta$, with $\Delta = 0.16$nm. In both cases, a small value of the positron work function is enough to raise the probability of finding the positron in a pickoff region way larger than the one used in TE.

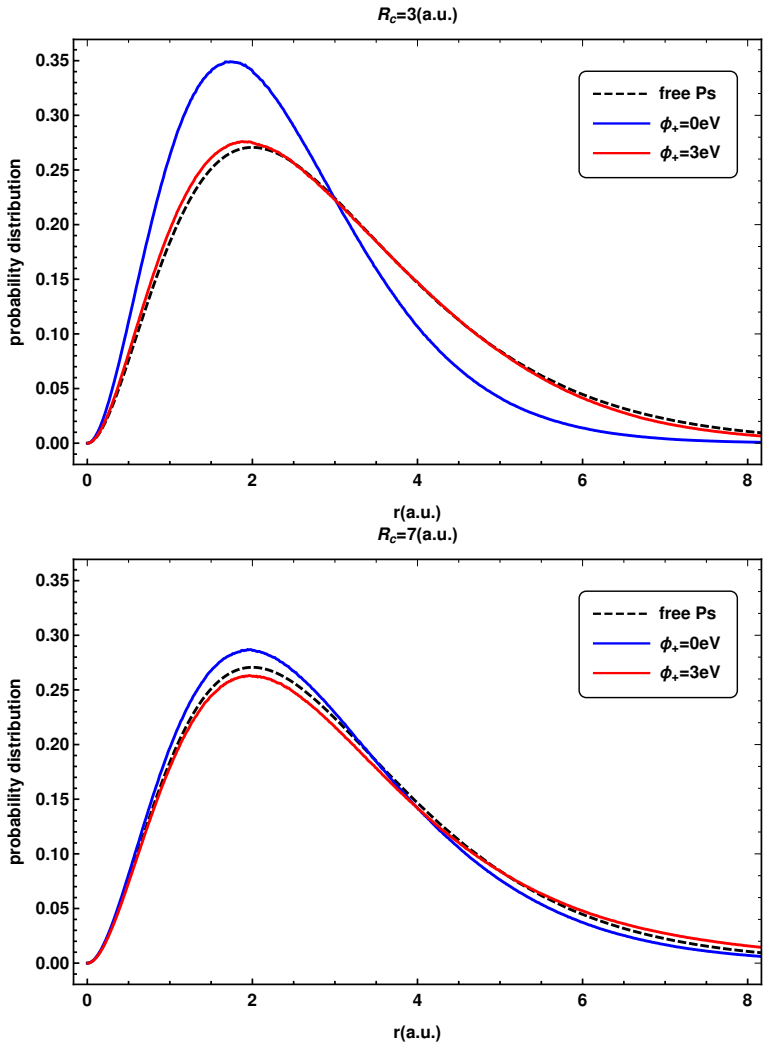

Figure 3.7: Radial distribution function of the relative distance r between the electron and the positron, for a cavity $R_c = 3$a.u. (top) and $R_c = 7$a.u. (bottom). The black dashed lines represent the same quantity for the 1S solution of free Ps in vacuum. Blue lines refer to the vanishing bulk potential solution with $\phi_+ = 0$eV. Red lines show the effect of adding a bulk potential term with $\phi_+ = 3$eV. It is clear that the confinement tends to squeeze the electron and the positron together while the bulk potential tends to pull them apart. Calculations were done with $M = 1000$, $\beta = 100$.

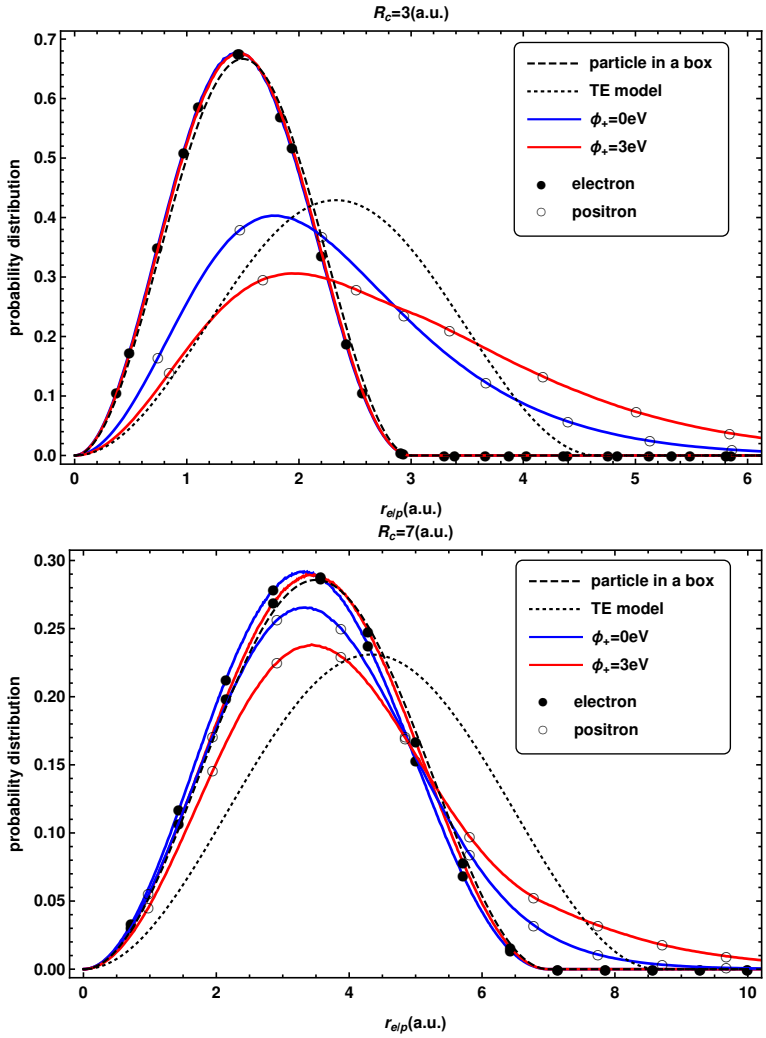

Figure 3.8: Distribution function of the radial distance $r_e(r_p)$ of the electron (positron) from the center of the cavity, for a cavity radius $R_c = 3$a.u. (top) and $R_c = 7$a.u. (bottom). The black dashed lines represent the same quantity for a particle in a spherical box with the same radius. Straight lines represent to the electron, while dashed are used for the positron. Blue lines refer to the vanishing bulk potential solution with $\phi_+ = 0$eV. Red lines show the effect of adding a bulk potential term with $\phi_+ = 3$eV. While the electron is strictly confined inside the cavity, the positron wavefunction spread out towards bulk. As a general trend, the higher the positron work function, the more probable is to find the positron outside R_c. Calculations were done with $M = 1000$, $\beta = 100$.

CHAPTER 4

Exchange effects on trapped Ps

In the context of Ps confinement in porous materials, it has long been assumed in literature that the interaction with surrounding electrons can be described as a small perturbation. This assumption is implicitly at the basis of every one-body and two-body theoretical models, where the introduction of an external electron layer accounts for pickoff annihilation but does not modify the nature and the form of Ps wavefunction. From another point of view, given the small energy gain in the Ps^- formation, Ps may not change significantly the spatial part of the N-electron wavefunction of the surrounding material, so that the two subsystems can be treated as independent.

Through PALS experiments, hints of Ps presence as a bound state can be deduced in materials showing different lifetime signatures, being this a direct evidence of the presence of different Ps states. In this sense, a description of a Ps atom weakly interacting with the environment is suggested in porous materials. However, this may not always be appropriate while, on the other hand, a more refined description of this kind of interactions is made complicated by the requirement of full electron indistinguishability. The validity of a theoretical treatment in which the Ps is seen as a separate "entity" and where the Ps electron is somehow privileged with respect to outer electrons must be questioned, especially given its direct relation to the pickoff annihilation.

In this chapter we will focus on a particular aspect of this problem, which we call "over-counting" and which is involved in the study of the annihilation process of Ps in cavities. Our ultimate goal is the formulation of a model better capable of explaining both the lowering of the contact density and the pickoff process, thus providing a simple tool to analyze the full spectrum of a PALS experiment.

4.1 The over-counting problem

As we saw in the first two chapters, the most common set of equations used to describe Ps annihilation in porous matter is given in literature by Eqs. 1.28:

$$\lambda_t = k_r \lambda_{3\gamma} + \lambda_{\mathrm{po}} \tag{4.1a}$$

$$\lambda_s = k_r \lambda_{2\gamma} + \lambda_{\mathrm{po}} \tag{4.1b}$$

These equations are considered valid when Ps interactions with external electrons and ions, which leads to pickoff annihilation, do not change significantly its wavefunction, i.e. its identity as a confined bound system.

For long time it has been thought of k_r, the usual relative contact density, as an intrinsic property of the confined Ps, whereas the term λ_{po}, which is identical in both Eq. 4.1a and 4.1b, was associated to the pickoff annihilation process with outer electrons. Given

that pickoff is by nature a *surface* process, in every model λ_{po} was assumed to be proportional to a geometrical probability, commonly denoted by P_{out}, of finding Ps outside the free-space (*inner*) region defining the cavity.

$$\lambda_{\text{po}} = P_{\text{out}}\lambda_b \tag{4.2}$$

In TE for example we saw that the proportionality constant λ_b was fixed to the average of singlet and triplet decay rates $\bar{\lambda} = 2.01[\text{ns}]^{-1}$, a value used by many other authors, including us[1]:

$$\lambda_{\text{po}} = P_{\text{out}}\bar{\lambda} \tag{4.3}$$

Being independent of the electronic properties of the surrounding medium, such an assumption must be regarded as an effective approximation, which holds provided that the geometry of the model (i.e. the value of Δ in the TE) is consequently adapted to fit the correct pickoff annihilation in real systems[2].

It came to our attention that there are many different opinions about the proper way of treating Ps in the *inner* and *surface* regions.

In many works (for example [94, 95, 96]), Ps, described as a single particle with $k_r = 1$, is considered affected on the same foot by both the intrinsic and the pickoff annihilations in the outer part of the cavity:

$$\begin{aligned} \lambda_t &= \lambda_{3\gamma} + P_{\text{out}}\lambda_b \\ \lambda_s &= \lambda_{2\gamma} + P_{\text{out}}\lambda_b \end{aligned} \tag{4.4}$$

On the other hand, a few one-particle models (to our knowledge this was done only in [61, 97, 98]) completely differentiate the *inner* and *surface* description of Ps. In these, Ps annihilates with its intrinsic vacuum annihilation rate only in the *inner* part of the cavity, whereas the *surface* region is dominated by pickoff. Following Goworek[97], Eqs. 4.4 are written in this picture as:

$$\begin{aligned} \lambda_t &= (1 - P_{\text{out}})\lambda_{3\gamma} + P_{\text{out}}\lambda_b \\ \lambda_s &= (1 - P_{\text{out}})\lambda_{2\gamma} + P_{\text{out}}\lambda_b \end{aligned} \tag{4.5}$$

being $(1 - P_{\text{out}}) = P_{\text{in}}$ the probability of finding Ps in the free-space region. Remarkably, a direct comparison between Eqs. 4.1 and Eqs. 4.5 show that the latter have by construction a relative contact density $k_r = P_{\text{in}}$ lower than the vacuum value. This is a direct consequence of the fact that, in this model, k_r exactly vanishes in the *surface* region. Surprisingly, to our knowledge, this important connection has gone unnoticed by the author and by the positronium community until now. In [97] this was due to an erroneous interpretation of the contact density, while in [61] no considerations about the contact density were done at all.

Finally, a somehow intermediate situation is found in all two-particle models (for example [68, 38, 39]), where pickoff annihilation is proportional to the probability P^+_{out} of having the positron outside the cavity

$$\begin{aligned} \lambda_{\text{po}} &= \lambda_b P^+_{\text{out}} \\ P^+_{\text{out}} &= \int_{r_p > R_c} |\Psi(\boldsymbol{r}_p, \boldsymbol{r}_e)|^2 \, d^3 r_p \, d^3 r_e \end{aligned} \tag{4.6}$$

which is somehow similar to P_{out}. In these models, intrinsic annihilation is assumed to take place only in the region allowed to the Ps-electron, which, analogously to Eqs 4.4

[1] As noted in Sec. 1.5, this value is identical to the Ps^- decay rate.

[2] See Section. 2.1.1 for a more accurate discussion.

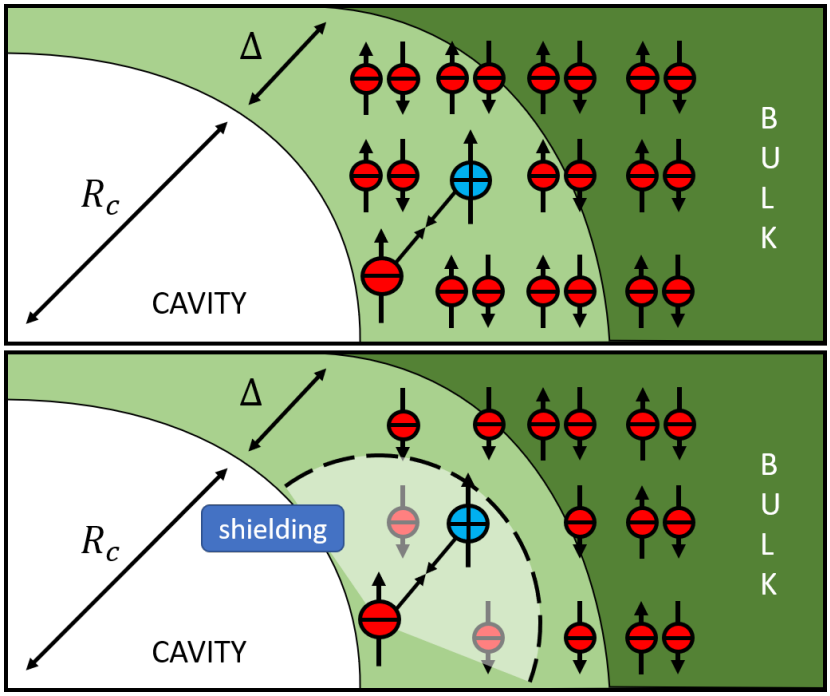

Figure 4.1: Effect of electron shielding on positron annihilation in bulk. Top: without shielding, the positron is free to annihilate with outer electrons of any spin configuration. Bottom: if shielding is considered, the positron will most likely annihilate with electrons having opposite spin with respect to Ps-electron.

and 4.5, can be either extended to the whole space [68] or limited to the *inner* cavity (if Ps-electron is striclty confined, like in [38]).

In our view, all these different approaches are due to a general confusion about the meaning of terms appearing in Eqs. 4.1. In particular, the fact that both the expressions for λ_t and λ_s in Eqs. 4.1 have the *same structure*, has been erroneously interpreted by some as the prove that *o*-Ps and *p*-Ps are affected by the *same pickoff annihilation rate*. In other words, it is assumed that the particular spin configuration of the Ps-electron does not affect in any way the pickoff annihilation behavior in the outer layer. As a direct consequence, the pickoff process was exclusively linked to the term $\lambda_{\rm po}$ in Eqs. 4.1, while k_r was associated to possible modifications of the internal structure of Ps.

In this picture, no "shielding" effect due to exchange correlation effects (Pauli exclusion) is ascribed to the Ps-electron, so that the positron is free to annihilate with all surrounding electrons (independently from their spin), with a consequent *over-counting* of annihilation processes inside the *surface* region (see Fig. 4.1).

Surprisingly, this no-shielding assumption was neither fully justified nor properly discussed from a theoretical point of view. The lack of such a discussion represents a minor problem to the positronium community since the over-counting has a negligible effect on the total annihilation rate of the *o*-Ps system, where $\lambda_{\rm po} \gg \lambda_{3\gamma}$. The same is not true for *p*-Ps , where pickoff and intrinsic annihilation rates may be comparable.

Given its connection to electrons indistinguishability, the question of whether this over-counting is legitimate or not must be answered in the framework of many-body

quantum mechanics. This will be given in detail in the following chapters, where we will show how the pickoff annihilation rate *is indeed different* for *o*-Ps and *p*-Ps . Here, we just note that this statement is not in contrast with Eqs. 4.1 as long as one realizes that they can be written as:

$$\lambda_t = \lambda_{3\gamma} + \left[(k_r - 1)\lambda_{3\gamma} + \lambda_{\rm po}\right] \tag{4.7a}$$

$$\lambda_s = \lambda_{2\gamma} + \left[(k_r - 1)\lambda_{2\gamma} + \lambda_{\rm po}\right] \tag{4.7b}$$

where the term in square brackets is the overall contribution to the annihilation due to the external electrons, i.e. the pickoff. This kind of formula has exactly the same form of the one that will be derived from the theory developed in the following Sections.

Before going on, we now review a discussion on the validity of Eqs. 4.1 which was given by Dupasquier et al. [9].

Trying to formulate a formal calculation of Ps annihilation, the most important feature on which the electron-positron annihilation process depends is the relative spin state of the two particles. Historically, spin is only taken into account when dealing with Ps in vacuum, while an averaged spin description is used for example in metals. There are just a few studies in literature which investigate how spin exchange affects intrinsic and pickoff annihilation rates for Ps confined inside a cavity.

In this framework, Brusa et al. [84] have studied the annihilation rate for a positron interacting with two unpaired-spin electrons in a close-shell environment. In their work they included exchange effects, hyperfine splitting and the coupling with an external magnetic field. Their numerical results depend on input parameters describing the form of the wavefunction called "symmetrized" electron-positron contact densities. However they keep a generic approach and do not give an explicit form for the spatial wavefunction.

A somehow similar approach was used by Dupasquier et al. [9] to extend the same formalism to a four particle system consisting of a Ps atom in a generic spin configuration χ_{jm} interacting with 2 electrons in a singlet state configuration χ_{00}. At variance with [84], in their work the authors didn't diagonalize any Hamiltonian to find a groundstate wavefunction, but instead they postulate its general form as a starting point. Focusing on the request of full exchange antisimmetry for the electrons, they introduced a total wavefunction of the form:

$$\begin{aligned}\Psi_{jm} =& \mathcal{A}\left[\phi(\boldsymbol{r}_p, \boldsymbol{r}_e; \boldsymbol{r}_1, \boldsymbol{r}_2)\chi_{jm}(p,e)\chi_{00}(1,2)\right] \\ =& \frac{1}{\sqrt{3}}\left[\phi(\boldsymbol{r}_p, \boldsymbol{r}_e; \boldsymbol{r}_1, \boldsymbol{r}_2)\chi_{jm}(p,e)\chi_{00}(1,2)\right. \\ & - \phi(\boldsymbol{r}_p, \boldsymbol{r}_1; \boldsymbol{r}_e, \boldsymbol{r}_2)\chi_{jm}(p,1)\chi_{00}(e,2) \\ & \left. -\phi(\boldsymbol{r}_p, \boldsymbol{r}_2; \boldsymbol{r}_1, \boldsymbol{r}_e)\chi_{jm}(p,2)\chi_{00}(1,e)\right]\end{aligned} \tag{4.8}$$

where $\mathcal{A}$ is the antisymmetrization operator, and calculate the expectation value of the annihilation operator 1.19. The main result of their calculation was to show that a common expression of both *o*-Ps and *p*-Ps pickoff annihilation rate can be given, which leads directly to the commonly accepted expression for Ps annihilation in matter:

$$\begin{aligned}\lambda_t &= k_r\lambda_{3\gamma} + \eta\bar{\lambda} \\ \lambda_s &= k_r\lambda_{2\gamma} + \eta\bar{\lambda}\end{aligned} \tag{4.9}$$

where the term proportional to $\bar{\lambda}$ depends on an "external" contact density parameter η related to the overlap between the positron and outer electrons. Explicit expressions for

k_r and η are:

$$\begin{aligned} k_r &= 8\pi a_0^3 \int |\phi(\boldsymbol{r}_p, \boldsymbol{r}_e; \boldsymbol{r}_1, \boldsymbol{r}_2)|^2 \delta^3(\boldsymbol{r}_p - \boldsymbol{r}_e)\, d^3r_p\, d^3r_e\, d^3r_1\, d^3r_2 \\ \eta &= 8\pi a_0^3 \int |\phi(\boldsymbol{r}_p, \boldsymbol{r}_1; \boldsymbol{r}_e, \boldsymbol{r}_2)|^2 \delta^3(\boldsymbol{r}_p - \boldsymbol{r}_e)\, d^3r_p\, d^3r_e\, d^3r_1\, d^3r_2 \end{aligned} \tag{4.10}$$

In their calculation, some "internal orthogonality" conditions (IO) on the 4 particles spatial wavefunction, which hides exchange terms, are imposed[3]:

$$\begin{aligned} &\int \phi(\boldsymbol{r}_p, \boldsymbol{r}_e; \boldsymbol{r}_1, \boldsymbol{r}_2)\delta^3(\boldsymbol{r}_p - \boldsymbol{r}_e)\phi(\boldsymbol{r}_p, \boldsymbol{r}_1; \boldsymbol{r}_2, \boldsymbol{r}_e)\, d^3r_p\, d^3r_e\, d^3r_1\, d^3r_2 = 0 \\ &\int \phi(\boldsymbol{r}_p, \boldsymbol{r}_e; \boldsymbol{r}_1, \boldsymbol{r}_2)\delta^3(\boldsymbol{r}_p - \boldsymbol{r}_e)\phi(\boldsymbol{r}_p, \boldsymbol{r}_2; \boldsymbol{r}_e, \boldsymbol{r}_1)\, d^3r_p\, d^3r_e\, d^3r_1\, d^3r_2 = 0 \end{aligned} \tag{4.11}$$

Because of these conditions, k_r and η in Eqs. 4.9 are both intrinsically connected to the presence of outer electrons, i.e. to the pickoff process. In particular, this means that the term $\lambda_{\text{po}} = \eta\bar{\lambda}$ alone is not representative of the whole process, being only its symmetrical contribution.

While we agree with their result, which however does not present the problem of over-counting by construction, we have some remarks on the interpretation and approach used to derive Eqs. 4.9.

First of all, in [9] the normalization condition of the total wavefunction is not explicitly taken into account. To us it is not clear whether the previously mentioned "internal orthogonality" conditions still hold adding this further requirement. We stress that, despite Eqs. 4.9 have been used by many authors for any form of Ps wavefunction, they are only valid when the total wavefunction satisfy Eqs. 4.11.

Secondly, as it will become clear in the next section[4], the form of 4.8 as it stands can not be related neither to a proper ground state, nor to a "first order" state. For this reason, while the evaluation of λ as a simple expectation value is theoretically valid for *any* quantum state, the connection of Eqs. 4.9 to the ground state annihilation rates is not fully justified.

In the next section, we will show how it's possible to provide a stronger theoretical approach and to extend their result to a system of Ps interacting with N electrons, by using a symmetry-adapted perturbation expansion.

4.2 Exchange perturbation theories

The detailed quantum state of an electron-positron pair inside a cavity is extremely complex. Whereas in the inner part of this free-space region it will resemble an isolate Ps bound state, in the outer part it will fade into a "spur state" (sometimes called quasi-Ps)[33] of a positron interacting with the full many-body environment. The main difficulty arises from the fact that in the first scenario one has a separate Ps-electron, while in the other full electron indistinguishability must be taken into account.

The formulation of a theoretical treatment capable of describing the transition between these two limiting situations is an old problem in both physics and chemistry.

[3] Even if this sounds somewhat arbitrary, they show how it is possible to build a wavefunction satisfying such conditions from a generic ground state.

[4] See the discussion following Eq.4.19.

There are many systems (for example atoms in molecules) wherein individual components are clearly identifiable and, in the non-interacting picture, may be described by an asymptotic-free hamiltonian H_0 where electrons are arbitrarily assigned to different subsystems. Since extramolecular interactions in these systems are often small compared with the low-lying intramolecular (or intraatomic or intraionic) level spacings, some sort of perturbative treatment based upon noninteracting components is suggested[99].

Historically, one of the first and most simple perturbation scheme is the so called *polarization approximation* (PA). In the PA for the interaction between two atoms, A and B, with total electron number N, one arbitrarily assigns electrons 1 through N_A to atom A, and N_A+1 through $N = N_A+N_B$ to B. If $H_A(H_B)$ is the Hamiltonian for atom $A(B)$ in the absence of $B(A)$ (i.e it operates only on the electronic coordinates assigned to A), the PA zero-order Hamiltonian H_0 is simply taken to be that for isolated sites $H_0 = H_A+H_B$, with no inter-site interaction[100]. The zero-order eigenstate is taken to be the Hartree product of isolated eigenstates $\psi^{(0)} = \phi_A\phi_B$, which in general has no symmetry for an interchange of coordinates between A and B. Given that V represents the interaction term between the two subsystems (hence the total Hamiltonian is $H = H_0 + V$), the basic assumption of PA is that a $\psi(\epsilon)$ exists such that:

$$[H_0 + \epsilon V]\,\psi(\epsilon) = E(\epsilon)\psi(\epsilon) \tag{4.12}$$

where both the energy and wavefunction can be expanded as a series of power of the perturbation parameter ϵ

$$\psi(\epsilon) = \sum_n \epsilon^n \psi^{(n)} \qquad \text{and} \qquad E(\epsilon) = \sum_n \epsilon^n E^{(n)} \tag{4.13}$$

in such a way that high order corrections to the wavefunction are orthogonal to the unperturbed solution

$$\left\langle \psi^{(0)} | \psi^{(n)} \right\rangle = 0 \qquad \text{for } n = 1, 2 \cdots \tag{4.14}$$

One expects that if the perturbation V is weak, then the expansion parameter ϵ smoothly links $\psi^{(0)}$ to $\psi(1)$ which must be an eigenfunction of the fully interacting H.

The expansion coefficients are then calculated with the standard framework of Rayleigh Schrödinger (RS) perturbation theory, for example:

$$E^{(1)} = \left\langle \psi^{(0)} \middle| V \middle| \psi^{(0)} \right\rangle \qquad \text{and} \qquad \left[H_0 - E^{(0)}\right] \psi^{(1)} = \left[E^{(1)} - V\right] \psi^{(0)} \tag{4.15}$$

However, it is clear that such a simplified approach can not give correct treatment of the exchange interactions since H_0, $H_0 + \epsilon V$ and $\psi^{(0)}$ have no symmetry under the interchange of pairs of electron coordinates belonging to different atoms, whereas $\psi(1)$ must be fully antisymmetric. This is a well known problem of PA which usually requires the introduction of so called unphysical states u_k which do not satisfy Pauli principle[101].

To overcome this problem, since the 1960s, a vast class of symmetry-adapted perturbation theory (SAPT) were proposed[102]. Most of these proposals agrees only on the first order expansion and they show qualitative differences even in low order[103]. An accurate review is beyond the scope of the present discussion and we report here only equations for the first order correction. In particular, in all SAPT formulations, the first order energy reads:

$$E^{(1)} = \frac{\left\langle \psi^{(0)} \middle| V \middle| \mathcal{A}\psi^{(0)} \right\rangle}{\left\langle \psi^{(0)} | \mathcal{A}\psi^{(0)} \right\rangle} \tag{4.16}$$

Here, $\mathcal{A}$ is an intermolecular antisymmetrizer operator, defined as[5]:

$$\mathcal{A} = \frac{1}{N!}\sum_{p}(-1)^p P \tag{4.17}$$

where P represents a permutation operator of N electrons, while $(-1)^p$ stands for the parity of the permutation. It's easy to see that $\mathcal{A}$ commutes with the total hamiltonian, but not with H_0 nor V :

$$[\mathcal{A}, H] = 0 \qquad [\mathcal{A}, H_0] \neq 0 \qquad [\mathcal{A}, V] \neq 0 \tag{4.18}$$

The factor $\left\langle \psi^{(0)} | \mathcal{A}\psi^{(0)} \right\rangle = \left\langle \psi^{(0)}\mathcal{A} | \mathcal{A}\psi^{(0)} \right\rangle$ at denominator of Eq. 4.16 explicitly takes into account the so-called intermediate-normalization condition[103].

On the other hand, first order correction to the state depends quite strongly on the chosen formalism[102]. As an example, with the choice given in [104]:

$$\psi^{(1)} = P\left[\epsilon O + P\left(E^{(1)} - H_0\right)P\right]^{-1} PH\mathcal{A}\psi^{(0)} \tag{4.19}$$

where $P = \left|\mathcal{A}\psi^{(0)}\right\rangle \left\langle \psi^{(0)}\right| / \left\langle \psi^{(0)} | \mathcal{A}\psi^{(0)} \right\rangle$ is the projector over the unperturbed state, $O = 1 - P$ is the orthogonal complement and ϵ is a small real number which makes sure that the operator in square brackets is invertible.

We stress that in SAPT context the antisymmetric state $\left|\mathcal{A}\psi^{(0)}\right\rangle$ is *not* the first order correction to the state, nor it can be considered a good ground state for the full hamiltonian H. This is particularly true if the product state $\psi^{(0)}$ already contains some kind of overlap between the subsystems.

4.3 Setting up the Ps-environment system

Now we proceed towards a suitable setting up of the Ps-environment system. The most general Hamiltonian of a system composed of a Ps atom interacting with an N-electron environment can be written as a sum of a free Ps Hamiltonian $\hat{H}^{(0)}_{\mathrm{Ps}}$, the Hamiltonian of the material $\hat{H}_b$ and an interaction potential acting between these two subsystems. Considering only Coulomb interactions and neglecting atomic nuclei, which are not involved in the annihilation process, we write $\hat{H}$ as:

$$\begin{aligned}\hat{H} &= \hat{H}^{(0)}_{\mathrm{Ps}}(\boldsymbol{r}_p, \boldsymbol{r}_e) + \hat{H}_b(\boldsymbol{r}_1, \boldsymbol{r}_2, \cdots, \boldsymbol{r}_N) + \sum_{i=1}^{N}\left[\hat{V}_{\mathrm{C}}(\boldsymbol{r}_e, \boldsymbol{r}_i) - \hat{V}_{\mathrm{C}}(\boldsymbol{r}_p, \boldsymbol{r}_i)\right] \\ &\equiv \hat{H}^{(0)}_{\mathrm{Ps}}(\boldsymbol{r}_p, \boldsymbol{r}_e) + \hat{H}_b(\boldsymbol{r}_1, \boldsymbol{r}_2, \cdots, \boldsymbol{r}_N) + \sum_{i=1}^{N}\hat{V}_{\mathrm{int}}(\boldsymbol{r}_p, \boldsymbol{r}_e, \boldsymbol{r}_i)\end{aligned} \tag{4.20}$$

where $\hat{V}_{\mathrm{C}}(\boldsymbol{r}_x, \boldsymbol{r}_y)$ is the Coulomb potential between the particles x and y. In the following we will denote p and e the spin-spatial coordinates of the Ps positron and electron (as defined is Section 1.1.2), respectively, while numbers refers to other electrons for convenience.

From the success of many theoretical models describing Ps in porous materials, we know that the overall effect of interactions can be well described by an effective potential

[5] With this definition, $\mathcal{A}$ is idempotent, i.e. $\mathcal{A}^2 = \mathcal{A}$.

$\hat{V}_{\text{eff}}(\boldsymbol{r}_p, \boldsymbol{r}_e)$ which acts only on Ps spatial coordinates. Despite this potential can be found in different formulations in literature, the most important feature they all share is the confining effect. As an example, in TE model $\hat{V}_{\text{eff}}(\boldsymbol{r}_p, \boldsymbol{r}_e) = \hat{V}_{\text{conf}}(\boldsymbol{R})$, being $\boldsymbol{R}$ the center of mass, while in our first model we used $\hat{V}_{\text{eff}}(\boldsymbol{r}_p, \boldsymbol{r}_e) = \hat{V}_{\text{conf}}(\boldsymbol{r}_e) + \hat{V}_{\text{bulk}}(\boldsymbol{r}_p)$.

Hence, it is convenient to include this generic potential in the definition of the Ps hamiltonian, so that Eq. 4.20 becomes:

$$\begin{aligned} \hat{H} &= \hat{H}_{\text{Ps}}(\boldsymbol{r}_p, \boldsymbol{r}_e) + \hat{H}_b(\boldsymbol{r}_1, \boldsymbol{r}_2, \cdots, \boldsymbol{r}_N) + \left[\sum_{i=1}^{N} \hat{V}_{\text{int}}(\boldsymbol{r}_p, \boldsymbol{r}_e, \boldsymbol{r}_i) - \hat{V}_{\text{eff}}(\boldsymbol{r}_p, \boldsymbol{r}_e) \right] \\ &\equiv \hat{H}_{\text{Ps}}(\boldsymbol{r}_p, \boldsymbol{r}_e) + \hat{H}_b(\boldsymbol{r}_1, \boldsymbol{r}_2, \cdots, \boldsymbol{r}_N) + \hat{V} \end{aligned} \tag{4.21}$$

where $\hat{H}_{\text{Ps}} = \hat{H}_{\text{Ps}}^{(0)} + \hat{V}_{\text{eff}}$.

If we neglect all interactions, hamiltonian 4.21 is separable and its ground state will be the product of the wavefunction of the bare wavefunction of the confined Ps (see Chapters 2 ,3) times the (antisymmetric) ground state of the N-electron system:

$$\begin{aligned} \psi^{(0)}(p, e, 1, \cdots, N) &= \Psi_{jm}(p, e)\phi(1, 2, \cdots, N) \\ &= \Psi_{jm}(p, e)\phi(\bar{b}) \end{aligned} \tag{4.22}$$

where j, m are the Ps spin $|S|^2$ and spin projection S_z quantum number ($j = 1$ for *o*-Ps and $j = 0$ for *p*-Ps). We used the symbol $\bar{b}$ to represent in a compact notation the vector of the N spin-space coordinates of external electrons. The wavefunction of the system $\psi^{(0)}(p, e; \bar{b})$ is by construction antisymmetric with respect to the exchange of two electrons in $\bar{b}$ since

$$\phi(b_1, \cdots, b_i, \cdots, b_j, \cdots, b_N) = -\phi(b_1, \cdots, b_j, \cdots, b_i, \cdots, b_N) \tag{4.23}$$

but it is not antisymmetric with respect to the exchange with Ps electron.

We introduce now some quantities which are usually well-known and will ease the notation in the following discussion. The external electron density is connected to the square modulus of the N-electron normalized wavefunction and it is defined as

$$n(\boldsymbol{r}) = N \sum_{\sigma_1} \int |\phi(\boldsymbol{r}, \sigma_1, 2, \cdots, N)|^2 \, d2 \cdots dN \tag{4.24}$$

We have used the compact notation $\int di = \sum_{\sigma_i} \int d^3 r_i$ to represent both spin summation and spatial integration. For simplicity in writing, in the following we may omit to specify integration variables di and domain when these are evident.

A powerful concept used in many body physics is that associated with reduced density matrices(RDM). RDM offer an intuitive way of describing the internal structure of a many body system of N indistinguishable particles without the complete knowledge of its wavefunction. The term "reduced" refers to the fact that attention is focused on a reduced number of electrons (or atom or molecule..) independently from positions of all the others. From a mathematical point of view, this means that the density matrix of the total system must be averaged over all coordinates except those of interest.

The simplest RDM is the one body reduced density matrix (1RDM), which is defined as:

$$\Gamma^{(1)}(x; y) \equiv N \int \phi(x, 2, \cdots, N)\phi^*(y, 2, \cdots, N) \, d2 \cdots dN \tag{4.25}$$

The 1RDM has in principle 4 components $\Gamma^{(1)}_{\uparrow\uparrow}$, $\Gamma^{(1)}_{\uparrow\downarrow}$, $\Gamma^{(1)}_{\downarrow\uparrow}$ and $\Gamma^{(1)}_{\downarrow\downarrow}$ resulting from expansion in a complete set of spin functions:

$$\Gamma^{(1)}(x;y) = \sum_{ij} \Gamma^{(1)}_{ij}(\boldsymbol{r}_x;\boldsymbol{r}_y) s_i(\sigma_x) s^*_j(\sigma_y) \tag{4.26}$$

where i and j may represent $\uparrow$ or $\downarrow$ spin states. Furthermore, we can define the spatial 1RDM integrating $\Gamma^{(1)}$ over the spin variables:

$$\begin{aligned}\Gamma^{(1)}(\boldsymbol{r}_x;\boldsymbol{r}_y) =& \sum_{\sigma_x,\sigma_y}\sum_{ij} \Gamma^{(1)}_{ij}(\boldsymbol{r}_x;\boldsymbol{r}_y) s_i(\sigma_x) s_j(\sigma_y) \\ =& N \sum_{\sigma_x,\sigma_y} \int \phi(\boldsymbol{r}_x,\sigma_x,2,\cdots,N)\phi^*(\boldsymbol{r}_y,\sigma_y,2,\cdots,N)\, d2\cdots dN\end{aligned} \tag{4.27}$$

In general, if no spin mixing potential appears in the hamiltonian of the bulk system, the wavefunction ϕ is an eigenstate of S_z and the two spin channels decouple, so that $\Gamma^{(1)}_{\uparrow\downarrow} = \Gamma^{(1)}_{\downarrow\uparrow} = 0$ and [105]:

$$\Gamma^{(1)}(\boldsymbol{r}_x;\boldsymbol{r}_y) = \Gamma^{(1)}_{\uparrow\uparrow}(\boldsymbol{r}_x;\boldsymbol{r}_y) + \Gamma^{(1)}_{\downarrow\downarrow}(\boldsymbol{r}_x;\boldsymbol{r}_y) \tag{4.28}$$

Finally, the diagonal part of the spatial 1RDM is just the electron density defined in Eq. 4.24:

$$n(\boldsymbol{r}) = \Gamma^{(1)}(\boldsymbol{r};\boldsymbol{r}) = n_\uparrow(\boldsymbol{r}) + n_\downarrow(\boldsymbol{r}) \tag{4.29}$$

We also introduce in a similar way the 1RDM of the Ps system, as the result of integration over the positron coordinate:

$$\Gamma^{(1)}_{\mathrm{Ps}}(1;2) \equiv \int \Psi^*_{jm}(p,2)\Psi_{jm}(p,1)\, dp \tag{4.30}$$

Another useful quantity is the two body reduced density matrix (2RDM), defined as:

$$\Gamma^{(2)}(x,x';y,y') \equiv \binom{N}{2} \int \phi(x,x',3,\cdots,N)\phi^*(y,y',3,\cdots,N)\, d3\cdots dN \tag{4.31}$$

which also can be expanded over a complete set of spin functions, with a total of 16 components:

$$\Gamma^{(2)}(x,x';y,y') = \sum_{ij,i'j'} \Gamma^{(2)}_{iji'j'}(\boldsymbol{r}_x,\boldsymbol{r}_{x'};\boldsymbol{r}_y,\boldsymbol{r}_{y'}) s_i(\sigma_x) s_j(\sigma_{x'}) s^*_{i'}(\sigma_y) s^*_{j'}(\sigma_{y'}) \tag{4.32}$$

As for spatial 1RDM, spatial 2RDM is introduced by integrating $\Gamma^{(2)}$ over the spin variables σ_x, $\sigma_{x'}$, σ_y and $\sigma_{y'}$. The diagonal part of the spatial 2RDM, $\Gamma^{(2)}(\boldsymbol{r}_x,\boldsymbol{r}_y;\boldsymbol{r}_x,\boldsymbol{r}_y) = P(\boldsymbol{r}_x,\boldsymbol{r}_y)$, is the pair distribution function, proportional to the conditional probability of having an electron in $\boldsymbol{r}_y$ given that another one is in $\boldsymbol{r}_x$. Given that correlation between two electrons vanish at long distances, in this limit they become independent and it is well known that $P(\boldsymbol{r}_x,\boldsymbol{r}_y)$satisfies the condition:

$$P(\boldsymbol{r}_x,\boldsymbol{r}_y) \approx n(\boldsymbol{r}_x)n(\boldsymbol{r}_y) \qquad \text{when} \qquad |\boldsymbol{r}_x - \boldsymbol{r}_y| \to \infty \tag{4.33}$$

On the other hand, the probability of having two electrons very close to each other is strongly suppressed in real systems by both the Pauli exclusion (if they have the same spin) and by the strong Coulomb repulsion.

When Ps approaches the electronic system, its wavefunction will begin to "overlap" with the system's one and exchange correlation effects must be considered. In this sense it is useful to introduce a parameter S to quantify this overlap. In the following, we will refer to S as "exchange overlap" and its definition reads:

$$\begin{aligned} S &= \sum_{i=1}^{N} \int \Psi^*_{jm}(p,e)\phi^*(i,2,\cdots,N)\Psi_{jm}(p,i)\phi(e,2,\cdots,N)\, dp\, de \cdots dN \\ &= N \int \Psi^*_{jm}(p,e)\phi^*(1,2,\cdots,N)\Psi_{jm}(p,1)\phi(e,2,\cdots,N)\, dp\, de \cdots dN \\ &= \int \Psi^*_{jm}(p,e)\Psi_{jm}(p,1)\Gamma^{(1)}(e;1)\, dp\, de\, d1 \\ &= \int \Gamma^{(1)}_{\mathrm{Ps}}(1;e)\Gamma^{(1)}(e;1)\, de\, d1 \end{aligned} \tag{4.34}$$

where we used the antisymmetry properties of the wavefunctions. In the following, we will assume that it is still correct to consider Ps as a perturbed singlet or triplet state as long as the exchange overlap is smaller than unity $S \ll 1$.

We anticipate here that assuming a Ps confined *a priori* in a certain free space (cavity) means that the interaction with the external electrons will take place only in limited surface domain so that the support of integral 4.34 is small by construction. The overlap S depends mainly on the electron density n_0 and, as we will see later, on a *geometrical parameter* representing the probability of having the two subsystems in the interacting region. To keep the notation of the TE model we may refer to this parameter as $P_{\mathrm{out}} \in [0,1]$. In terms of this parameter, the limit $P_{\mathrm{out}} = 1$ represents a fully-interacting regime where the Ps wave function completely overlap with the external electron density, while the opposite limit $P_{\mathrm{out}} = 0$ corresponds to Ps in vacuum, where the ground state is (almost) degenerate with respect to the internal spin configuration and Ps can be projected on a specif triplet/singlet state.

4.4 Perturbative approach to annihilation rate

As we saw in Sec. 1.2, the annihilation process can be formally described as the effect of an imaginary potential term which accounts for particle loss. This peculiar characteristic of the annihilation operator makes possible its description in terms of imaginary part of the energy of the system. In particular, the first order correction to the annihilation rate can thus be derived from the (imaginary part of) first order correction to energy. This correction can in turn be calculated in SAPT framework using Eq. 4.16, with just the knowledge of the unperturbed ground state of the system [6].

To take advantage of SAPT description, we introduce the absorption potential described in 1.18 in the expression of the total Hamiltonian 4.21:

$$\hat{H} = \hat{H}_{\mathrm{Ps}}(\boldsymbol{r}_p, \boldsymbol{r}_e) - i\frac{\hbar}{2}\hat{\lambda}_e + \hat{H}_b(\boldsymbol{r}_1, \boldsymbol{r}_2, \cdots, \boldsymbol{r}_N) + \left[\hat{V} - i\frac{\hbar}{2}\sum_{i=1}^{N}\hat{\lambda}_i\right] \tag{4.35}$$

where we have separated the *intrinsic* annihilation term due to the Ps electron e from the pickoff annihilations coming from the other N electrons. It is now straightforward

[6] This is not restricted to SAPT but it is also true for standard RS perturbation theory. It is a well-known fact that the first order correction in energy is given by $E^{(1)} = \langle \psi^{(0)} | V | \psi^{(0)} \rangle$ and does not require the calculation of the first order correction to the ground state $|\psi^{(1)}\rangle$.

to calculate the total annihilation rate for Ps

$$\lambda = \lambda^{(0)} + \lambda^{(1)} \tag{4.36}$$

where the zero-order term is simply the *intrinsic* annihilation rate, which does not depends on external electrons

$$\begin{aligned}\lambda^{(0)} &= \left\langle \psi^{(0)}_{jm} \right| \hat{\lambda}_e \left| \psi^{(0)}_{jm} \right\rangle \\ &\equiv \langle \Psi_{jm} | \, \hat{\lambda}_e \, | \Psi_{jm} \rangle \\ &= 8\pi a_0^3 \int |\Psi_{jm}(p,p)|^2 \begin{cases} \lambda_{2\gamma} & \text{if } j=0 \text{ (p-Ps)} \\ \lambda_{3\gamma} & \text{if } j=1 \text{ (o-Ps)} \end{cases}\end{aligned} \tag{4.37}$$

while the first-order correction represents the pickoff contribution coming from Eq. 4.16:

$$\lambda^{(1)} = \frac{\left\langle \psi^{(0)}_{jm} \right| \sum_{i=1}^{N} \hat{\lambda}_i \left| \mathcal{A}\psi^{(0)}_{jm} \right\rangle}{\left\langle \psi^{(0)}_{jm} | \mathcal{A}\psi^{(0)}_{jm} \right\rangle} \tag{4.38}$$

Explicitly, using the definition given in Eq. 4.17, we have[7]:

$$\begin{aligned}\left| \mathcal{A}\psi^{(0)}_{jm} \right\rangle =& \frac{1}{(N+1)} \left[\Psi_{jm}(p,e)\phi(1,2,\cdots,N) \right. \\ & \left. - \sum_{i=1}^{N} \Psi_{jm}(p,i)\phi(1,\cdots,i-1,e,i+1,\cdots,N) \right] \\ \left\langle \psi^{(0)}_{jm} | \mathcal{A}\psi^{(0)}_{jm} \right\rangle =& \frac{\mathcal{N}}{N+1}\end{aligned} \tag{4.39}$$

where the factor $(N+1)$ at the denominator is the total number of extra permutations of the Ps electron, while $\mathcal{N}$ depends only on the overlap S:

$$\begin{aligned}\mathcal{N} &= 1 - N\Re \int \Psi^*_{jm}(p,e)\phi^*(1,2,\cdots,N)\Psi_{jm}(p,1)\phi(e,2,\cdots,N) \\ &= 1 - \int \Psi^*_{jm}(p,e)\Psi_{jm}(p,1)\Gamma^{(1)}(e;1) \\ &= 1 - S\end{aligned} \tag{4.40}$$

From now on we will focus on *o*-Ps , so that we fix $\{jm\} = \{11\}$ for simplicity, but analogous calculation can be done for *p*-Ps . Taking $\mathcal{N}$ on the left side of Eq. 4.38, this

[7]Note that ${}_* \left\langle \mathcal{A}\psi^{(0)} | \mathcal{A}\psi^{(0)} \right\rangle_* \neq 1$

last one becomes:

$$\begin{aligned}
\mathcal{N}\lambda^{(1)} =& \int \Psi^*(p,e)\phi^*(1,2,\cdots,N)\sum_{i=1}^{N}\hat{\lambda}_i \\
& [\Psi(p,e)\phi(1,2,\cdots,N) - \Psi(p,1)\phi(e,2,\cdots,N) - \Psi(p,2)\phi(1,e,\cdots,N)\cdots] \\
=& \int \Psi^*(p,e)\phi^*(1,2,\cdots,N)\sum_{i=1}^{N}\hat{\lambda}_i\Psi(p,e)\phi(1,2,\cdots,N) \\
& - \int \Psi^*(p,e)\phi^*(1,2,\cdots,N)\sum_{i=1}^{N}\hat{\lambda}_i\Psi(p,1)\phi(e,2,\cdots,N) \\
& - \int \Psi^*(p,e)\phi^*(1,2,\cdots,N)\sum_{i=1}^{N}\hat{\lambda}_i\Psi(p,2)\phi(1,e,\cdots,N) \\
& - \cdots \\
=& N\int \Psi^*(p,e)\phi^*(1,2,\cdots,N)\hat{\lambda}_1\Psi(p,e)\phi(1,2,\cdots,N) \\
& - N\int \Psi^*(p,e)\phi^*(1,2,\cdots,N)\hat{\lambda}_1\Psi(p,1)\phi(e,2,\cdots,N) \\
& - \binom{N}{2}2\int \Psi^*(p,e)\phi^*(1,2,\cdots,N)\hat{\lambda}_1\Psi(p,2)\phi(1,e,\cdots,N)
\end{aligned} \tag{4.41}$$

where we have used the antisymmetric property of ϕ to group together terms corresponding to the same contribution The last line of Eq 4.41 shows that the correction to the annihilation rate is the sum of 3 different terms:

$$\mathcal{N}\lambda^{(1)} = \lambda_{\text{po}} + \lambda_{\text{ex}} + \lambda_{\text{ex-po}} \tag{4.42}$$

The first contribution λ_{po} represent an *external* annihilation, which has the same expression of the "standard" pickoff annihilation rate[8]. To show that, we write λ_{po} separating the spatial and spin part and using the electron density representation over the single particle spin basis as described in Eqs. 4.24 and 4.29[9]:

$$\begin{aligned}
\lambda_{\text{po}} =& \int |\Psi(\boldsymbol{r}_p,\boldsymbol{r}_e)|^2 n_\uparrow(\boldsymbol{r}_1)\left[\chi_{11}(\sigma_p,\sigma_e)s_\uparrow(\sigma_1)\hat{\lambda}_1\chi_{11}(\sigma_p,\sigma_e)s_\uparrow(\sigma_1)\right] \\
& + \int |\Psi(\boldsymbol{r}_p,\boldsymbol{r}_e)|^2 n_\downarrow(\boldsymbol{r}_1)\left[\chi_{11}(\sigma_p,\sigma_e)s_\downarrow(\sigma_1)\hat{\lambda}_1\chi_{11}(\sigma_p,\sigma_e)s_\downarrow(\sigma_1)\right] \\
=& 8\pi a_0^3 \int |\Psi(\boldsymbol{r}_p,\boldsymbol{r}_e)|^2\delta(\boldsymbol{r}_1-\boldsymbol{r}_p)\left[\lambda_{3\gamma}n_\uparrow(\boldsymbol{r}_1) + \frac{\lambda_{2\gamma}+\lambda_{3\gamma}}{2}n_\downarrow(\boldsymbol{r}_1)\right] \\
=& 8\pi a_0^3\bar{\lambda}\int |\Psi(\boldsymbol{r}_p,\boldsymbol{r}_e)|^2 n(\boldsymbol{r}_p)\,d^3r_p\,d^3r_e
\end{aligned} \tag{4.43}$$

where we have assumed uniform spin distribution of the outer electrons, which implies

[8] As already discussed in Section 4.1, the symbol λ_{po} represents only the *symmetric* part of the pickoff annihilation, whereas the full pickoff annihilation, which is given by $\lambda^{(1)}$, has different expressions for *o*-Ps and *p*-Ps states.

[9] Despite here we're dealng only with the $m = 1$ component of *o*-Ps , an identical expression for λ_{po} is obtained starting from any Ps state.

that the local spin-up(down) electron density satisfies:

$$n_\uparrow(\boldsymbol{r}) = n_\downarrow(\boldsymbol{r}) = \frac{1}{2} n(\boldsymbol{r}) \tag{4.44}$$

and $\bar{\lambda}$ is the spin averaged annihilation rate defined in 1.6. In the second line, the expectation value of the spin exchange operator inside $\hat{\lambda}_1$ has been obtained expanding the spin part over the eigenstates of $\Sigma_{p,1}$ using the identities (see Appendix B):

$$\begin{aligned}
\chi_{11}(\sigma_p,\sigma_e)s_\uparrow(\sigma_1) &= \chi_{11}(\sigma_p,\sigma_1)s_\uparrow(\sigma_e) \\
\chi_{11}(\sigma_p,\sigma_e)s_\downarrow(\sigma_1) &= \frac{1}{\sqrt{2}}\left[\chi_{00}(\sigma_p,\sigma_1) + \chi_{1,0}(\sigma_p,\sigma_1)\right] s_\uparrow(\sigma_e) \\
\chi_{00}(\sigma_p,\sigma_e)s_\uparrow(\sigma_1) &= \frac{1}{\sqrt{2}}\left[\chi_{11}(\sigma_p,\sigma_1)s_\downarrow(\sigma_e) + \frac{1}{\sqrt{2}}\left(\chi_{00}(\sigma_p,\sigma_1) - \chi_{10}(\sigma_p,\sigma_1)\right) s_\uparrow(\sigma_e)\right] \\
\chi_{00}(\sigma_p,\sigma_e)s_\downarrow(\sigma_1) &= \frac{1}{\sqrt{2}}\left[-\chi_{1-1}(\sigma_p,\sigma_1)s_\uparrow(\sigma_e) + \frac{1}{\sqrt{2}}\left(\chi_{00}(\sigma_p,\sigma_1) + \chi_{10}(\sigma_p,\sigma_1)\right) s_\downarrow(\sigma_e)\right]
\end{aligned} \tag{4.45}$$

The last two identities are written for completeness, because are useful in the analogue calculation on the *p*-Ps state (which however gives the same result).

The second and last integrals λ_{ex} and $\lambda_{\text{ex-po}}$ in 4.41 are exchange contributions to annihilation. In λ_{ex} the annihilation operator directly acts on the Ps spin wavefunction, so that the remaining spin sum is easily performed. It can be shown that only one contribution remains for *o*-Ps , which can be written in a simpler form using the definition of the one-body reduced density matrix Eq. 4.25:

$$\begin{aligned}
\lambda_{\text{ex}} =& -N \sum_{\sigma_p,\sigma_1,\sigma_e} \int \Psi^*(\boldsymbol{r}_p,\boldsymbol{r}_e)\Psi(\boldsymbol{r}_p,\boldsymbol{r}_1)\phi^*(\boldsymbol{r}_1,\sigma_1,2,\cdots,N)\phi(\boldsymbol{r}_e,\sigma_e,2,\cdots,N) \\
&\times \left[\chi_{11}(\sigma_p,\sigma_e)\hat{\lambda}_1\chi_{11}(\sigma_p,\sigma_1)\right] d^3r_p\, d^3r_e\, d^3r_1\, d2\cdots dN \\
=& -8\pi a_0^3 \lambda_{3\gamma} \int \Psi^*(\boldsymbol{r}_p,\boldsymbol{r}_e)\Psi(\boldsymbol{r}_p,\boldsymbol{r}_p)\Gamma^{(1)}_{\uparrow\uparrow}(\boldsymbol{r}_e;\boldsymbol{r}_p)\, d^3r_p\, d^3r_e
\end{aligned} \tag{4.46}$$

For *p*-Ps λ_{ex} has the same expression of the equation above after substituting $\lambda_{3\gamma}$ with $\lambda_{2\gamma}$ (this is a consequence of the uniform spin distribution and the fact that $\Gamma^{(1)}_{\uparrow\uparrow} = \Gamma^{(1)}_{\downarrow\downarrow}$).

Finally, the last integral in 4.41 is an exchange-correlation contribution to annihilation which depends on the two body reduced density matrix of the system $\Gamma^{(2)}$. The expectation value of the annihilation operator can be calculated using the spin expansion of $\Gamma^{(2)}$ described in Eq. 4.32, so that $\lambda_{\text{ex-po}}$ becomes a sum over $2^4 = 16$ terms with different spin configurations.

$$\begin{aligned}
\lambda_{\text{ex-po}} =& -2 \sum_{ij,i'j'} \sum_{\sigma_e\sigma_p}^{\sigma_1,\sigma_2} \int d^3r_p\, d^3r_e\, d^3r_1\, d^3r_2 \\
&\times \Psi^*(\boldsymbol{r}_p,\boldsymbol{r}_e)\Psi(\boldsymbol{r}_p,\boldsymbol{r}_2)\Gamma^{(2)}_{iji'j'}(\boldsymbol{r}_1,\boldsymbol{r}_e;\boldsymbol{r}_1,\boldsymbol{r}_2) \\
&\times \left[\chi_{11}(\sigma_p,\sigma_e)s_i(\sigma_1)s_j(\sigma_2)\hat{\lambda}_1\chi_{11}(\sigma_p,\sigma_2)s_{i'}(\sigma_1)s_{j'}(\sigma_e)\right]
\end{aligned} \tag{4.47}$$

After some algebra, using the identities reported in Appendix B, one gets only two non-

vanishing contributions for *o*-Ps :

$$\begin{aligned}\lambda_{\text{ex-po}} = &-2(8\pi a_0^3)\int d^3r_p\, d^3r_e\, d^3r_2 \Psi^*(\boldsymbol{r}_p,\boldsymbol{r}_e)\Psi(\boldsymbol{r}_p,\boldsymbol{r}_2)\\ &\times\left[\lambda_{3\gamma}\Gamma^{(2)}_{\uparrow\uparrow\uparrow\uparrow}(\boldsymbol{r}_p,\boldsymbol{r}_e;\boldsymbol{r}_p,\boldsymbol{r}_2)+\frac{\lambda_{2\gamma}+\lambda_{3\gamma}}{2}\Gamma^{(2)}_{\downarrow\uparrow\downarrow\uparrow}(\boldsymbol{r}_p,\boldsymbol{r}_e;\boldsymbol{r}_p,\boldsymbol{r}_2)\right]\end{aligned} \tag{4.48}$$

With the same reasoning, but slightly more lengthy calculations, similar expressions can be easily obtain for the other *o*-Ps configurations and, in particular, for *p*-Ps one obtains:

$$\begin{aligned}\lambda_{\text{ex-po}} = &-2(8\pi a_0^3)\int d^3r_p\, d^3r_e\, d^3r_2 \Psi^*(\boldsymbol{r}_p,\boldsymbol{r}_e)\Psi(\boldsymbol{r}_p,\boldsymbol{r}_2)\\ &\times\left[\frac{\lambda_{2\gamma}+\lambda_{3\gamma}}{2}\frac{1}{2}\left[\Gamma^{(2)}_{\uparrow\uparrow\uparrow\uparrow}(\boldsymbol{r}_p,\boldsymbol{r}_e;\boldsymbol{r}_p,\boldsymbol{r}_2)+\Gamma^{(2)}_{\downarrow\downarrow\downarrow\downarrow}(\boldsymbol{r}_p,\boldsymbol{r}_e;\boldsymbol{r}_p,\boldsymbol{r}_2)\right]\right.\\ &+\frac{\lambda_{2\gamma}-\lambda_{3\gamma}}{2}\frac{1}{2}\left[\Gamma^{(2)}_{\uparrow\downarrow\downarrow\uparrow}(\boldsymbol{r}_p,\boldsymbol{r}_e;\boldsymbol{r}_p,\boldsymbol{r}_2)+\Gamma^{(2)}_{\downarrow\uparrow\uparrow\downarrow}(\boldsymbol{r}_p,\boldsymbol{r}_e;\boldsymbol{r}_p,\boldsymbol{r}_2)\right]\\ &\left.+\lambda_{3\gamma}\frac{1}{2}\left[\Gamma^{(2)}_{\uparrow\downarrow\uparrow\downarrow}(\boldsymbol{r}_p,\boldsymbol{r}_e;\boldsymbol{r}_p,\boldsymbol{r}_2)+\Gamma^{(2)}_{\downarrow\uparrow\downarrow\uparrow}(\boldsymbol{r}_p,\boldsymbol{r}_e;\boldsymbol{r}_p,\boldsymbol{r}_2)\right]\right]\end{aligned} \tag{4.49}$$

Up to this point, the only assumption we made about the system interacting with Ps is that of uniform spin distribution (Eq 4.44), a condition which translates in the absence of local spin polarization near the cavity region. In particular, no assumption on the form of ϕ has been done so that the formulation of the annihilation rate as given in Eq. 4.42 is completely general. To provide more physical insight we need to introduce further approximations.

In the next section we will introduce LDA formalism to a simplified model which enables us to provide explicit expressions for the electron density and $\Gamma^{(1)}$.

4.5 Local density approximation

To find accurate expressions of the electron density and reduced density matrices of a N electron system is a cumbersome task which requires expensive numerical calculations and, moreover, have to be related to the specific crystalline structure and composition of the medium under consideration. In order to maintain a general approach in our discussion, we need to introduce some kind of approximations.

In condensed matter physics, one of the simplest approaches used to describe exchange correlation effects in metals is the homogeneous electron gas (HEG, also known as Jellium) approximation. In HEG, electrons move in a uniform positive charge distribution which simulates the ionic background, whence the electron density is a uniform quantity as well. Even in the absence of interactions, i.e. considering a free electron gas, this model is capable of showing the formation of exchange correlation "holes" due to electron indistinguishability. The peculiarity of the non-interacting HEG is that both $1RDM$ and $2RDM$ are well known and have a simple analytical expression. In particular, for a paramagnetic non-interacting HEG of constant electron density ρ_e, the ground state is best described using Restricted Hartree Fock (RHF) formalism, i.e. as a single

Slater determinant, and the following relations are valid[106]:

$$\begin{aligned} n(\boldsymbol{r}) &= \rho_e \\ n_\uparrow(\boldsymbol{r}) = n_\downarrow(\boldsymbol{r}) &= \frac{1}{2}\rho_e \\ \Gamma^{(1)}(x;y) &= \delta_{\sigma_x\sigma_y}\frac{\rho_e}{2}B(k_F|\boldsymbol{r}_x - \boldsymbol{r}_y|) \end{aligned} \tag{4.50}$$

where

$$B(x) = 3\frac{\sin(x) - x\cos(x)}{x^3} \tag{4.51}$$

with $\rho_e = \frac{(k_F)^3}{3\pi^2}$ and k_F is the Fermi momentum. Eq. 4.50 implies that $\Gamma^{(1)}$ is diagonal in the spin space and its components are equally given by:

$$\Gamma^{(1)}_{\uparrow\uparrow}(\boldsymbol{r}_x;\boldsymbol{r}_y) = \Gamma^{(1)}_{\downarrow\downarrow}(\boldsymbol{r}_x;\boldsymbol{r}_y) = \frac{\rho_e}{2}B(k_F|\boldsymbol{r}_x - \boldsymbol{r}_y|) \tag{4.52}$$

The function $B(x)$ is plotted in Fig. 4.2. It satisfies $B(0) = 1$ at the origin and it exponentially decays to zero on a length $\sigma^2 = 5/k_F^2$, as shown by a fit of its first order expansion:

$$B(r) = 1 - \frac{k_F^2 r^2}{10} + o(r^2) \approx \exp\left[-\frac{k_F^2 r^2}{10}\right] \tag{4.53}$$

We note also that another important relation exists which connects $\Gamma^{(2)}$ to $\Gamma^{(1)}$ and holds for states described by a single Slater determinant:

$$\Gamma^{(2)}(x,x';y,y') = \frac{1}{2}\left[\Gamma^{(1)}(x;y)\Gamma^{(1)}(x';y') - \Gamma^{(1)}(x';y)\Gamma^{(1)}(x;y')\right] \tag{4.54}$$

Moreover, taking the diagonal part $\Gamma^{(2)}(x,y;x,y)$ and summing over spin, the famous result for the pair density function of a noninteracting gas is found:

$$P(r = |\boldsymbol{x} - \boldsymbol{y}|) = \rho_e^2\left[1 - \frac{1}{2}B(k_F r)^2\right] \tag{4.55}$$

which is plotted in Fig. 4.3. In particular, the probability of finding two electron at the same position is given by $P(0) = \frac{1}{2}\rho_e^2$. The one half factor is easily understood since half the electrons have parallel spin, so the exclusion principle prevents them to be at the same position. However, it is well known that the form 4.55 strongly overestimates $P(r)$ at short distances with respect to real systems, where Coulomb repulsion plays an important role in keeping electrons separated. As an example, for a fully interacting electron gas, it is found[107]:

$$P(0) = \frac{32}{(8 + 3r_s + \frac{383}{1200}r_s^2)^2}\rho_e^2 \tag{4.56}$$

being r_s the electron gas parameter (see Eq. 2.47). As shown in Fig. 4.4, this value is considerably smaller than $1/2$ and vanishes in the low density limit.

Going back to the general problem, knowledge of expressions 4.50, which are uniquely determined by the value of ρ_e, suggests that it is possible to approximately describe some properties of a real system knowing its electron density function only. Since the

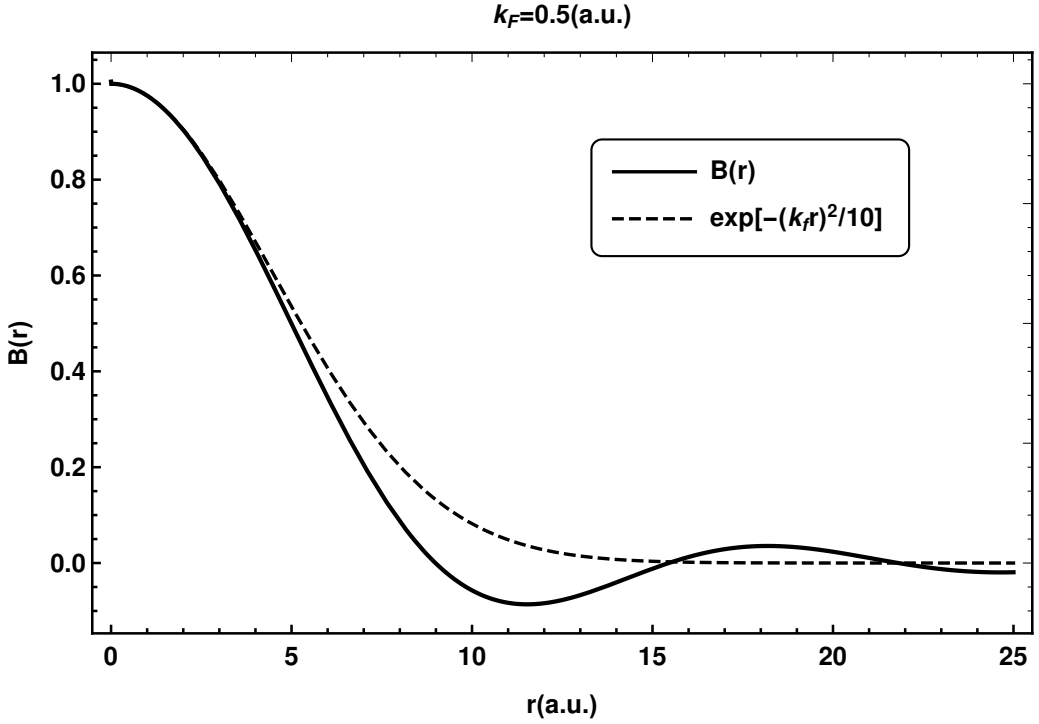

Figure 4.2: The function $B(r)$ and its exponential approximation as given in Eq. 4.53, for $k_F = 0.5$ atomic units. The main difference is the cutting off of the long range oscillations, while there's a good agreement at short range.

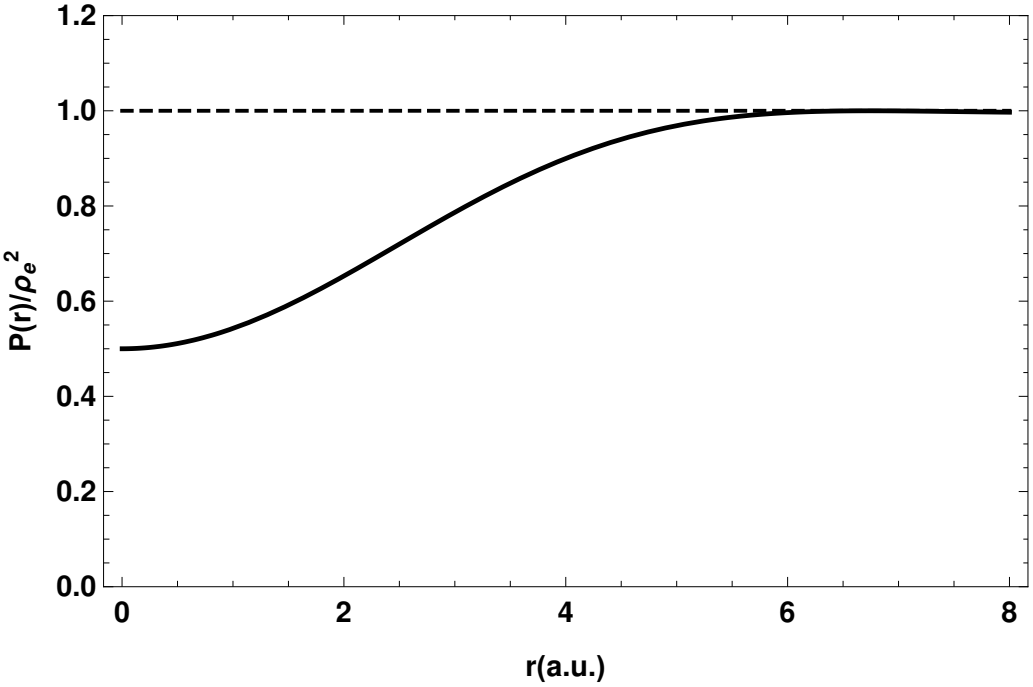

Figure 4.3: The normalized pair density $\frac{P(r)}{\rho_e^2}$ as a function of the radial distances between two electrons r for a reference electron density value of $\rho_e = k_0/4$. For comparison, the dotted line represents the case of independent particles.

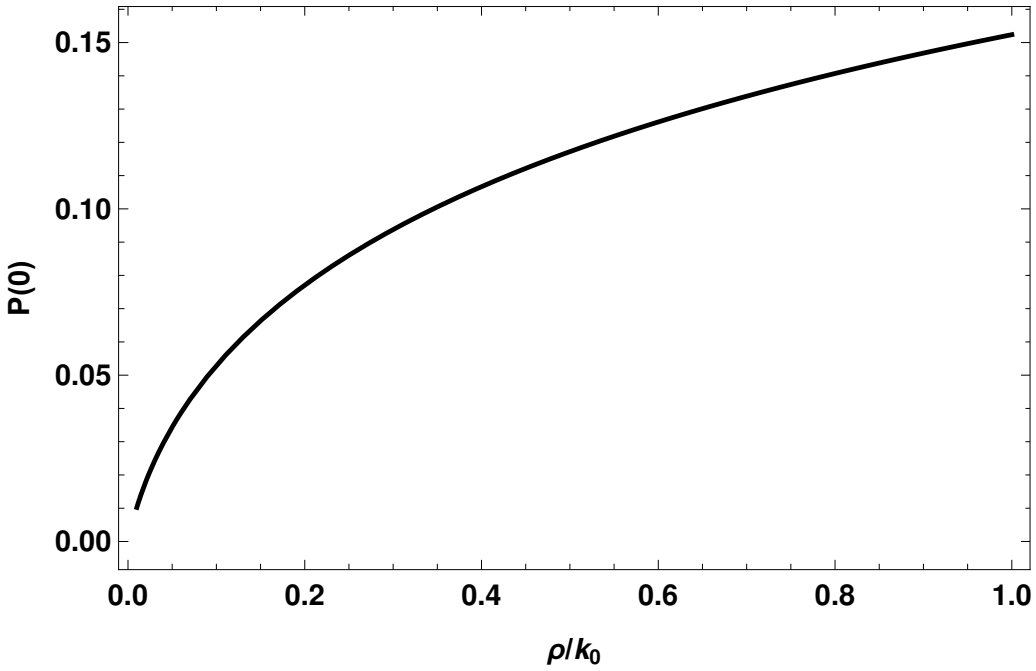

Figure 4.4: The normalized pair density at zero distance $P(0)/\rho_e^2$ for an interacting electron gas as a function of electron density.

determination of a realistic density profile is outside the scope of the current theoretical treatment, we will just assume for the moment that it can be described by a suitable function $n(\boldsymbol{r})$, postponing the discussion about its qualitative form to next section.

Given $n(\boldsymbol{r})$, we can extend the 1RDM definition in Eq. 4.50 by using the so called local density approximation (LDA). In LDA, the properties of an electronic system are locally modeled at $\boldsymbol{r}$ as given by a free electron gas with density $n(\boldsymbol{r})$. In this simple model, the 1RDM can be written using the density evaluated in the middle point as [106]:

$$\begin{aligned} \Gamma^{(1)}(x;y) &= \delta_{\sigma_x\sigma_y}\frac{n(\boldsymbol{R}_{xy})}{2}B\big(k_F(\boldsymbol{R}_{xy})\,|\boldsymbol{r}_{xy}|\big) \\ \Gamma^{(1)}(\boldsymbol{R}_{xy};\boldsymbol{r}_{xy}) &= \Gamma^{(1)}_{\uparrow\uparrow}(\boldsymbol{R}_{xy};\boldsymbol{r}_{xy}) + \Gamma^{(1)}_{\downarrow\downarrow}(\boldsymbol{R}_{xy};\boldsymbol{r}_{xy}) \\ k_F(\boldsymbol{R}_{xy}) &= \big(3\pi^2 n(\boldsymbol{R}_{xy})\big)^{1/3} \end{aligned} \tag{4.57}$$

where a local fermi momentum $k_F(\boldsymbol{r})$ is introduced in a natural way. In Eq. 4.57 and in the following we have used the notation

$$\begin{aligned} \boldsymbol{R}_{xy} &= \frac{\boldsymbol{x}+\boldsymbol{y}}{2} \\ \boldsymbol{r}_{xy} &= \boldsymbol{x}-\boldsymbol{y} \end{aligned} \tag{4.58}$$

to denote the average and the relative position of two particles x and y, respectively.

Whereas the LDA extension of 1RDM is successfully used in standard DFT calculations, the same result does not hold for the two body reduced density, which strongly depends on the system under examination. In particular, as we already noted in the discussion following Eq. 4.55, its non-interacting expression 4.54 fails at short inter-electron

distances. This is particularly relevant for the calculation of λ_{ex-po}, which is proportional to (Eq. 4.48):

$$\lambda_{\text{ex-po}} \propto \int d^3r_p\, d^3r_e\, d^3r_2 \Psi^*(\boldsymbol{r}_p, \boldsymbol{r}_e)\Psi(\boldsymbol{r}_p, \boldsymbol{r}_2)\Gamma^{(2)}(\boldsymbol{r}_p, \boldsymbol{r}_e; \boldsymbol{r}_p, \boldsymbol{r}_2) \tag{4.59}$$

In fact, by construction, Ps wavefunctions $\Psi^*(\boldsymbol{r}_p, \boldsymbol{r}_e)\Psi(\boldsymbol{r}_p, \boldsymbol{r}_2)$ exponentially vanish at large inter particles separation, i.e. when $r_{pe}, r_{p1} \gtrsim 2a_0$. On the contrary, a straightforward LDA extension of Eq. 4.54 would lead to a overestimation of λ_{ex-po}, since any realistic form of $\Gamma^{(2)}$ should rapidly vanish when inter particles separation lies in the so called "exchange-correlation hole" region, whose size is roughly given by the the electron gas parameter $r_s = \left(\frac{3}{4\pi n}\right)^{1/3}$. Given that $r_s \gtrsim 2a_0$ for common value of n, the integration domain in Eq. 4.59 is extremely reduced, thus making λ_{ex-po} an higher order contribution to the annihilation rate. For these qualitative reasoning, and given that we're considering only first order corrections to λ, in the following we will neglect λ_{ex-po}. However we stress that the theory presented here and in particular Eqs. 4.43, 4.46, 4.48 and 4.49 can be evaluated starting from *any* given Ps and bulk wavefunctions.

Finally, using 4.57 we can give explicit expressions to the various contributions to the total annihilation rate of Eq. 4.42.

The exchange overlap factor inside the normalization $\mathcal{N}$ becomes:

$$S = \int \Psi^*(\boldsymbol{r}_p, \boldsymbol{r}_1)\Psi(\boldsymbol{r}_p, \boldsymbol{r}_1)\Gamma^{(1)}_{\uparrow\uparrow}(\boldsymbol{R}_{e1}; \boldsymbol{r}_{e1})\, d^3r_p\, d^3r_e\, d^3r_1 \tag{4.60}$$

while λ_{po} and λ_{ex} are given respectively by:

$$\begin{aligned} \lambda_{\text{po}} =& 8\pi a_0^3 \bar{\lambda} \int |\Psi(\boldsymbol{r}_p, \boldsymbol{r}_e)|^2 n(\boldsymbol{r}_p)\, d^3r_p\, d^3r_e \\ \lambda_{\text{ex}} =& -8\pi a_0^3 \lambda_{3\gamma} \int \Psi^*(\boldsymbol{r}_p, \boldsymbol{r}_e)\Psi(\boldsymbol{r}_p, \boldsymbol{r}_p)\Gamma^{(1)}_{\uparrow\uparrow}(\boldsymbol{R}_{pe}; \boldsymbol{r}_{pe})\, d^3r_p\, d^3r_e \end{aligned} \tag{4.61}$$

Using the definition introduced above, the exchange overlap and all the corrections to the annihilation rate can in principle be calculated if the electron density function $n(\boldsymbol{r})$ and the form of Ps spatial wavefunction are known from other computations. In the next section we will show how it is possible to include basic qualitative features of these two quantities into the discussion.

4.5.1 Spatial form of Ps wavefunction

In order to find the expression of the spatial Ps wavefunction $\Psi(\boldsymbol{r}_p, \boldsymbol{r}_e)$, one has to specify the form of its hamiltonian, hence choosing some suitable effective potentials acting on the two particles. As previously anticipated, there are many possible models describing Ps confinement, which were extensively discussed in Chapters 2 and 3. For the sake of simplicity, having in mind a comparison with the TE model, we will focus on a spherical cavity geometry and we assume that Ψ can be written in simple product form using the relative and center of mass coordinates as:

$$\Psi(\boldsymbol{r}_p, \boldsymbol{r}_e) = \psi(r_{pe})\Psi_{\text{TE}}(R_{pe}) \tag{4.62}$$

Here Ψ_{TE} has the same form of Eq. 2.3 and describes the confining effect acting on the Ps system as a whole:

$$\Psi_{\text{TE}}(R) = \begin{cases} \dfrac{1}{\sqrt{2\pi(R_c+\Delta)}} \dfrac{\sin\left(\pi R/(R_c+\Delta)\right)}{R} & \text{if} \quad R \leq R_c + \Delta \\ 0 & \text{if} \quad R > R_c + \Delta \end{cases} \tag{4.63}$$

However, we will admit the possibility that the value of Δ may be different from the TE value $\Delta^{\text{TE}} \approx 0.17$nm.

Since we're neglecting all Coulomb potentials except the one leading to the bound Ps atom, the radial part is supposed to be the same as to the unperturbed Ps, i.e. an Hydrogen like 1S orbital (see Eq. 1.10):

$$\psi(r_{pe}) = \sqrt{k_0} e^{-\frac{r_{pe}}{2a_0}} \tag{4.64}$$

In particular we have:

$$\begin{aligned} \Psi(\boldsymbol{r}_p, \boldsymbol{r}_p) &= \sqrt{k_0}\Psi_{\text{TE}}(R_{pp}) \\ \int |\Psi^{\text{Ps}}(\boldsymbol{r}_p, \boldsymbol{r}_p)|^2 \, d^3 r_p &= k_0 \end{aligned} \tag{4.65}$$

4.5.2 An approximate expression for the electron density

Giving an accurate expression for the electron density function $n(\boldsymbol{r})$ is an extremely complicated task if one has to consider all the interactions naturally present in the system. Whereas electron-electron repulsion may add a negligible contribution to annihilation, the opposite is true for positron-electron correlation.

As we explained in Sec. 2.3.1 for the case of a single positron in HEG, turning on the interactions leads to an enhancement of the electron density at the positron position due to the strong Coulomb attraction. In turn, this pile up of electrons greatly increases the annihilation rate by an enhancement factor which expression is given in Eq. 2.46 for an electron gas. In particular, we saw in Eq. 2.48 that when the mean density of the electron gas tends to zero, its value at the positron position tends to that of Ps in vacuum, i.e. k_0.

In the present treatment, this last condition is automatically satisfied being Ps the starting point of the perturbative approach. Nevertheless, a realistic profile for the external electron density function $n(\boldsymbol{r})$ should still satisfy a "light" enhancement condition:

$$n(\boldsymbol{r}_p) \gtrsim \overline{n(\boldsymbol{r})} \tag{4.66}$$

being $\overline{n(\boldsymbol{r})}$ the average value of $n(\boldsymbol{r})$ far from the positron position.
Theoretically, parametrization of the electron density on the material in the field of Ps can be done by means of DFT calculations. However, we note that in all the expressions of $\lambda_{\text{po}}, \lambda_{\text{ex}}$ and S, the outer electron density is evaluated at (or very close to) the positron position. Hence, without any knowledge of the amount of the enhancement, we can just re-define ρ_e to be the electron density *felt* by the Ps, that is:

$$n(\boldsymbol{r}) \approx \rho_e \qquad \text{if} \qquad \boldsymbol{r} \sim \boldsymbol{r}_p \tag{4.67}$$

Furthermore, to keep an analogy with TE-like models where the interaction region is limited to a shell layer, the outer electron density must smoothly vanish in the inner part

of the cavity[10]:

$$n(\boldsymbol{r}) \approx 0 \qquad \text{if} \qquad r < R_c \tag{4.68}$$

In the context of porous material, it is commonly assumed that the positron interacts only with a low-density surface layer of electrons belonging to outer atomic orbitals. We believe that, in order to catch the basic features of Ps annihilation in this framework, the real form of $n(\boldsymbol{r})$ can be replaced by a simpler one which only retains the most important qualitative aspects, i.e. conditions 4.67 and 4.68. The simplest possible expression of $n(\boldsymbol{r})$ is then given by the piecewise function:

$$n(\boldsymbol{r}) = \begin{cases} \rho_e & \text{if} \quad r \geq R_c \\ 0 & \text{if} \quad r < R_c \end{cases} \tag{4.69}$$

which is the exact analogous of the TE model.

4.6 Formal calculation of pickoff annihilation

Using Eqs. 4.62 and 4.69, the exchange overlap and the symmetric contribution to the annihilation read:

$$\begin{aligned} S &= \frac{\rho_e}{2} \int_{R_{e1}>R_c} \Psi_{\text{TE}}(R_{pe})\Psi_{\text{TE}}(R_{p1})\psi(r_{pe})\psi(r_{p1})B(k_F\, r_{e1})\, d^3r_p\, d^3r_e\, d^3r_1 \\ \lambda_{\text{po}} &= \bar{\lambda}\frac{\rho_e}{k_0} \int_{r_p>R_c} |\Psi_{\text{TE}}(R_{pe})|^2 |\psi(r_{pe})|^2\, d^3r_p\, d^3r_e \end{aligned} \tag{4.70}$$

whereas the exchange correction is given for *o*-Ps and *p*-Ps respectively by:

$$\begin{aligned} \lambda_{\text{ex}}^{3\gamma} &= -\lambda_{3\gamma}\frac{\rho_e}{2\sqrt{k_0}} \int_{R_{pe}>R_c} \Psi^*_{\text{TE}}(R_{pe})\Psi_{\text{TE}}(r_p)\psi(r_{pe})B(k_F\, r_{pe})\, d^3r_p\, d^3r_e \\ \lambda_{\text{ex}}^{2\gamma} &= -\lambda_{2\gamma}\frac{\rho_e}{2\sqrt{k_0}} \int_{R_{pe}>R_c} \Psi^*_{\text{TE}}(R_{pe})\Psi_{\text{TE}}(r_p)\psi(r_{pe})B(k_F\, r_{pe})\, d^3r_p\, d^3r_e \end{aligned} \tag{4.71}$$

Finally, adding the first order corrections (as defined in 4.42) to the unperturbed intrinsic annihilation, the formal expressions for the total annihilation rates of *o*-Ps and *p*-Ps are found:

$$\begin{aligned} \lambda_t &= \left[\lambda_{3\gamma} - \frac{\lambda_{\text{ex}}^{3\gamma}}{1-S}\right] + \frac{\lambda_{\text{po}}}{1-S} \\ \lambda_s &= \left[\lambda_{2\gamma} - \frac{\lambda_{\text{ex}}^{2\gamma}}{1-S}\right] + \frac{\lambda_{\text{po}}}{1-S} \end{aligned} \tag{4.72}$$

Despite all the approximations used, the integrals appearing in these terms have no analytical expression, so that one still needs to use numerical methods. This are easily done and we will show calculation results in the following section.

However some insights about their qualitative behavior can be deduced using simple geometrical considerations, as follow.

Considering for example the integrand function in the expression of S, we note that the radial distances between the three particles p, e and 1 have a distribution shaped by

[10]The reader may note that in TE formalism the potential barrier of the confining potential is located at $R_c + \Delta$ and not at R_c, being this last quantity the radius of the free space region.

the exponentials factors $\psi(r_{pe})\psi(r_{p1}) = \exp[-(r_{pe}+r_{p1})/2a_0]$. In particular, this means that the integral will be sensibly different from zero only when $r_{pe}, r_{p1} \lesssim 2a_0$, i.e. when the two electrons lay altogether around the positron position in a sphere roughly the size of Ps. Hence, the center of mass positions R_{pe}, R_{p1} and R_{e1}, which are midway from the corresponding particles, will in turn lay in a sphere of radius $\approx a_0$ around r_p. Since this value is small compared to the range of variation of $\Psi_{\text{TE}}(R)$, we may assume $R_{pe} \sim R_{p1} \sim R_{e1} \sim r_p \equiv R$ and write

$$\Psi_{\text{TE}}(R_{pe})\Psi_{\text{TE}}(R_{p1})n(R_{e1}) \approx |\Psi_{\text{TE}}(R)|^2 n(R) \tag{4.73}$$

Given that $n(R)$ has a step behavior, it's convenient to introduce the quantity P'_{out}:

$$P'_{\text{out}} \equiv 4\pi \int_{R_c}^{R_c+\Delta} |\Psi_{\text{TE}}(R)|^2 R^2 \, dR \tag{4.74}$$

which is the probability of finding the Ps center of mass in the interaction region outside R_c, in spherical coordinates. Of course this quantity reproduces the TE P_{out} of Eq. 2.4 if one fixes Δ to the TE value $\Delta^{\text{TE}} = 0.17$nm. By using the same approximation to all annihilation contributions, and changing integration variables from $(\boldsymbol{r}_p, \boldsymbol{r}_i, \cdots)$ to $(\boldsymbol{R}, \boldsymbol{r}_{pi}, \cdots)$, Eqs. 4.70 become:

$$\begin{aligned}
S &\approx \frac{\rho_e}{2} P'_{\text{out}} \int \psi(r_{pe})\psi(r_{p1}) B(k_F\, r_{e1})\, d^3 r_{pe}\, d^3 r_{p1} \\
\lambda_{\text{po}} &\approx \bar{\lambda} \frac{\rho_e}{k_0} P'_{\text{out}} \int |\psi(r_{pe})|^2\, d^3 r_{pe} = \bar{\lambda} \frac{\rho_e}{k_0} P'_{\text{out}} \\
\lambda_{\text{ex}}^{3\gamma} &\approx -\lambda_{3\gamma} \frac{\rho_e}{2\sqrt{k_0}} P'_{\text{out}} \int \psi(r_{pe}) B(k_F\, r_{ep})\, d^3 r_{pe}
\end{aligned} \tag{4.75}$$

and similarly for $\lambda_{\text{ex}}^{2\gamma}$. Finally, summing the first and second order corrections (as defined in 4.42), the total annihilation rate for *o*-Ps is obtained in the usual form showing the two separate contributions due to the pickoff process:

$$\lambda_t = \left[1 - \frac{P'_{\text{out}} A[\nu]}{1 - P'_{\text{out}} C[\nu]}\right] \lambda_{3\gamma} + \left[\frac{\rho_e}{k_0} \frac{P'_{\text{out}}}{1 - P'_{\text{out}} C[\nu]}\right] \bar{\lambda} \tag{4.76}$$

and the analogue expression for *p*-Ps can be obtained

$$\lambda_s = \left[1 - \frac{P'_{\text{out}} A[\nu]}{1 - P'_{\text{out}} C[\nu]}\right] \lambda_{2\gamma} + \left[\frac{\rho_e}{k_0} \frac{P'_{\text{out}}}{1 - P'_{\text{out}} C[\nu]}\right] \bar{\lambda} \tag{4.77}$$

where $\nu = 2k_F a_0$, and we have used the analytical results:

$$\begin{aligned}
&\frac{\rho_e}{2\sqrt{k_0}} \int \psi(r_{pe}) B(k_F\, r_{ep})\, d^3 r_{pe} = A[\nu] \\
&A[x] = \frac{2}{\pi}\left[\arctan(x) - \frac{x}{1+x^2}\right] \\
&\frac{\rho_e}{2} \int \psi(r_{pe})\psi(r_{p1}) B(k_F\, r_{e1})\, d^3 r_{pe}\, d^3 r_{p1} = C[\nu] \\
&C[x] = \frac{2}{\pi}\left[\arctan(x) - \frac{x - \frac{8}{3}x^3 - x^5}{(1+x^2)^3}\right]
\end{aligned} \tag{4.78}$$

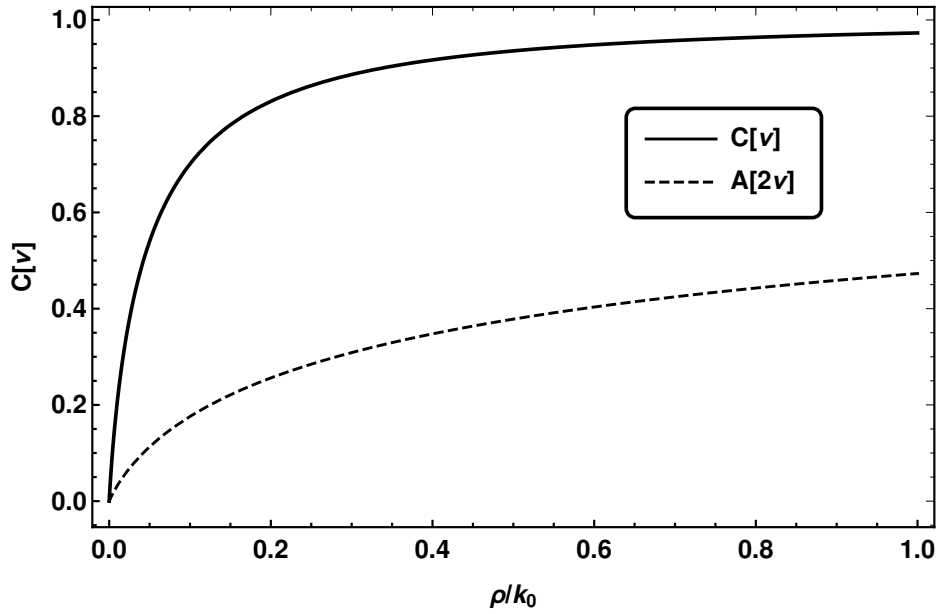

Figure 4.5: Plot of $C[\nu]$ and $A[\nu]$, with $\nu = k_F a_0$, as a function of the electron density ρ_e felt by the positron in the material.

The main advantage of approximation 4.73 is that in Eqs. 4.76 and 4.77 geometrical effects are well separated from the that due to electron exchange. In Fig. 4.5 we plotted the functions A and C respectively, as a function of the electron density ρ_e felt by the positron in the material. Both these functions increase for increasing density values while they vanish at the low density limit.

Within this approximation, the relative contact density is given by

$$k_r = \left[1 - \frac{P'_{\text{out}} A[\nu]}{1 - P'_{\text{out}} C[\nu]}\right] \tag{4.79}$$

By definition, k_r is a useful indicator of the dissociation degree of Ps atom, i.e. of the separability of the Ps-electron. Its maximum value $k_r = 1$ (Ps in vacuum) is lowered by the overlap with surrounding electrons and it vanishes as the original Ps state fades. When $k_r = 0$ no distinction between *o*-Ps and *p*-Ps annihilation rates is possible because all electrons are taken on equal footings. Note that the vanishing behavior of the contact density is only due to electron indistinguishability and it is by no means related to a spatial deformation of Ps wavefunction, as previously believed. In order to show k_r behavior between these two limits, in Fig. 4.6 we plotted its value as a function of both P'_{out} and ρ_e.

4.6.1 Comparison with TE model

It is interesting to compare Eq. 4.76 with the analogous TE expression Eq. 2.2. Equivalence between the symmetric parts of pickoff annihilation rates predicted by the two

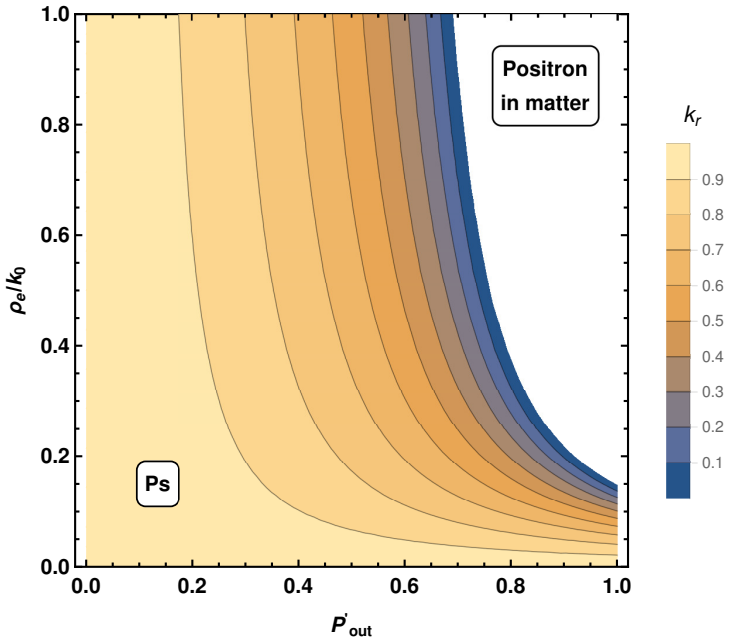

Figure 4.6: Plot of k_r as a function of the geometrical parameter P'_{out} and the electron density ρ_e felt by the positron in the material (Eq. 4.79). In the top-right region, k_r assumes negative values since the description os a Ps atom weakly interacting with the environment is no more possible.

models is obtain by setting[11]:

$$P_{\text{out}} = \frac{\rho_e}{k_0} \frac{P'_{\text{out}}}{1 - P'_{\text{out}} C[\nu]} \tag{4.80}$$

This condition holds only if $0 \leq P_{\text{out}} \leq 1$, i.e. when

$$P'_{\text{out}} \leq \frac{1}{\frac{\rho_e}{k_0} + C[\nu]} \tag{4.81}$$

which is satisfied for realistic choices of the parameters R_c, Δ and ρ_e. In particular, In the high density limit $\rho_e = k_0$ condition 4.81 reads $P'_{\text{out}} \lesssim 0.5$, while 4.80 implies:

$$P_{\text{out}} = \frac{P'_{\text{out}}}{1 - P'_{\text{out}} C[\nu]} \geq P'_{\text{out}} \tag{4.82}$$

In turn, by fixing the total length $R_c + \Delta$ of the confining region, it is easy to see that

$$\Delta^{\text{TE}} \geq \Delta \tag{4.83}$$

which means that the actual interaction region Δ may be much smaller than the one predicted by standard TE-like models.

[11] This condition can be easily satisfied for any electron density value remembering that the geometrical parameters R_c and Δ, on which P'_{out} depends, can be different from the TE values R_c^{TE} and $\Delta^{\text{TE}} = 0.17$nm.

Another meaningful physical insight can be obtained by using the scaling condition 4.80 to write Eq. 4.76 as:

$$\begin{aligned}\lambda_t &= \left[1 - \frac{k_0}{\rho_e} A[\nu] P_{\text{out}}\right] \lambda_{3\gamma} + P_{\text{out}} \bar{\lambda} \\ \lambda_s &= \left[1 - \frac{k_0}{\rho_e} A[\nu] P_{\text{out}}\right] \lambda_{2\gamma} + P_{\text{out}} \bar{\lambda}\end{aligned} \tag{4.84}$$

which are very similar to Eqs. 4.5, and of course can be interpreted as in Eqs. 4.7. In this equivalent version of the TE model, the relative contact density in the *surface* region, i.e. in the outer shell of thickness Δ^{TE}, is be equal to:

$$k_{\text{out}} = 1 - \frac{k_0}{\rho_e} A[\nu] \tag{4.85}$$

In the limit in which the probability of having an external electron at the positron position reach the same value of free Ps, i.e. when $\rho_e \to k_0$, the value of k_{out} becomes:

$$\lim_{\rho_e \to k_0} k_{\text{out}} = 1 - 0.472 = 0.527 \tag{4.86}$$

which is close to Ps^- contact density value ≈ 0.52 (Eq. 1.61).

This result can be easily explained with the following simple argument. Taking as a reference Fig. 4.1, where particles are represented by rigid spheres, we focus on the $m = 1$ *o*-Ps , so that both Ps positron and electron will have $\uparrow$ spin configuration. Then, the pickoff annihilation contribution due only to outer electrons of opposite spin will be proportional to the probability $P_\downarrow(\boldsymbol{r}_p)$ of finding a spin-down electron at the positron position:

$$\Lambda_{\uparrow\downarrow} = P_\downarrow(\boldsymbol{r}_p) \lambda_{\uparrow\downarrow} \tag{4.87}$$

where $\lambda_{\uparrow\downarrow}$ is the mean annihilation rate for opposite-spin configuration. At the same way, the contribution due only to outer electrons of the same spin will be given by the product:

$$\Lambda_{\uparrow\uparrow} = P_\uparrow(\boldsymbol{r}_p) \lambda_{\uparrow\uparrow} \tag{4.88}$$

From the general expression of the annihilation operator Eq. 1.19, it's easy to find that

$$\begin{aligned}\lambda_{\uparrow\downarrow} &= \frac{\rho_e}{k_0} \frac{\lambda_{2\gamma} + \lambda_{3\gamma}}{2} \\ \lambda_{\uparrow\uparrow} &= \frac{\rho_e}{k_0} \lambda_{3\gamma}\end{aligned} \tag{4.89}$$

so that the total annihilation rate reads:

$$\begin{aligned}\lambda_t &= \lambda_{3\gamma} + \Lambda_{\uparrow\downarrow} + \Lambda_{\uparrow\uparrow} \\ \lambda_t &= \lambda_{3\gamma} + P_\downarrow(\boldsymbol{r}_p) \frac{\rho_e}{k_0} \frac{\lambda_{2\gamma} + \lambda_{3\gamma}}{2} + P_\uparrow(\boldsymbol{r}_p) \frac{\rho_e}{k_0} \lambda_{3\gamma}\end{aligned} \tag{4.90}$$

If no shielding effect is present, and considering uniform spin distribution for outer electrons, then $P_\downarrow(\boldsymbol{r}_p)$ and $P_\uparrow(\boldsymbol{r}_p)$ would be equally given by:

$$P_\downarrow(\boldsymbol{r}_p) = P_\uparrow(\boldsymbol{r}_p) = \frac{1}{2} P_{\text{out}} \tag{4.91}$$

where as usual P_{out} is the probability of having Ps in the interaction region. However, the Ps electron "repels" electrons with the same spin, so that $P_{\uparrow}(\boldsymbol{r}_p) < \frac{1}{2}P_{\text{out}}$. The range of this repulsion is usually associated to the size of the exchange hole, which in turn is inversely proportional to the electron density. If we assume that, when $\rho_e = k_0$, i.e. when the electron density at the positron matches the same value of a $1S$ ground state wavefunction, at most two electrons can be found at the positron position (the Ps electron and an outer one with opposite spin), we have $P_{\uparrow}(\boldsymbol{r}_p) = 0$ and:

$$\begin{aligned} \lambda_t &= \lambda_{3\gamma} + \frac{1}{2}P_{\text{out}}\frac{\lambda_{2\gamma} + \lambda_{3\gamma}}{2} \\ &= (1 - \frac{1}{2}P_{\text{out}})\lambda_{3\gamma} + P_{\text{out}}\bar{\lambda} \end{aligned} \tag{4.92}$$

which is just result 4.86.

This suggests a simplified picture in which Ps can be considered as such in the internal cavity region, whereas it becomes a Ps^- when inside the interaction region in the external shell. For lower electron density values, the range of the shielding effect will be wider and in particular for $\rho_e = \rho_0 \approx 0.3k_0$ it is found that the contact density vanishes in the *surface* region:

$$k_{\text{out}} = 1 - \frac{k_0}{\rho_e}A[2\nu]\bigg|_{\rho_e=\rho_0} = 0 \tag{4.93}$$

so that Eqs. 4.84 become identical to Eq. 4.5:

$$\begin{aligned} \lambda_t\big|_{\rho_0} &= [1 - P_{\text{out}}]\,\lambda_{3\gamma} + P_{\text{out}}\bar{\lambda} \\ \lambda_s\big|_{\rho_0} &= [1 - P_{\text{out}}]\,\lambda_{2\gamma} + P_{\text{out}}\bar{\lambda} \end{aligned} \tag{4.94}$$

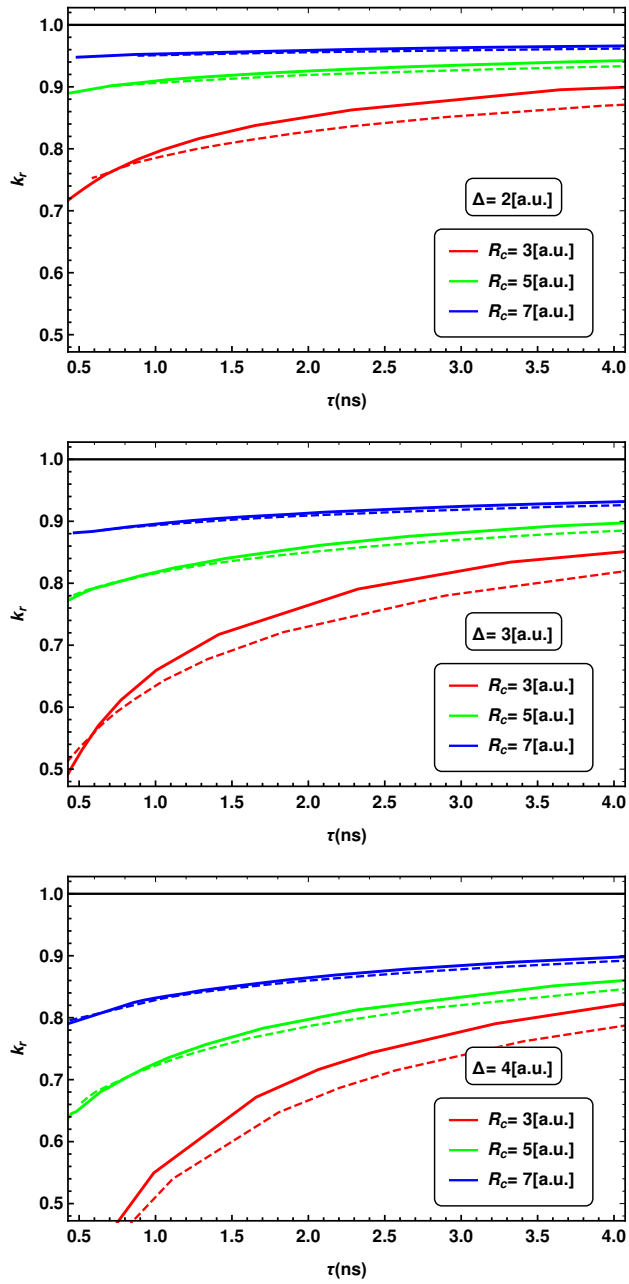

Figure 4.7: Relationship between o-Ps lifetime τ and relative contact density k_r, for 3 different values of cavity radius R_c. The length of the interaction layer Δ was fixed to $2, 3$ and 4 atomic units respectively from top to bottom. Curves are obtained by varying the electron density ρ_e felt by Ps. Increasing values of ρ_e correspond to smaller lifetimes and smaller k_r. Straight lines are numerically calculated from Eqs. 4.70, while dotted lines refer to the analytical approximation given in Eqs. 4.76. Qualitatively, a lower value of Δ reproduces the same result of a larger one, if the cavity radius R_c is consequently scaled.

Table 4.1: PALS data fo some materials. The relative contact density k_r is mostly obtained by magnetic quenching experiments.

Name	τ_1	$I_1\%$	τ_2	$I_2\%$	τ_3	$I_3\%$	τ_4	$I_4\%$	k_r	Sym.	Ref.
Ttactic polypropylene(PPA)	0.211	14.3	0.344	54.3	0.887	10.2	2.66 ± 0.05	21.2	0.66 ± 0.04	$\star$	[58]
Polymethylmethacrylate(PMMA)	0.146	14.1	0.346	52.9	0.875	12.4	2.23 ± 0.04	20.6	0.65 ± 0.03	$\bullet$	[58]
Isotactic polypropylene(PPI)	0.102	14.7	0.334	62.1	1.15	9.	2.33	14.2	0.55	$*$	[58]
Teflon(PTFE)	0.204	25.2	0.458	46.5	1.58	12.4	4.47	15.9	1 ± 0.08	$\blacktriangleleft$	[58]
Polyethylene(PE)	0.133	14.7	0.367	59.2	0.989	9.9	2.6 ± 0.05	16.2	0.6 ± 0.06	$\blacksquare$	[58]
Naphthalene	0.16 ± 0.02	$18. \pm 3.$	0.35 ± 0.01	$65. \pm 3.$	1.03 ± 0.01	17.3 ± 0.3	-	-	0.82 ± 0.07	$\blacktriangle$	[108]
Acenaphtene	0.142 ± 0.01	7.5 ± 0.4	0.333 ± 0.004	$69.9 \pm 1.$	0.915 ± 0.026	$22.5 \pm 1.$	-	-	0.75 ± 0.06	$\blacktriangledown$	[2]
Byphenil	0.139 ± 0.011	7.5 ± 0.6	0.339 ± 0.004	$70. \pm 9.$	1.148 ± 0.016	22.5 ± 0.3	-	-	0.82 ± 0.06	$\triangle$	[2]
KCl	0.127 ± 0.013	15.3 ± 0.5	0.304 ± 0.004	$37.1 \pm 2.$	0.68 ± 0.01	45.9 ± 1.5	-	-	0.56 ± 0.04	KCl	[2]
Octadecane (solid)	0.133 ± 0.007	7.5 ± 0.2	0.331 ± 0.003	$70. \pm 0.8$	1.504 ± 0.0015	22.5 ± 0.6	-	-	0.85 ± 0.05	$\bullet$	[51]
Octadecane (liquid)	0.169 ± 0.016	11.4 ± 0.2	0.463 ± 0.031	54.4 ± 0.7	2.919 ± 0.036	34.2 ± 0.6	-	-	0.69 ± 0.07	$\blacksquare$	[51]
2,5-Diphenyloxazole (PPO)	0.142 ± 0.008	6.8 ± 0.5	0.239 ± 0.005	$32.4 \pm 3.$	0.44 ± 0.021	40.3 ± 1.1	1.065 ± 0.025	20.5 ± 1.4	0.78 ± 0.04	$\blacktriangleright$	[109]
2,5-Diphenyl 1,3,4 oxadiazole (PPD)	0.261 ± 0.011	$53.6 \pm 7.$	0.51 ± 0.045	$35.1 \pm 6.$	1.217 ± 0.015	11.2 ± 0.4	-	-	1.05 ± 0.11	$\blacktriangledown$	[109]
Butyl-PBD	0.21 ± 0.016	$28.8 \pm 9.$	0.366 ± 0.019	59.8 ± 8.5	1.409 ± 0.07	11.4 ± 0.4	-	-	0.88 ± 0.11	$\diamond$	[109]
p–terphenyl (doped with anthracene)	-	-	0.313 ± 0.004	-	1.438 ± 0.015	19.9 ± 0.2	-	-	0.8 ± 0.02	$\blacklozenge$	[110]
p–terphenyl (doped with chrysene)	-	-	0.317 ± 0.003	-	1.16 ± 0.013	22.5 ± 0.3	-	-	0.83 ± 0.02	$\triangledown$	[110]
NaCl	-	-	-	-	0.68 ± 0.02	-	-	-	0.42 ± 0.07	NaCl	[111]
Hexane (dagassed)	0.29 ± 0.02	$40. \pm 3.$	0.86 ± 0.04	$16. \pm 2.$	3.93 ± 0.02	$33. \pm 1.$	-	-	0.82 ± 0.03	Hex	[112]
Benzene	0.148 ± 0.018	18.1 ± 2.2	0.416 ± 0.007	$37.4 \pm 1.$	1.18 ± 0.18	5.3 ± 0.8	3.26 ± 0.02	39.2 ± 0.8	0.71 ± 0.06	$\blacktriangle$	[113]
Alpha-SiO2	-	-	-	-	0.27 ± 0.01	-	-	-	0.31 ± 0.02	$\spadesuit$	[114]
Amorphous-SiO2	-	-	-	-	1.59 ± 0.02	-	-	-	0.95 ± 0.03	$\square$	[115]

4.7 Numerical results

To better see how the geometry affects the results, in Fig. 4.7 we plotted the relationship between lifetime $\tau = \lambda_t^{-1}$ and relative contact density k_r of a confined *o*-Ps , for 3 different choices of the length parameters R_c and Δ. The electron density ρ_e varies in the range $0 \leq \rho_e \leq 2k_0$ and increasing values of ρ_e correspond to shorter lifetime values. In these pictures, continuous lines refers to the exact numerical result obtained from Eqs. 4.72, while dashed lines are calculated using the analytical approximation given in Eqs. 4.76.

As expected from the discussion in the previous section, k_r always lie below the vacuum limit $k_r = 1$, and gets lower with increasing values of Δ or ρ_e (i.e. of the overlap S) . It is quite clear that approximations 4.73 do not hold for small $R_c + \Delta$ values, where the heavily distorted wavefunction of the confined Ps undergoes big variations over short distances[12]. On the other hand, there is a general good agreement for larger radii. Also, the variance in predictions between Eqs. 4.72 and Eqs. 4.76 seems not to be influenced by the value of the electron density, being mainly related to the system geometry.

In Fig. 4.8 we plotted the relationship between *o*-Ps lifetime τ and relative contact density k_r, for different values of electron density ρ_e, together with known experimental data taken from Table. 4.1. Points are numerically calculated from Eqs. 4.72 as a function of the couple (R_c, Δ), while lines are obtained by the corresponding analytical approximation given by Eqs. 4.76.

Here, each color corresponds to a specific value of ρ_e. In particular, red values represent the $\rho_e = k_0$ limit, where the pickoff process can be related to a *surface* formation of Ps^-, as discussed after Eq. 4.86. On the other hand, green values represents the $\rho_e = \rho_0 \approx 0.3k_0$ limit, where the electron-shielding effect exactly matches Ps contact density in vacuum, as shown in Eqs. 4.93 and 4.5. Finally, we also plotted an intermediate region $\rho_e = 0.5k_0$ (in green) and a low density limit $\rho_e = 0.1k_0$ (in blue) for comparison.

In the top picture, the shell thickness Δ was limited to vary in the range $1 \leq \Delta \leq 4$ a.u., a choice in line with the standard picture in which the interaction layer is small compared to the cavity radius R_c. For comparison, in the TE model, the value of Δ is usually fixed at ≈ 3.13 a.u.. In the bottom picture, instead, we show the effect of having an extended range for Δ, which can be as large as 10 a.u. (~ 0.5nm). As expected, points tend to saturate to the analytical approximation in the limit $\Delta \gg R_c$, which corresponds to the situation of Ps confined in a relatively wide quantum well completely filled with electron gas.

To compare our model with experimental data, we used known results on the contact density and PALS spectra obtained for some polymers and porous materials, which are reported in Table. 4.1. Here, spectra are decomposed in 3 or 4 lifetime components. As described in Sec. 1.6, the shorter component $\tau_1 \sim 0.125$ns is associated to *p*-Ps annihilation, the intermediate lifetime $\tau_2 \sim 0.3$ns is due to direct positron annihilation while the longest $\tau_3, \tau_4 \sim 1 - 10$ns are associated to *o*-Ps annihilating via pickoff process[13]. We note that only a few spectra show the correct $1/3$ ratio between the detected intensities of *p*-Ps and *o*-Ps annihilations, a problem which was already addressed in the discussion following Eq. 1.63, and which may implicate a bias in the estimate of

[12]This distortion is to be ascribed to the center of mass motion only, given that there are no potentials acting on the relative part of Ps wavefunction.

[13]In the present discussion there is no need for a rescaled *o*-Ps lifetime τ', as the one we introduced in our previous model, since electron density explicitly enters into the description and there are no other empirical parameters that need to be fitted.

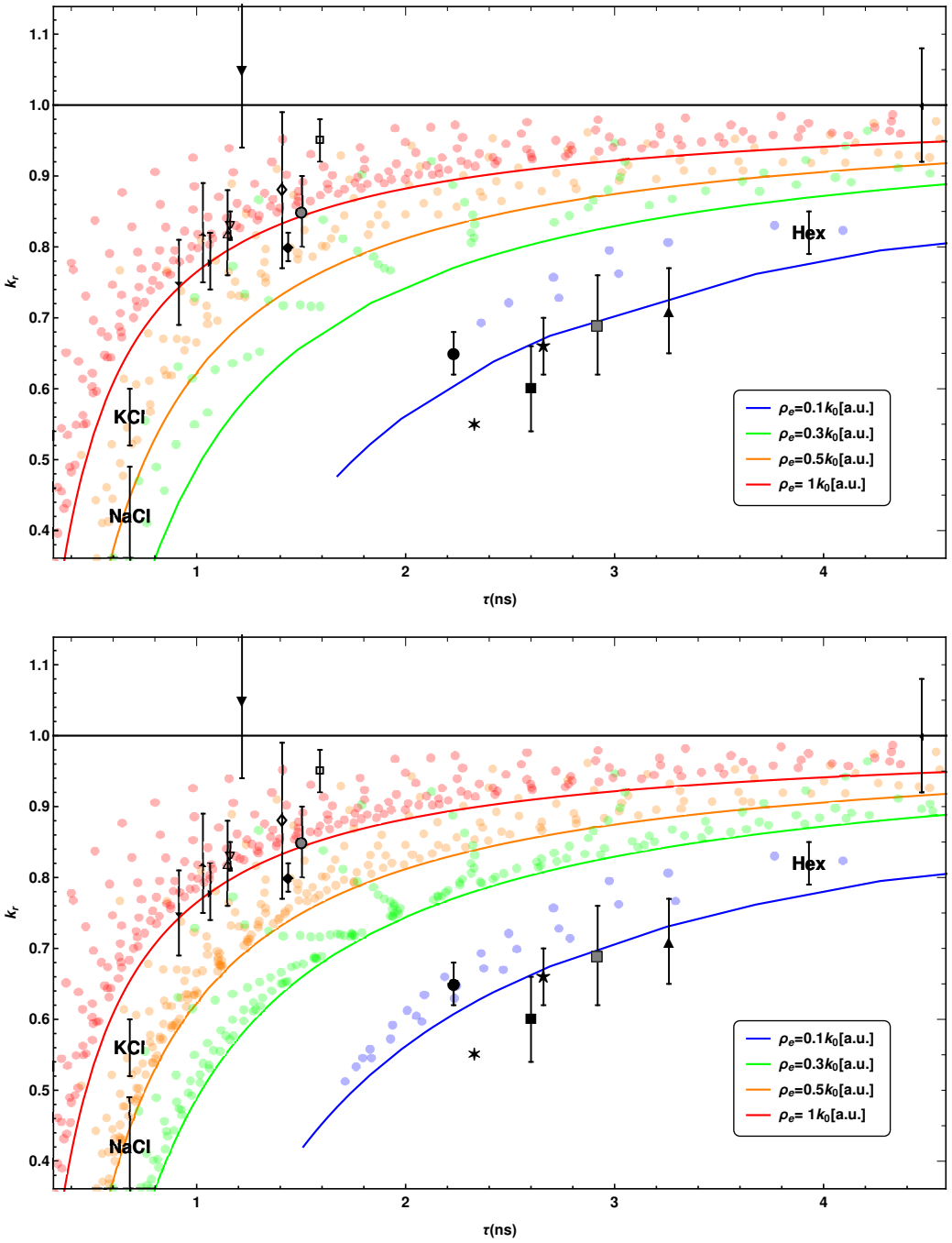

Figure 4.8: Relationship between o-Ps lifetime τ and relative contact density k_r, for different values of electron density ρ_e (each represented by a different color). Each point was numerically calculated from Eqs. 4.72 as a function of (R_c, Δ), while lines are obtained by the corresponding analytical approximation given by Eqs. 4.76. In the top picture, Δ was limited to vary in the range $1 \leq R_c, \Delta \leq 4$a.u., while in the bottom Δ can be as high as 10a.u.. As expected, curves tend to saturate to the analytical approximation at the high Δ limit, which corresponds to the situation of a cavity being completely filled with electron gas. Known experimental data taken from Table. 4.1 are plotted for comparison.

the shorter and longer components of the spectra (i.e. the one associated to p-Ps and o-Ps respectively). On the other hand, the relative contact density values k_r in Table. 4.1 are mostly obtained via magnetic quenching experiments, so that they are independent of any possible bias in the PALS analysis.

Fig. 4.8 shows a general good agreement between our predictions and a substantial group of the experimental data, which tend to accumulate in the $\rho_e = k_0$ region associated to the *surface* Ps^-formation process. The case of both sodium and potassium chlorides is someway different: they are found in a region characterized by low values of contact density and cavity size. Here, Ps wavefunction has a high overlap with surrounding electrons, so that its description as a distinct system is blurry. This is not surprising, given that in such ionic compounds the presence of internal pores or cavity is not expected. We note that the other data showing a bad agreement with our model are mostly obtained by a PALS analysis characterized by a wrong I_1/I_3 ratio. For example, 4 of the 6 points[14] lying in the down-right corner of Fig. 4.8 present a o-Ps / p-Ps intensity ratio $I_1/I_3 \gtrsim 0.5 > 1/3$. Thus it is not clear if they are effectively linkable to a Ps trapped in a relatively big cavity ($R_c + \Delta \approx 10$, a.u with $R_c \approx 1$ a.u), completely filled with a low density electron gas ($\rho_e \lesssim 0.1 k_0$), as would be predicted by the current model. In particular, the unnaturally high vaue $k_r > 1$ found in PPD is associated to an intensity ratio $I_1/I_3 = 4.8 \gg 1/3$ which can not be linked to Ps.

At variance with results obtained with our old model (previous chapter, Fig. 3.6) where in the small cavity limit the relative contact density was raised up to the (unphysical) Hydrogen value $k_r = 8$, here k_r tends to vanish. This different behavior is rapidly explained given the lack, in the current picture, of a confining potential acting on Ps-electron only. Moreover, the present discussion is characterize by the complete lack of *any* potential that could pull the electron and positron apart. Indeed the relative wavefunction of the Ps atom is exactly the same as in vacuum. The vanishing of the contact density for small values of R_c is then a mere consequence of having an higher overlap with outer electrons. In other words, it is the concept of Ps itself which inevitably fades when electrons can no more be distinguished.

Another useful relationship predicted by our model is the one between o-Ps and p-Ps lifetime components, which is plotted in Fig. 4.9 for different values of electron density ρ_e. Like in Fig. 4.8, points are numerically calculated from Eqs. 4.72, while lines are obtained by the corresponding analytical approximation given by Eqs. 4.76. The straight black line represents p-Ps lifetime in vacuum $\lambda_{2\gamma}^{-1} = 0.125$ns. We can see that most data lay in the range predicted by our model. Again, the few exceptions present a wrong I_1/I_3 ratio. For example, a particularly bad analysis may be the cause of the unphysical low value of $\tau_1 < \lambda_{2\gamma}^{-1}$ found in the PPI sample.

In general, by looking both at Fig. 4.8 and 4.9, it is not easy to establish the goodness of this model, given the lack of independent information regarding pore dimension, relative geometries and effective electron densities around the voids. To overcome this problem we now separately analyze an interesting series of annihilation data taken by Brusa et al. on a vitreous SiO_2 sample [116]. The peculiarity of their work is that PALS spectra were captured while an increasing pressure was applied to the sample. In particular, in Table 4.2 we list three series of PALS spectra taken with a pressure of $0, 4$ and 6 GPa respectively (these are shown in Fig. 4.11, 4.12 and 4.13). The great importance of such a series is that it should give insight about how the relationship between λ_t and λ_s (i.e. the pickoff annihilation) is affected by the pores geometry alone.

[14] For these materials, points are given in the form (τ_4, k_r), i.e. as a function of the longest o-Ps lifetime component.

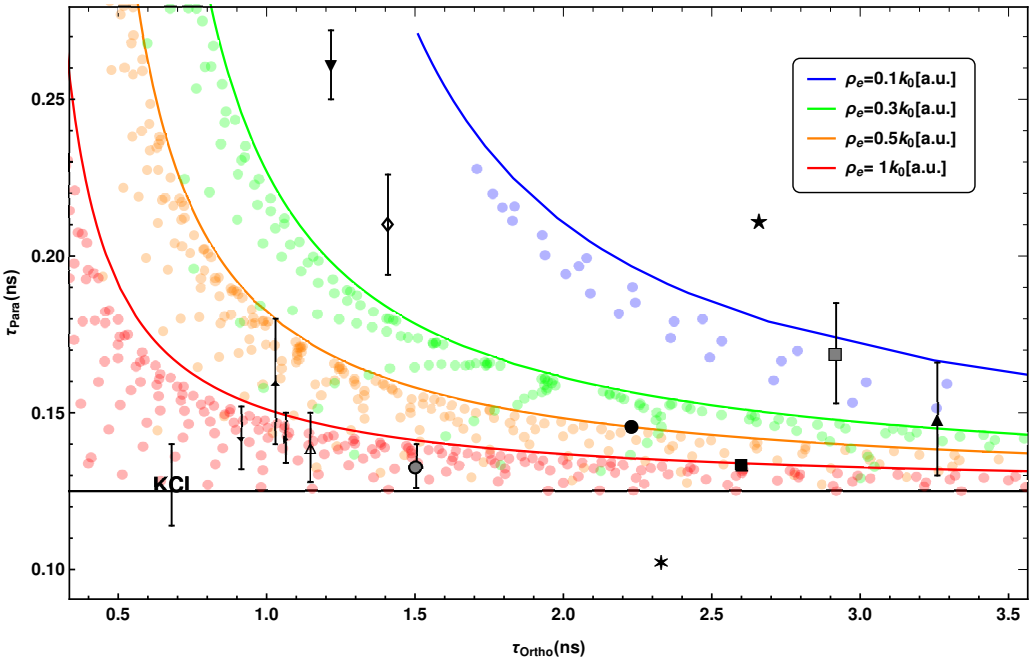

Figure 4.9: Relationship between *o*-Ps and *p*-Ps lifetimes, τ_{Ortho} and τ_{Para}, for different values of electron density ρ_e (each represented by a different color). Each point was numerically calculated from Eqs. 4.72 as a function of (R_c, Δ), while lines are obtained by the corresponding analytical approximation given by Eqs. 4.76. As already seen in Fig. 4.8, curves tend to saturate to the analytical approximation at the high Δ limit, which corresponds to the situation of a cavity being completely filled with electron gas. Known experimental data taken from Table. 4.1 are plotted for comparison. For materials with more than 3 lifetime components, only the longer one is used. The straight black line represents *p*-Ps lifetime in vacuum $\lambda_{2\gamma}^{-1} = 0.125$ns.

Table 4.2: PALS spectra of a vitreous SiO_2 sample, taken at different values P of pressure[116, 117].

P (GPa)	τ_1	$I_1\%$	τ_2	$I_2\%$	τ_3	$I_3\%$
0	0.139 ± 0.0009	24.7	0.646 ± 0.009	16.1 ± 0.4	1.591 ± 0.005	59.1 ± 0.4
4	0.161 ± 0.001	24.81	0.526 ± 0.004	27.3 ± 0.2	1.491 ± 0.003	47.9 ± 0.2
6	0.167 ± 0.001	23.6	0.498 ± 0.002	43.4 ± 0.3	1.218 ± 0.005	32.9 ± 0.3

Indeed, whereas we expect that higher pressures would tend to squeeze cavities inside the material, on the other hand they will not affect the chemical properties of the sample, i.e. the electron density felt by the Ps. This fact is crucial since it makes us able to fit our model without knowing the value of ρ_e.

Furthermore, looking at Table 4.2, we note both τ_2 and τ_3 decrease with increasing pressure. If τ_2 should be related only to positron direct annihilation in bulk, as we discussed in Section 1.6, this behavior could not be explained. However, since τ_2 values in Table 4.2 are bigger than those usually found in intermediate components (≈ 0.3ns as found in Table 4.1), they most likely must be associated to an *o*-Ps state as well. Hence, τ_2 can be interpreted as corresponding to *o*-Ps pickoff annihilation in small interatomic voids, whereas τ_3 can be related to *o*-Ps pickoff in the intrinsic voids of the amorphous structure[116]. In this case, the $1/3$ ratio between the intensities is recovered if

$$I_1 \approx \frac{1}{3}\left[I_2 + I_3\right] \tag{4.95}$$

a condition which finds good agreement with data. Since we do not have magnetic quenching data, the relative contact density is directly extrapolated from PALS using Eq. 1.64:

$$\begin{aligned} k_r^{(12)} &= \frac{\lambda_1 - \lambda_2}{\lambda_{2\gamma} - \lambda_{3\gamma}} \\ k_r^{(13)} &= \frac{\lambda_1 - \lambda_3}{\lambda_{2\gamma} - \lambda_{3\gamma}} \end{aligned} \tag{4.96}$$

where we admitted the possibility of having two different *o*-Ps contributes to the PALS spectra.

As shown in Fig. 4.10, both the series of data show a confined-Ps behavior. In particular, for increasing pressure, both series of points tend to approach the nearest saturation curve. This means that, while the free-space region R_c, and the total range of the confinement $R_c + \Delta$, are effectively squeezed, the length of the interaction layer Δ grows. Furthermore, a part from geometrical differences, the pore structures associated to τ_2 and τ_3 may be also related to different local values of the electron density, i.e. $\rho_e \approx k_0$ for τ_2 and $\rho_e \approx 0.5k_0$ for τ_3.

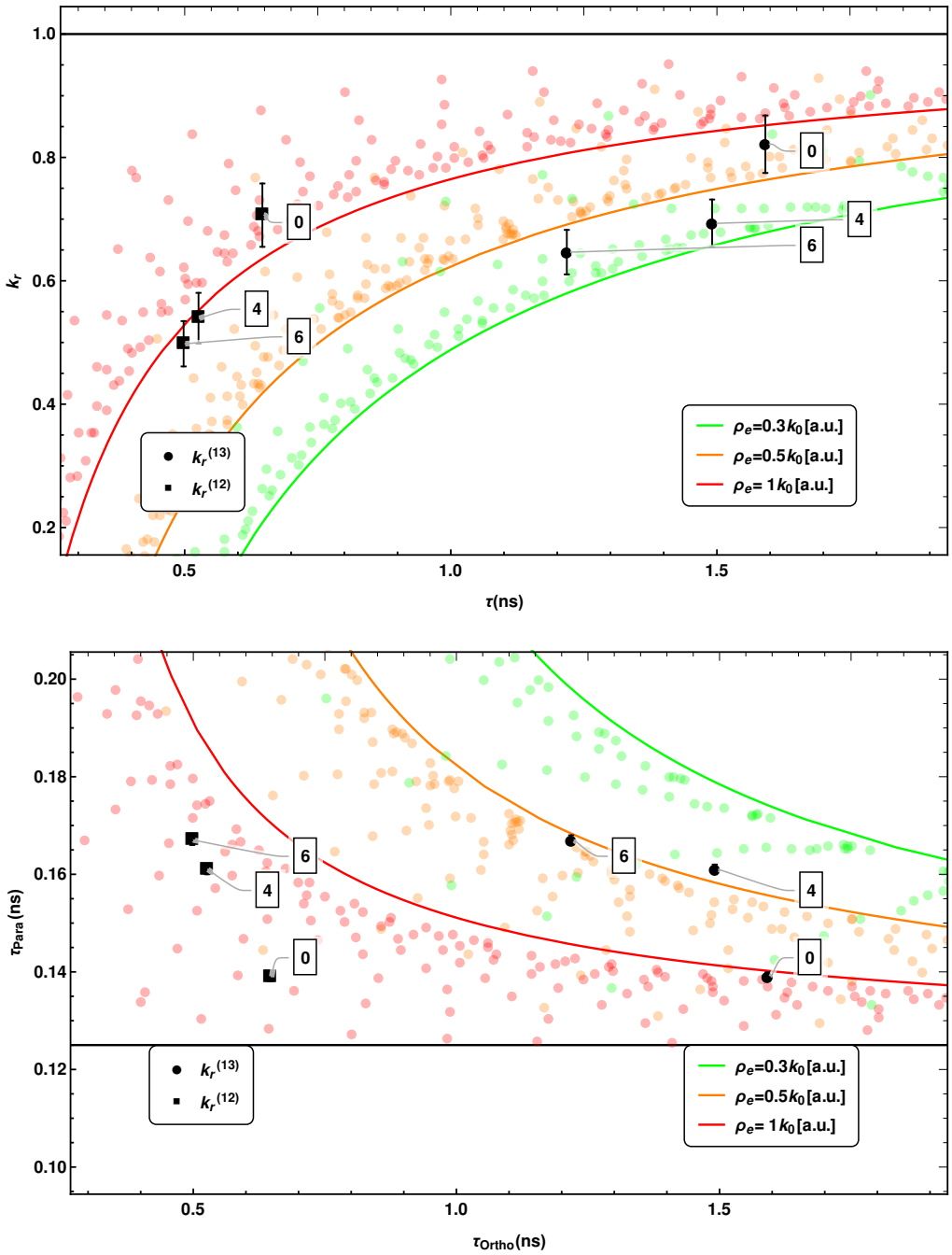

Figure 4.10: Top: same as Fig. 4.8. Bottom: same as Fig. 4.9. All data are taken from Table. 4.2 and are referred to different values of pressure, i.e. $0, 4$ and 6GPa respectively. Contact densities $k_r^{(12)}$ and $k_r^{(13)}$ are calculated using Eqs. 4.96 as explained in the text.

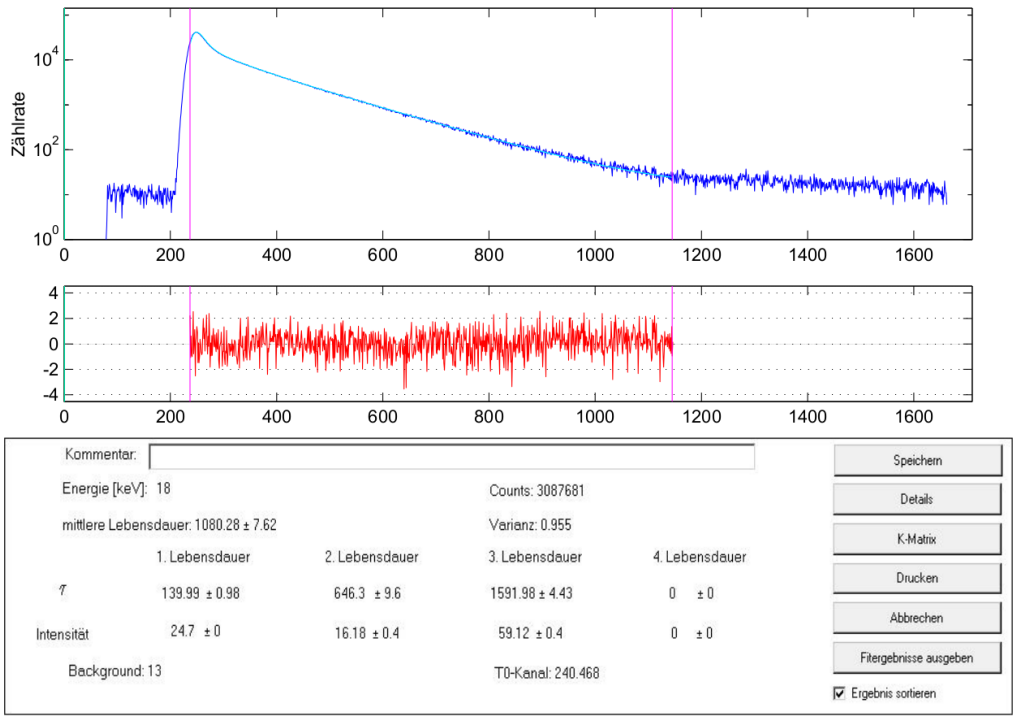

Figure 4.11: PALS analysis of a SiO_2 sample with at zero pressure.

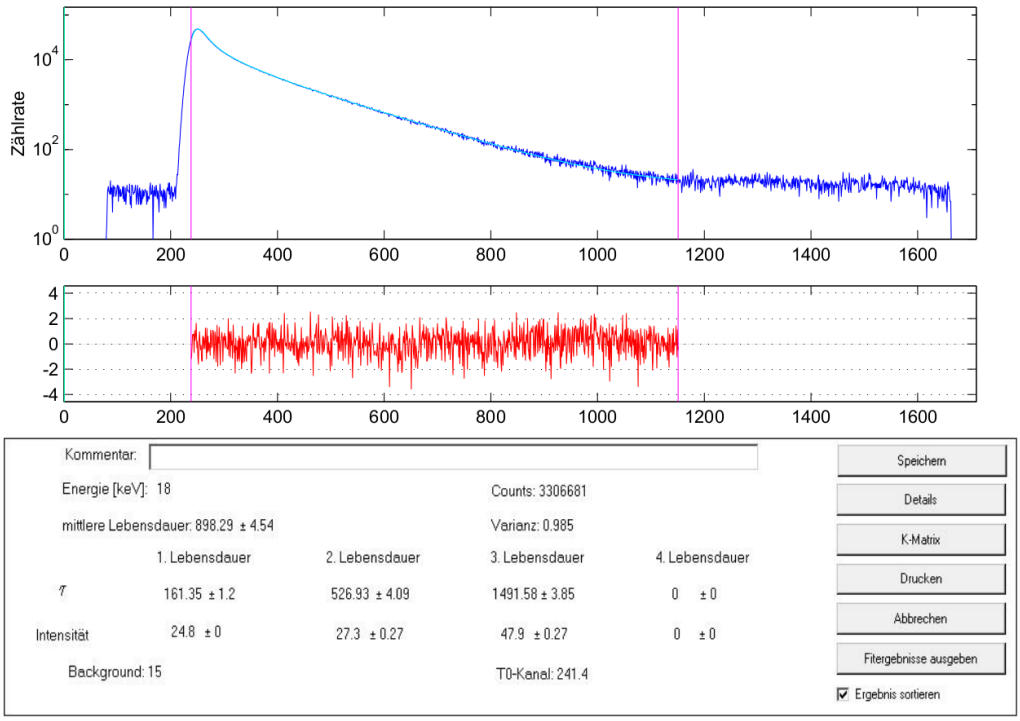

Figure 4.12: PALS analysis of a SiO_2 sample with at pressure $P = 4\,\text{GPa}$.

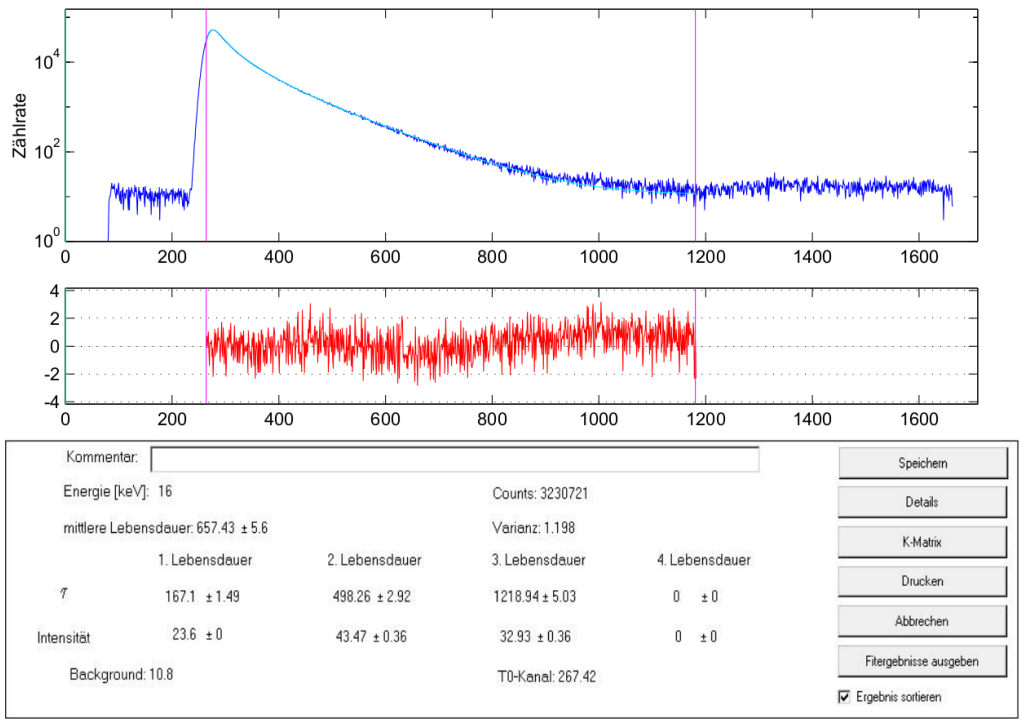

Figure 4.13: PALS analysis of a SiO_2 sample with at pressure $P = 6\,\mathrm{GPa}$.

Conclusions

The main objective of this thesis work was to find a theory which could describe in a simple yet powerful way the behavior of Ps in porous materials. The motivation is strictly related to the increased experimental interest for using Ps as a probe in the context of structural analysis of materials. In particular, positron annihilation lifetimes (PALS) experiments are one of the few available methods to obtain information about sub-nanometric porous structures (i.e. voids, cavities and free spaces in general) which may be present inside a sample. As a matter of fact, a complete theory of Ps formation and annihilation inside matter is needed in order to extract useful information about the medium itself from PALS data.

Any model which aims to accurately describe Ps in porous material must include an appropriate treatment of the pickoff process, i.e. the possibility for the positron to annihilate with an electron of the surrounding environment, different from that to which is bound in a Ps state. At present, the most used models describing Ps inside small cavities are based on the Tao-Eldrup (TE) approach, which relates pick-off annihilation rates λ_{po} to pore sizes by considering Ps as a single quantum particle trapped inside an infinite potential well. At the state of the art, these models have been greatly extended to describe various cavity geometries and temperature effects. Despite also fully *ab initio* treatments of a two particle bound system inside a host material can in principle be done, they are usually avoided given the huge computational efforts required.

After having reviewed many existing models which deals with Ps trapped in nanometric cavities, we found out that some of its annihilation characteristics still lacked a proper theoretical explanation. The most important of these mis-predicted features, usually observed in many solids where Ps is formed, is the lowering of the so-called intrinsic relative contact density, a fundamental measurable quantity of interests defined as the probability of finding the Ps-electron at the positron position, with respect to its vacuum value.

Like other authors, we addressed this peculiar aspect first by picturing Ps as affected by a confining potential which models the cavity. Our initial assumption was that the confining effects was due to Pauli exchange forces, and as such it was to be ascribed to the electron only. Given that a description of the intrinsic contact density requires by definition the knowledge of the internal structure of Ps, we naturally introduced a two-particle model by combining the generality of TE approach with specific chemical properties of the surrounding material. In particular, we believed that a positive value for the positron work function, as found, for example, in silica, could attract the positron toward the medium, effectively pulling it apart from the Ps-electron.

By applying approximate semi-analytical techniques, the variational method and, more recently, QMC calculations, we were able to demonstrate that our model can indeed correctly describe the lowering of the contact density, obtaining promising results in the comparison with experimental data.

Despite that, the great number of unknown parameters and the extreme conditions needed to explain such a lowering effect were not satisfactory. This led us to reconsider the whole problem of Ps confinement in porous materials using a different approach, i.e. taking into full account exchange interaction with surrounding electrons. In literature, these interactions have been always considered small, in the sense that a description of a Ps atom weakly interacting with the environment is suggested.

For this reason, we decided to study Ps annihilation using perturbation theories, which are made complicated by the requirement of full electron indistinguishability. Using symmetry adapted perturbation theory (SAPT) we managed to set up a theoretical framework in which Ps can be seen as a separate "entity" and where the Ps electron is somehow privileged with respect to outer electrons.

With this, we were able to clarify some concepts that had had many different interpretations in literature. In particular, we managed to provide insights about the meaning of the relative contact density k_r, which for long time has been related only to the spatial part of the confined Ps wavefunction, and about the form of the pickoff annihilation term, which has been always taken to be identical for *o*-Ps and *p*-Ps . Furthermore, we focused on a particular aspect of this problem, which we call "over-counting" and which is involved in the study of the annihilation process of Ps in cavities.

Using a simplified model of a Ps interacting with an N-electrons environment, we showed how the pickoff annihilation rate is indeed different for *o*-Ps and *p*-Ps . In practice, we found that a spin-shielding effect must be ascribed to the Ps-electron, which makes the pickoff process asymmetric with respect to the two Ps spin configurations, a feature often misunderstood and never previously analyzed in literature. On the other hand, it is possible to reconnect known results with ours by recasting this difference in a symmetric form directly related to the observed lowering of the intrinsic contact density, hence with a parallel and new interpretation of the whole annihilation processes.

Indeed, within SAPT framework, k_r essentially becomes an indicator of the dissociation degree of Ps atom, i.e. of the separability of the Ps-electron with respect to other electrons of the surrounding. Its maximum value $k_r = 1$ (Ps in vacuum) is lowered by the overlap with surrounding electrons and it vanishes as the original Ps state fades. When $k_r = 0$ no distinction between *o*-Ps and *p*-Ps annihilation rates is possible because all electrons are taken on equal footings.

In particular, we suggested a new model which only depends on 3 parameters, namely the size R_c of the free space region (cavity), the length of the interaction layer Δ and the value of the outer electron density felt by the positron ρ_e. Finally, our main result can be summarized with the expressions of the total annihilation rate of *o*-Ps and *p*-Ps which can be written in the form (Eqs. 4.72):

$$\begin{aligned} \lambda_t &= \left[\lambda_{3\gamma} - \frac{\lambda_{\text{ex}}^{3\gamma}}{1-S}\right] + \frac{\lambda_{\text{po}}}{1-S} \\ \lambda_s &= \left[\lambda_{2\gamma} - \frac{\lambda_{\text{ex}}^{2\gamma}}{1-S}\right] + \frac{\lambda_{\text{po}}}{1-S} \end{aligned} \tag{4.97}$$

where symbols are explained in the text.

Remarkably, we found that this model is capable to provide a simple explanation

for the lowering of the contact density despite it is characterized by the complete lack of *any* potential that could pull the electron and positron apart. Indeed, we used an expression for the Ps relative wavefunction which is exactly the same as in vacuum. The vanishing of the contact density for small values of R_e or for high values of ρ_e is then a mere consequence of having an higher overlap with outer electrons, and it is by no means related to a spatial deformation of Ps wavefunction, as previously believed. In other words, it is the concept of Ps itself which inevitably fades when electrons can no more be distinguished.

Further investigations are necessary to test and validate the relationships provided by our model. In particular, PALS and magnetic quenching experiments on materials subjected to external pressure can be extremely useful as they reduce the number of unknown free parameters. As also recommended above, to avoid interpretation bias, future PALS analysis should be performed assuming the correct intensity ratio between *p*-Ps and *o*-Ps lifetime components, a condition which can be easily achieved by a constrained fitting procedure.

Appendices

APPENDIX A

Unperturbed solution

In this section we will derive the general solution of the Schrödinger equation introduced in Chapter 3.1:

$$\hat{H}_0 \Psi_n(\boldsymbol{r}_e, \boldsymbol{r}) = E_n^0 \Psi_n(\boldsymbol{r}_e, \boldsymbol{r}) \tag{A.1}$$

where n symbolizes a suitable quantum number set, which can be found with standard method of quantum mechanics and which will be a useful starting point both for the variational method and QMC. Since Hamiltonian $\hat{H}_0$ is separable, the original problem reduce to two distinct Schrödinger equations, one for the confined particle (electron with coordinates $\boldsymbol{r}_e$) and one for the relative motion with coordinates $\boldsymbol{r}$.

It's easy to see that the relative motion wavefunction $\psi_{n,l,m}(\boldsymbol{r})$ satisfies:

$$\left[-\nabla_r^2 - \frac{1}{r}\right] \psi_{n,l,m}(\boldsymbol{r}) = E'_n \psi_{n,l,m}(\boldsymbol{r}) \tag{A.2}$$

which is just the relative time independent Schrödinger equation of an hydrogen atom with half the reduced mass. Its solutions are given in terms of the standard quantum numbers (n, l, m) and using a spherical coordinate system (r, θ, ϕ) constructed with the z axis parallel to $\boldsymbol{r}_e$:

$$\psi_{n,l,m}(r, \theta, \phi) = Y_{l,m}(\theta, \phi) R_{n,l}(r) \tag{A.3}$$

where $Y_{l,m}$ are spherical harmonic functions of degree l and order m, while the well known radial functions $R_{n,l}$ can be expanded in term of generalized Laguerre polynomials [118].

On the other hand, the wavefunctions $F_{i,l',m'}(\boldsymbol{r}_e)$ of a free particle in an infinite spherical quantum well satisfy:

$$\left[-\frac{1}{2}\nabla_{r_e}^2 + V_{\text{conf}}(r_e)\right] F_{i,l',m'}(\boldsymbol{r}_e) = E''_{i,l'} F_{i,l',m'}(\boldsymbol{r}_e) \tag{A.4}$$

Again, Eq. A.4 is easily solved in spherical coordinates (r_e, θ_e, ϕ_e) since the angular solution is given by the spherical harmonics functions $Y_{l',m'}(\theta_e, \phi_e)$. To find the radial solution, we first recall here that, without the confining potentials (free-particle) this is given in terms of Spherical Bessel Functions of the first kind $j_{l'}(z)$:

$$j_{l'}(z) = z^{l'} \left[-\frac{1}{z}\frac{d}{dz}\right]^{l'} \left(\frac{\sin z}{z}\right) \tag{A.5}$$

where $z = k r_e$ and $k^2 = \frac{2mE}{\hbar^2}$. To include the confining potential we just have to impose the vanishing boundary condition at the cavity walls $j_{l'}(kR_c) = 0$ which in turns results

in quantized energy levels:

$$\begin{aligned} k_{i,l'} &= \frac{z_{i,l'}}{R_c} \\ E''_{i,l'} &= z^2_{i,l'} \frac{\hbar^2}{2mR_c^2} \end{aligned} \tag{A.6}$$

where $z_{i,l'}$ represents the *i* zero of the *l'* spherical Bessel Functions $j_{l'}(z_{i,l'}) = 0$. $z_{i,l'}$ can be numerically computed and some of the lowest values are reported here:

$$\begin{aligned} z_{i,0} &= i\pi \\ z_{1,0} &= 3.142 \\ z_{1,1} &= 4.493 \\ z_{1,2} &= 5.763 \end{aligned} \tag{A.7}$$

Finally we have:

$$F_{i,l',m'}(r_e, \theta_e, \phi_e) = \frac{1}{N} Y_{l',m'}(\theta_e, \phi_e) j_{l'}(k_{i,l'} r_e) \tag{A.8}$$

where N is the normalization factor and the total unperturbed wavefunction reads:

$$\begin{aligned} \Psi_{i,l',m',n,l,m}(\boldsymbol{r}_e, \boldsymbol{r}) &= F_{i,l',m'}(r_e, \theta_e, \phi_e) \psi_{n,l,m}(r, \theta, \phi) \\ &= \frac{1}{N} Y_{l',m'}(\theta_e, \phi_e) j_{l'}(k_{i,l'} r_e) Y_{l,m}(\theta, \phi) R_{n,l}(r) \end{aligned} \tag{A.9}$$

The total energy of the unperturbed system depends only on 3 quantum numbers and it reads:

$$\begin{aligned} E^{tot}_{i,l',n} &= E'_n + E''_{i,l'} \\ &= -E_{HA} \frac{1}{4n^2} + z^2_{i,l'} \frac{\hbar^2}{2mR_c^2} \end{aligned} \tag{A.10}$$

In particular, the ground state solution of Eq. A.1 is

$$\Psi_{1,0,0,1,0,0}(\boldsymbol{r}_e, \boldsymbol{r}) = \frac{1}{N} \left[\frac{\sin(\pi r_e / R_c)}{\pi r_e / R_c} \right] \cdot \exp[-\frac{r}{2\alpha_b}] \tag{A.11}$$

Regarding excited levels, they depend on the cavity radius and we note for example that if $R_c \gtrsim 5$a.u., the first excited state of the unperturbed system will be 3 times degenerate:

$$\Psi_{1,1,0,1,0,0}, \Psi_{1,1,-1,1,0,0}, \Psi_{1,1,+1,1,0,0}$$

Instead if $R_c \lesssim 5$a.u., the first excited state of the unperturbed system will be (4 times degenerate):

$$\Psi_{1,0,0,2,0,0}, \Psi_{1,0,0,2,1,0}, \Psi_{1,0,0,2,1,-1}, \Psi_{1,0,0,2,1,+1}$$

APPENDIX B

Spin notation and identities

As it is well known from standard quantum mechanics, the wave functions of a fermion (i.e. electron and positron in this work) depends on the coordinates $\boldsymbol{r} = (r_x, r_y, r_z)$ and on the z-component of spin $\hat{S}_z$ (given that total spin S^2 is fixed by statistics). While the coordinates can be anything, the spin S_z can only take on two eigenvalues $\hbar/2$ and $-\hbar/2$. In turn, these lead to the two values of the spin quantum number $m_s = \pm 1/2$. The value $m_s = 1/2 = \uparrow$ is usually associated to the so called *spin-up* state while $m_s = -1/2 = \downarrow$ is what we call *spin-down*. In particular,

$$\begin{aligned} S^2 \left|s, m_s\right\rangle &= \hbar^2 s(s+1) \left|s, m_s\right\rangle \\ S_z \left|s, m_s\right\rangle &= \hbar m_s \left|s, m_s\right\rangle \end{aligned} \tag{A.1}$$

where $s = \frac{1}{2}$ for fermions.

In many body physics, it is useful to describe these states introducing a spin variable $\sigma \equiv \hbar m_s$ and a spin wavefunction $s_{m_s}(\sigma)$ associated to it. Since σ can take on only two values $\pm\hbar/2$, each spin wave function will only have two values:

$$\begin{aligned} s_\uparrow(\frac{\hbar}{2}) &= 1 \qquad & s_\uparrow(-\frac{\hbar}{2}) &= 0 \\ s_\downarrow(\frac{\hbar}{2}) &= 0 \qquad & s_\downarrow(-\frac{\hbar}{2}) &= 1 \end{aligned} \tag{A.2}$$

The meaning of this wave function is that Using this wave functions, the probability that a measurement of S_z will yield a certain value is easily understood in terms of squared modulus. For example, when the electron is in the spin-up state, the probability of finding it at $\sigma = \hbar/2$ is $P(\sigma = \hbar/2) = |s_\uparrow(\hbar/2)|^2 = 1$, while the probability that its value will be $-\hbar/2$ is 0. Note that the spin wave functions are normalized and mutually orthogonal:

$$\begin{aligned} \sum_{\sigma=-\hbar/2}^{\hbar/2} |s_{m_s}(\sigma)|^2 &= 1 \\ \sum_{\sigma=-\hbar/2}^{\hbar/2} s_\uparrow(\sigma) s_\downarrow(\sigma) &= 0 \end{aligned} \tag{A.3}$$

so they are a basis on the single particle spin space. Using this notation, the well known

singlet and triplet spin configuration of two particles can be written as:

$$\begin{aligned}
\chi_{00}(\sigma_1,\sigma_2) &= \frac{s_\uparrow(\sigma_1)s_\downarrow(\sigma_2) - s_\downarrow(\sigma_1)s_\uparrow(\sigma_2)}{\sqrt{2}} \\
\chi_{10}(\sigma_1,\sigma_2) &= \frac{s_\uparrow(\sigma_1)s_\downarrow(\sigma_2) + s_\downarrow(\sigma_1)s_\uparrow(\sigma_2)}{\sqrt{2}} \\
\chi_{11}(\sigma_1,\sigma_2) &= s_\uparrow(\sigma_1)s_\uparrow(\sigma_2) \\
\chi_{1-1}(\sigma_1,\sigma_2) &= s_\downarrow(\sigma_1)s_\downarrow(\sigma_2)
\end{aligned} \tag{A.4}$$

where χ_{s,s_z} are eigenfunctions of the total spin S^2 and its z component S_z.

In this thesis we use the following identities for the spin configurations of a system of 3 particles :

$$\begin{aligned}
\chi_{11}(\sigma_p,\sigma_e)s_\uparrow(\sigma_1) &= \chi_{11}(\sigma_p,\sigma_1)s_\uparrow(\sigma_e) \\
\chi_{11}(\sigma_p,\sigma_e)s_\downarrow(\sigma_1) &= \frac{1}{\sqrt{2}}\left[\chi_{00}(\sigma_p,\sigma_1) + \chi_{1,0}(\sigma_p,\sigma_1)\right] s_\uparrow(\sigma_e) \\
\chi_{00}(\sigma_p,\sigma_e)s_\uparrow(\sigma_1) &= \frac{1}{\sqrt{2}}\left[\chi_{11}(\sigma_p,\sigma_1)s_\downarrow(\sigma_e) + \frac{1}{\sqrt{2}}\left(\chi_{00}(\sigma_p,\sigma_1) - \chi_{10}(\sigma_p,\sigma_1)\right) s_\uparrow(\sigma_e)\right] \\
\chi_{00}(\sigma_p,\sigma_e)s_\downarrow(\sigma_1) &= \frac{1}{\sqrt{2}}\left[-\chi_{1-1}(\sigma_p,\sigma_1)s_\uparrow(\sigma_e) + \frac{1}{\sqrt{2}}\left(\chi_{00}(\sigma_p,\sigma_1) + \chi_{10}(\sigma_p,\sigma_1)\right) s_\downarrow(\sigma_e)\right]
\end{aligned} \tag{A.5}$$

Also similar results can easily be extended to 4 particles:

$$\begin{aligned}
\chi_{11}(\sigma_p,\sigma_2)s_\uparrow(\sigma_1)s_\uparrow(\sigma_e) &= \chi_{11}(\sigma_p,\sigma_1)s_\uparrow(\sigma_2)s_\uparrow(\sigma_e) \\
\chi_{11}(\sigma_p,\sigma_2)s_\uparrow(\sigma_1)s_\downarrow(\sigma_e) &= \chi_{11}(\sigma_p,\sigma_1)s_\uparrow(\sigma_2)s_\downarrow(\sigma_e) \\
\chi_{11}(\sigma_p,\sigma_2)s_\downarrow(\sigma_1)s_\uparrow(\sigma_e) &= \frac{1}{\sqrt{2}}\left[\chi_{00}(\sigma_p,\sigma_1) + \chi_{10}(\sigma_p,\sigma_1)\right] s_\uparrow(\sigma_2)s_\uparrow(\sigma_e) \\
\chi_{11}(\sigma_p,\sigma_2)s_\downarrow(\sigma_1)s_\downarrow(\sigma_e) &= \frac{1}{\sqrt{2}}\left[\chi_{00}(\sigma_p,\sigma_1) + \chi_{10}(\sigma_p,\sigma_1)\right] s_\uparrow(\sigma_2)s_\downarrow(\sigma_e) \\
\chi_{00}(\sigma_p,\sigma_2)s_\uparrow(\sigma_1)s_\uparrow(\sigma_e) &= \frac{1}{\sqrt{2}}\Big[\chi_{11}(\sigma_p,\sigma_1)s_\downarrow(\sigma_2) + \\
&\quad + \frac{1}{\sqrt{2}}\left[\chi_{00}(\sigma_p,\sigma_1) - \chi_{10}(\sigma_p,\sigma_1)\right] s_\uparrow(\sigma_2)\Big] s_\uparrow(\sigma_e) \\
\chi_{00}(\sigma_p,\sigma_2)s_\uparrow(\sigma_1)s_\downarrow(\sigma_e) &= \frac{1}{\sqrt{2}}\Big[\chi_{11}(\sigma_p,\sigma_1)s_\downarrow(\sigma_2) + \\
&\quad + \frac{1}{\sqrt{2}}\left[\chi_{00}(\sigma_p,\sigma_1) - \chi_{10}(\sigma_p,\sigma_1)\right] s_\uparrow(\sigma_2)\Big] s_\downarrow(\sigma_e) \\
\chi_{00}(\sigma_p,\sigma_2)s_\downarrow(\sigma_1)s_\uparrow(\sigma_e) &= \frac{1}{\sqrt{2}}\Big[- \chi_{1-1}(\sigma_p,\sigma_1)s_\uparrow(\sigma_2) + \\
&\quad + \frac{1}{\sqrt{2}}\left[\chi_{00}(\sigma_p,\sigma_1) + \chi_{10}(\sigma_p,\sigma_1)\right] s_\downarrow(\sigma_2)\Big] s_\uparrow(\sigma_e) \\
\chi_{00}(\sigma_p,\sigma_2)s_\downarrow(\sigma_1)s_\downarrow(\sigma_e) &= \frac{1}{\sqrt{2}}\Big[- \chi_{1-1}(\sigma_p,\sigma_1)s_\uparrow(\sigma_2) + \\
&\quad + \frac{1}{\sqrt{2}}\left[\chi_{00}(\sigma_p,\sigma_1) + \chi_{10}(\sigma_p,\sigma_1)\right] s_\downarrow(\sigma_2)\Big] s_\downarrow(\sigma_e)
\end{aligned} \tag{A.6}$$

Bibliography

[1] H. Nakanishi and Y Ujihira. *J. Phys. Chem.*, 86:4446–50, 1982.

[2] G. Consolati and F. Quasso. The experimental determination of the qps contact density in matter. *Applied Physics A*, 52(5):295–298, May 1991.

[3] D. W. Gidley, W. E. Frieze, T. L. Dull, A. F. Yee, E. T. Ryan, and H.-M. Ho. Positronium annihilation in mesoporous thin films. *Phys. Rev. B*, 60:R5157–R5160, Aug 1999.

[4] L. Xie, G. B. DeMaggio, W. E. Frieze, J. DeVries, D. W. Gidley, H. A. Hristov, and A. F. Yee. Positronium formation as a probe of polymer surfaces and thin films. *Phys. Rev. Lett.*, 74:4947–4950, Jun 1995.

[5] J.W.Humberston M.Charlton. *Positron Physics*.

[6] P.E. Mallon Y.C.Jean and D.M.Schrader. *Positron and positronium chemistry*.

[7] S.V.Stepanov and V.M.Byakov. *Principles and Application of Positron & Positronium Chemistry*.

[8] V.I. Goldanskii. Physical chemistry of the positron and positronium.

[9] A. Dupasquier, P. De Natale, and A. Rolando. Formal calculation of the pick-off annihilation rate for ortho- and parapositronium. *Phys. Rev. B*, 43:10036–10041, May 1991.

[10] Giovanni Consolati, Fiorenza Quasso, and Davide Trezzi. Swelling of positronium confined in a small cavity. *PLOS ONE*, 9(10):1–5, 10 2014.

[11] M.

[12] Martin Deutsch. Evidence for the formation of positronium in gases. *Physical Review*, 82(3):455, 1951.

[13] Richard A Ferrell. The positronium fine structure. *Physical Review*, 84(4):858, 1951.

[14] Stephan Berko and Hugh N Pendleton. Positronium. *Annual Review of Nuclear and Particle Science*, 30(1):543–581, 1980.

[15] Aadne Ore and JL Powell. Three-photon annihilation of an electron-positron pair. *Physical Review*, 75(11):1696, 1949.

[16] Jinfeng Yang, Masami Chiba, Ryosuke Hamatsu, Tachishige Hirose, Toshihiro Matsumoto, and Jie Yu. Four-photon decay of orthopositronium: A test of charge-conjugation invariance. *Physical Review A*, 54(3):1952, 1996.

[17] L Wolfenstein and DG Ravenhall. Some consequences of invariance under charge conjugation. *Physical Review*, 88(2):279, 1952.

[18] Toshihiro Matsumoto, Masami Chiba, Ryosuke Hamatsu, Tachishige Hirose, Jinfeng Yang, and Jie Yu. Measurement of five-photon decay in orthopositronium. *Physical Review A*, 54(3):1947, 1996.

[19] John Archibald Wheeler. Polyelectrons. *Annals of the New York Academy of Sciences*, 48(3):219–238, 1946.

[20] AI Alekseev. Two-photon annihilation of positronium in the p-state. *Zhur. Eksptl'. i Teoret. Fiz.*, 34, 1958.

[21] Akinori Igarashi, Mineo Kimura, Isao Shimamura, and Nobuyuki Toshima. Inseparable positron annihilation and positronium formation in positron-atom collisions: Description in terms of an absorption potential. *Physical Review A*, 68(4):042716, 2003.

[22] RJ Drachman and J Sucher. Annihilation in positron—atom collisions: A new approach. *Physical Review A*, 20(2):442, 1979.

[23] GE Lee-Whiting. Thermalization of positrons in metals. *Physical Review*, 97(6):1557, 1955.

[24] S Kahana. Positron annihilation in metals. *Physical Review*, 129(4):1622, 1963.

[25] DC Connors and RN West. Positron annihilation and defects in metals. *Physics Letters A*, 30(1):24–25, 1969.

[26] T Korhonen, Martti J Puska, and Risto M Nieminen. First-principles calculation of positron annihilation characteristics at metal vacancies. *Physical Review B*, 54(21):15016, 1996.

[27] M Manninen, Risto Nieminen, P Hautojärvi, and J Arponen. Electrons and positrons in metal vacancies. *Physical Review B*, 12(10):4012, 1975.

[28] P Jena, AK Gupta, and KS Singwi. Positron annihilation in small metal voids. *Solid State Communications*, 21(3):293–296, 1977.

[29] JA Ludlow and GF Gribakin. Many-body theory calculations of positron binding to negative ions. *arXiv preprint arXiv:1002.3125*, 2010.

[30] Richard A Ferrell. Theory of positron annihilation in solids. *Reviews of Modern Physics*, 28(3):308, 1956.

[31] M. J. Puska and R. M. Nieminen. Theory of positrons in solids and on solid surfaces. *Rev. Mod. Phys.*, 66:841–897, Jul 1994.

[32] Egil A Hylleraas and Aadne Ore. Binding energy of the positronium molecule. *Physical Review*, 71(8):493, 1947.

[33] O-E. Mogensen. Spur reaction model of positronium formation. *The Journal of Chemical Physics*, 60(3):998–1004, 1974.

[34] Ennio Lazzarini. A comprehensive model for positronium formation and related phenomena of its inhibition and enhancement. *International Journal of Radiation Applications and Instrumentation. Part C. Radiation Physics and Chemistry*, 28(1):49–54, 1986.

[35] M Eldrup, A Vehanen, Peter J Schultz, and KG Lynn. Positronium formation and diffusion in crystalline and amorphous ice using a variable-energy positron beam. *Physical Review B*, 32(11):7048, 1985.

[36] Lea Di Noto. *Positronium in the AEgIS experiment: study on its emission from nanochanneled samples and design of a new apparatus for Rydberg excitations*. PhD thesis, University of Trento, 2014.

[37] David W Gidley, Hua-Gen Peng, and Richard S Vallery. Positron annihilation as a method to characterize porous materials. *Annu. Rev. Mater. Res.*, 36:49–79, 2006.

[38] G Marlotti Tanzi, F Castelli, and G Consolati. Positronium confinement in small cavities: A two-particle model for the lowering of contact density. *Physical review letters*, 116(3):033401, 2016.

[39] G Marlotti Tanzi, F Castelli, and G Consolati. Numerical solution of a two-particle

model of positronium confined in small cavities. *Acta Physica Polonica, A.*, 132(5), 2017.

[40] T. Fulop, Z. Farkas, A. Seeger, and J. Major. On the inner structure of confined positronium. *eprint arXiv:cond-mat/0304442*, April 2003.

[41] T McMullen and MJ Stott. Dependence of the positronium hyperfine interaction on the environment: a simple model. *Canadian Journal of Physics*, 61(3):504–507, 1983.

[42] Otto Halpern. Magnetic quenching of the positronium decay. *Physical Review*, 94(4):904, 1954.

[43] A Bisi, A Fiorentini, E Gatti, and L Zappa. Magnetic quenching of positronium in solids and positron helicity. *Physical Review*, 128(5):2195, 1962.

[44] VL Telegdi, JC Sens, DD Yovanovitch, and SD Warshaw. Magnetic quenching of 3-photon annihilation in solids. *Physical Review*, 104(4):867, 1956.

[45] Michael A Stroscio. Positronium: A review of the theory. *Physics Reports*, 22(5):215–277, 1975.

[46] ML Lewis and VW Hughes. Higher-order relativistic contributions to the combined zeeman and motional stark effects in positronium. *Physical Review A*, 8(2):625, 1973.

[47] A Bisi, Gr Consolati, Gr Gambarini, and L Zappa. Effects of collisions with paramagnetic ions on the magnetic quenching of positronium. *Il Nuovo Cimento B (1971-1996)*, 65(2):442–454, 1981.

[48] A Bisi, G Consolati, G Gambarini, and L Zappa. Normal and anomalous positronium in matter. *Il Nuovo Cimento D*, 6(3):183–192, 1985.

[49] A Bisi, G Consolati, and L Zappa. Contact density and hyperfine splitting of positronium in naphthalene. *Hyperfine Interactions*, 36(1):29–37, 1987.

[50] Giovanni Consolati and Fiorenza Quasso. A comparison between the magnetic quenching of positronium in atactic polypropylene and that in isotactic polypropylene. *Journal of Physics C: Solid State Physics*, 21(22):4143, 1988.

[51] G Consolati and F Quasso. Anomalous magnetic quenching of quasi-positronium in solid octadecane. *Journal of Physics: Condensed Matter*, 2(17):3941, 1990.

[52] Giovanni Consolati. Magnetic quenching of positronium. *Journal of radioanalytical and nuclear chemistry*, 210(2):273–292, 1996.

[53] John Archibald Wheeler. Polyelectrons. *Annals of the New York Academy of Sciences*, 48(3):219–238, 1946.

[54] S. H. Patil. Boundary-condition-determined wave function for the ground state of positronium ion $\bar{e}ee$. *Phys. Rev. A*, 58:728–731, Jul 1998.

[55] YK Ho. Positron annihilation in the positronium negative ion. *Journal of Physics B: Atomic and Molecular Physics*, 16(8):1503, 1983.

[56] Alexei M Frolov. Positron annihilation in the positronium negative ion ps-. *Physics Letters A*, 342(5-6):430–438, 2005.

[57] Richard J Drachman. The interaction of positrons and positronium with small atoms. *Canadian Journal of Physics*, 60(4):494–502, 1982.

[58] Giovanni Consolati and Fiorenza Quasso. On the origin of the intermediate component in the positron lifetime spectra in polymers. *Applied Physics A*, 50(1):43–48, 1990.

[59] S. J. Tao. Positronium annihilation in molecular substances. *The Journal of Chemical Physics*, 56(11):5499–5510, 1972.

[60] M. Eldrup, N. J. Pedersen, and J. N. Sherwood. Positron annihilation study of

defects in succinonitrile. *Phys. Rev. Lett.*, 43:1407–1410, Nov 1979.

[61] D. W. Gidley, W. E. Frieze, T. L. Dull, A. F. Yee, E. T. Ryan, and H.-M. Ho. Positronium annihilation in mesoporous thin films. *Phys. Rev. B*, 60:R5157–R5160, Aug 1999.

[62] Dhanadeep Dutta, Bichitra Nandi Ganguly, Debarshi Gangopadhyay, Tapas Mukherjee, and Binayak Dutta-Roy. General trends of positronium pick-off annihilation in molecular substances. *Journal of Physics: Condensed Matter*, 14(32):7539, 2002.

[63] A Zubiaga, M M Ervasti, I Makkonen, A Harju, F Tuomisto, and M J Puska. Modeling positronium beyond the single particle approximation. *Journal of Physics B: Atomic, Molecular and Optical Physics*, 49(6):064005, 2016.

[64] Werner Brandt, S. Berko, and W. W. Walker. Positronium decay in molecular substances. *Phys. Rev.*, 120:1289–1295, Nov 1960.

[65] Giovanni Consolati, Rafael Ferragut, Anne Galarneau, Francesco Di Renzo, and Fiorenza Quasso. Mesoporous materials for antihydrogen production. *Chem. Soc. Rev.*, 42:3821–3832, 2013.

[66] B. Zgardzinska. Can tao-eldrup model be used at short o-ps lifetime? *Acta Physica Polonica A*, 125(3):700–701, 2014.

[67] Ken Wada and Toshio Hyodo. A simple shape-free model for pore-size estimation with positron annihilation lifetime spectroscopy. In *Journal of Physics: Conference Series*, volume 443, page 012003. IOP Publishing, 2013.

[68] Sergey V Stepanov, Vsevolod M Byakov, Dmitrii S Zvezhinskiy, Gilles Duplâtre, Roman R Nurmukhametov, and Petr S Stepanov. Positronium in a liquid phase: formation, bubble state and chemical reactions. *Advances in Physical Chemistry*, 2012, 2012.

[69] Amy LR Bug, Timothy W Cronin, PA Sterne, and Zachary S Wolfson. Simulation of positronium: Toward more realistic models of void spaces in materials. *Radiation Physics and Chemistry*, 76(2):237–242, 2007.

[70] David Ceperley and Berni Alder. Quantum monte carlo. *Science*, 231(4738):555–560, 1 1986.

[71] E. L. Pollock and D. M. Ceperley. Simulation of quantum many-body systems by path-integral methods. *Phys. Rev. B*, 30:2555–2568, Sep 1984.

[72] D. M. Ceperley. Path integrals in the theory of condensed helium. *Rev. Mod. Phys.*, 67:279–355, Apr 1995.

[73] L. Larrimore, R. N. McFarland, P. A. Sterne, and Amy L. R. Bug. A two-chain path integral model of positronium. *The Journal of Chemical Physics*, 113(23):10642–10650, 2000.

[74] Levere Hostler and R. H. Pratt. Coulomb green's function in closed form. *Phys. Rev. Lett.*, 10:469–470, Jun 1963.

[75] R. G. Storer. Path-integral calculation of the quantum-statistical density matrix for attractive coulomb forces. *Journal of Mathematical Physics*, 9(6):964–970, 1968.

[76] E.L. Pollock. Properties and computation of the coulomb pair density matrix. *Computer Physics Communications*, 52(1):49 – 60, 1988.

[77] A.L.R. Bug and P.A. Sterne. *Phys. Rev. B*, 73:094106, 2006.

[78] P.A. Sterne, L. Larrimore, P. Hastings, and A.L.R. Bug. New theories for positrons in insulators. *Radiation Physics and Chemistry*, 68(3):409 – 414, 2003. Proceedings of the 7th International Conference on Positron and Positronium Chemistry.

[79] Amy L.R. Bug, Melaku Muluneh, Jillian Waldman, and P.A. Sterne. Positronium

in solids: Computer simulation of pick-off and self-annihilation. In *Positron Annihilation - ICPA-13*, volume 445 of *Materials Science Forum*, pages 375–379. Trans Tech Publications, 2 2004.

[80] Dario Bressanini, Massimo Mella, and Gabriele Morosi. Positronium chemistry by quantum monte carlo. i. positronium-first row atom complexes. *The Journal of chemical physics*, 108(12):4756–4760, 1998.

[81] Massimo Mella, Gabriele Morosi, Dario Bressanini, and Stefano Elli. Positron and positronium chemistry by quantum monte carlo. v. the ground state potential energy curve of e+ lih. *The Journal of Chemical Physics*, 113(15):6154–6159, 2000.

[82] Massimo Mella, Gabriele Morosi, and Dario Bressanini. Positron and positronium chemistry by quantum monte carlo. iv. can this method accurately compute observables beyond energy? *The Journal of chemical physics*, 111(1):108–114, 1999.

[83] A Zubiaga, F Tuomisto, and MJ Puska. Pick-off annihilation of positronium in matter using full correlation single particle potentials: solid he. *The Journal of Physical Chemistry B*, 119(4):1747–1755, 2015.

[84] R. S. Brusa, A. Dupasquier, S. Longano, and S. Oss. Positron-electron annihilation in the proximity of a second electron in a dense medium. *Phys. Rev. B*, 43:12715–12722, Jun 1991.

[85] JP Carbotte and S Kahana. Positron annihilation in an interacting electron gas. *Physical Review*, 139(1A):A213, 1965.

[86] B Barbiellini, P Genoud, and T Jarlborg. Calculation of positron lifetimes in bulk materials. *Journal of Physics: Condensed Matter*, 3(39):7631, 1991.

[87] Ilja Makkonen, Mikko M Ervasti, Topi Siro, and Ari Harju. Enhancement models of momentum densities of annihilating electron-positron pairs: The many-body picture of natural geminals. *Physical Review B*, 89(4):041105, 2014.

[88] E Boroński and RM Nieminen. Electron-positron density-functional theory. *Physical Review B*, 34(6):3820, 1986.

[89] J Mitroy and B Barbiellini. Enhancement factors for positron annihilation studies. *Physical Review B*, 65(23):235103, 2002.

[90] ND Drummond, P López Ríos, CJ Pickard, and RJ Needs. First-principles method for impurities in quantum fluids: Positron in an electron gas. *Physical Review B*, 82(3):035107, 2010.

[91] Y. Nagashima, Y. Morinaka, T. Kurihara, Y. Nagai, T. Hyodo, T. Shidara, and K. Nakahara. Origins of positronium emitted from sio_2. *Phys. Rev. B*, 58:12676–12679, Nov 1998.

[92] S J Brawley, S Armitage, J Beale, D E Leslie, A I Williams, and G Laricchia. Electron-like scattering of positronium. 330:789, 11 2010.

[93] A_ Bondi. van der waals volumes and radii. *The Journal of physical chemistry*, 68(3):441–451, 1964.

[94] T Goworek, K Ciesielski, B Jasińska, and J Wawryszczuk. Positronium states in the pores of silica gel. *Chemical physics*, 230(2-3):305–315, 1998.

[95] Kenji Ito, Hiroshi Nakanishi, and Yusuke Ujihira. Extension of the equation for the annihilation lifetime of ortho-positronium at a cavity larger than 1 nm in radius. *The Journal of Physical Chemistry B*, 103(21):4555–4558, 1999.

[96] YC Jean, J David Van Horn, Wei-Song Hung, and Kuier-Rarn Lee. Perspective of positron annihilation spectroscopy in polymers. *Macromolecules*, 46(18):7133–7145, 2013.

[97] T Goworek. Comments on the relation: positronium lifetime–free volume size pa-

rameters of the tao–eldrup model. *Chemical physics letters*, 366(1-2):184–187, 2002.

[98] R Zaleski, J Wawryszczuk, and T Goworek. Electron density at positron's site in mcm-41 ordered silica. *Chemical physics letters*, 372(5-6):800–804, 2003.

[99] Klein D. J. Exchange perturbation theories. *International Journal of Quantum Chemistry*, 32(3):377–396.

[100] Adams William H. Perturbation theory of intermolecular interactions: What is the problem, are there solutions? *International Journal of Quantum Chemistry*, 38(24):531–547.

[101] William H Adams. The problem of unphysical states in the theory of intermolecular interactions. *Journal of mathematical chemistry*, 10(1):1–23, 1992.

[102] Krzysztof Szalewicz, Konrad Patkowski, and Bogumil Jeziorski. Intermolecular interactions via perturbation theory: from diatoms to biomolecules. In *Intermolecular forces and clusters II*, pages 43–117. Springer, 2005.

[103] Douglas J Klein and Josep M Oliva. Composite-system models. *International Journal of Quantum Chemistry*, 110(15):2784–2800, 2010.

[104] JN Murrell and G Shaw. Intermolecular forces in the region of small orbital overlap. *The Journal of Chemical Physics*, 46(5):1768–1772, 1967.

[105] Ernest Davidson. *Reduced density matrices in quantum chemistry*, volume 6. Elsevier, 2012.

[106] Joachim Alexander Maruhn, Paul-Gerhard Reinhard, and Eric Suraud. *Simple models of many-fermion systems*. Springer Science & Business Media, 2010.

[107] AW Overhauser. Pair-correlation function of an electron gas. *Canadian journal of physics*, 73(11-12):683–686, 1995.

[108] Giovanni Consolati and Fiorenza Quasso. Magnetic quenching of the three-photon annihilation rate in some molecular solids. *Physical Review B*, 50(9):5848, 1994.

[109] Giovanni Consolati, N Gambara, and Fiorenza Quasso. Positron annihilation in some organic scintillators: magnetic quenching and three gamma spectroscopy results. *Zeitschrift für Physik D Atoms, Molecules and Clusters*, 21(3):259–264, 1991.

[110] T Goworek, A Badia, and G Duplatre. Normal and anomalous positronium states in ionic and molecular solids investigated via magnetic field effects. *Journal of the Chemical Society, Faraday Transactions*, 90(11):1501–1506, 1994.

[111] A Bisi, A Dupasquier, and L Zappa. Properties of the magnetically quenchable positron state in alkali halides. *Journal of Physics C: Solid State Physics*, 6(7):1125, 1973.

[112] A Bisi, Giovanni Consolati, G Gambarini, and L Zappa. Positronium-oxygen interaction in hexane. *Il Nuovo Cimento D*, 1(6):725–736, 1982.

[113] G Consolati, D Gerola, and F Quasso. An unusual three-quantum yield from positrons annihilated in benzene. *Journal of Physics: Condensed Matter*, 3(39):7739, 1991.

[114] Y Nagai, Y Nagashima, and T Hyodo. Lifetime of delocalized positronium in α-SiO_2. *Physical Review B*, 60(11):7677, 1999.

[115] Yasuyuki Nagashima, Yasuyoshi Nagai, and Takeo Hyodo. Positronium contact density in crystalline and amorphous sio 2. In *Materials Science Forum*, volume 363, pages 567–569, 2001.

[116] M Zanatta, G Baldi, RS Brusa, W Egger, A Fontana, E Gilioli, S Mariazzi, G Monaco, L Ravelli, and F Sacchetti. Structural evolution and medium range order in permanently densified vitreous sio 2. *Physical review letters*, 112(4):045501, 2014.

[117] R.S.Brusa. Università degli studi di trento, private communication. 2018.
[118] Hans A Bethe and Edwin E Salpeter. *Quantum mechanics of one-and two-electron atoms*. Springer Science & Business Media, 2012.

Acknowledgments

Firstly, I would like to express my sincere gratitude to my advisor Fabrizio, for the continuous support of my Ph.D study and related research, for his knowledge, motivation, and, above all, his strong optimism. His guidance helped me in all the time of research and writing of this thesis. Besides, I would like to thank my co-advisor Gianni, for his availability, his insightful comments and his vast experience and knowledge of the field. I could not have imagined having better advisors for my Ph.D study.

I thank my fellow colleagues Simo, Marci, Silvia, Marco and Lorenzo for all the lunch breaks, for the stimulating discussions, for the beers, the board games, the escape rooms and for all the fun we have had in the last three years. I would never have survived so long without such a company.

I thank all my dearest friends, despite they were constantly mocking me for choosing such a crazy career. I guess that's probably what friends are there for.

I thank my family, my parents and my brother for supporting me spiritually throughout writing this thesis and my my life in general.

Last but not the least, I would like to thank my girlfriend, Vale. There are too many reasons and too little space here, but I'm lucky having you by my side.